

Spring 2020

An Examination Between Neighborhood Characteristics and Alzheimer's Disease and Related Dementias and Caregiver Mental Health in South Carolina

Mohammad Jahirul Islam

Follow this and additional works at: <https://scholarcommons.sc.edu/etd>



Part of the [Chemistry Commons](#)

Recommended Citation

Islam, M. J.(2020). *An Examination Between Neighborhood Characteristics and Alzheimer's Disease and Related Dementias and Caregiver Mental Health in South Carolina*. (Doctoral dissertation). Retrieved from <https://scholarcommons.sc.edu/etd/5688>

This Open Access Dissertation is brought to you by Scholar Commons. It has been accepted for inclusion in Theses and Dissertations by an authorized administrator of Scholar Commons. For more information, please contact digres@mailbox.sc.edu.

CHEMISTRY OF PYRIDYLCARBORANE MULTIDENTATE LIGANDS
AND THEIR METAL COMPLEXES

by

Mohammad Jahirul Islam

Bachelor of Science
University of Dhaka, 2010

Master of Science
University of Dhaka, 2012

Submitted in Partial Fulfillment of the Requirements

For the Degree of Doctor of Philosophy in

Chemistry

College of Arts and Sciences

University of South Carolina

2020

Accepted by:

Dmitry V. Peryshkov, Major Professor

Aaron K. Vannucci, Committee Member

Sheryl L. Wiskur, Committee Member

Christopher Williams, Committee Member

Cheryl L. Addy, Vice Provost and Dean of the Graduate School

© Copyright by Mohammad Jahirul Islam, 2020
All Rights Reserved.

DEDICATION

To my parents, wife Humaiara Akter, daughter Ruaydaa Zaarin, Mini aunt and
Jamal uncle for all their love and support.

ACKNOWLEDGEMENTS

I would like to express my deepest appreciation to Dr. Dmitry Peryshkov for his great supervision and guidance. Your amazing encouragement and support allowed me to achieve my educational goals and focus my efforts on my academic pursuits. Thank you for always being there to answer all my questions whenever I was in trouble. I truly appreciate you for giving me a chance to work with you that will shape my future career.

I would like to thank all the professors at the University of South Carolina who have helped me to broaden my knowledge and guided me to grow as a researcher. I am also grateful to all the past and present members of the Peryshkov Group and Shustova Group. Lastly, I would like to express my deepest gratitude to my parents, wife, daughter, relatives and friends for their unconditional motivation, love, and support.

ABSTRACT

Carboranes are of topical interest due to their unique structures and applications in the fields of catalysis, polymers, material sciences and supramolecular chemistry. Icosahedral *closo*-dicarbadodecaboranes are remarkably robust three-dimensional boron-carbon clusters with two slightly acidic C-H bonds. Moreover, coordinatively unsaturated transition-metal complexes containing C-functionalized *ortho*-carborane are considered as potential catalysts for activation of small molecules.

Recently, we reported the synthesis of a pyridine-backbone pincer complex $\{(C_5H_3N)(C_2B_{10}H_{10})_2\}Ni(CH_3CN)$ (**1**) in which two C-functionalized *ortho*-carborane clusters act as the arms of the pincer ligand. The complex **1** was determined to be a competent catalyst for nucleophilic addition of piperidine to acetonitrile. Upon addition of KO^tBu, activation of a C-H bond of a labile acetonitrile ligand at the nickel center afforded a C-bound cyanomethyl ligand bearing complex $K\{(C_5H_3N)(C_2B_{10}H_{10})_2\}Ni(CH_2CN)$ (**2**). Oxidation of **2** by introducing oxygen yielded a cyano complex $K\{(C_5H_3N)(C_2B_{10}H_{10})_2\}Ni(CN)$ (**3**), along with HCHO, CO₂ and HO-CH₂CN *via* a free radical mechanism. The complexes, **1** and **2**, also mediated the formation of acrylamide through C-C coupling of acetonitrile with aldehyde. The double deboronation of the pincer ligand by a methanolic potassium hydroxide solution, followed by homometalation by Ru resulted in the formation of a mixture of racemic and meso ruthenacarborane clusters.

The bidentate (*ortho*-carboranyl)pyridine ligand bearing complex $\text{RuCl}(\text{C}_{10}\text{H}_{14})(\text{C}_7\text{H}_{14}\text{B}_{10}\text{N})$ (**4**) was synthesized by the addition of $[\text{Ru}(p\text{-cymene})\text{Cl}_2]_2$ into a solution of $\{(\textit{ortho}\text{-carboranyl})\text{pyridine}\}$ potassium in tetrahydrofuran. The synthesis of a cationic complex $[\text{Ru}(\text{CH}_3\text{CN})(\text{C}_{10}\text{H}_{14})(\text{C}_7\text{H}_{14}\text{B}_{10}\text{N})](\text{BF}_4)$ (**5**) was accomplished by reacting **4** with AgBF_4 using acetonitrile as the solvent. The complexes, **4** and **5**, were characterized by an array of multinuclear NMR spectroscopic techniques and single crystal X-ray crystallography. Both complexes were found to be competent catalysts for transfer hydrogenation of a wide range of aliphatic and aromatic ketones.

The *C,N*-chelating ligand (*ortho*-carboranyl)pyridine was also employed to obtain an intramolecularly coordinated nickel (II) complex $\{(\text{C}_5\text{H}_3\text{N})(\text{C}_2\text{B}_{10}\text{H}_{10})\}_2\text{Ni}$ (**6**). Interestingly, the coordination of the two *ortho*-carborane bearing *C,N*-chelating ligands to the Ni(II) center afforded an unusual distorted square planar geometry, in which two chelates occupied adjacent positions.

TABLE OF CONTENTS

Dedication.....	iii
Acknowledgements.....	iv
Abstract.....	v
List of Schemes.....	viii
List of Figures.....	x
Chapter 1 Carboranes in the Realm of Organometallic Chemistry	1
Chapter 2 Sterically Encumbered Dianionic Dicarboranyl Pincer Ligand (C ₅ H ₃ N)(C ₂ B ₁₀ H ₁₁) ₂ and its CNC Nickel(II) Complex.....	23
Chapter 3 Activation of C–H and C–CN Bonds of Acetonitrile by a Dianionic Dicarboranyl Pincer Ligand (C ₅ H ₃ N)(C ₂ B ₁₀ H ₁₁) ₂ Bearing CNC Nickel(II) Complex	43
Chapter 4 Formation of Acrylamide <i>via</i> Coupling of Acetonitrile with Aldehyde, Mediated by a CNC Ni(II) Complex: A Mechanistic Study	68
Chapter 5 Synthesis and Characterization of Doubly Deboronated 2,6–bis { <i>nido</i> –(<i>ortho</i> –carborane)} pyridine Ligand and its Ruthenacarborane Clusters.....	89
Chapter 6 Synthesis and Characterization of Ru(II) Complexes of (<i>ortho</i> –Carboranyl)pyridine and their Role on Transfer Hydrogenation of Ketones.....	105
Chapter 7 Synthesis and Characterization of a Pyridine–Functionalized Carborane Bearing Distorted Square Planar Complex of Nickel(II)	128
Appendix A: Permission to Reprint.....	139

LIST OF SCHEMES

Scheme 1.1 A general overview to afford <i>C</i> -functionalized <i>ortho</i> -carborane. The second deprotonation can be done by employing another equivalent of base. ¹⁰	4
Scheme 1.2 Deboronation of <i>ortho</i> -carborane by anionic nucleophile (Nu ⁻) to yield 7,8- <i>nido</i> -carborane. ^{10,43}	7
Scheme 1.3 Strategies for activation of C–CN bond of nitriles.	9
Scheme 1.4 Activation of C–CN bond by Ni(0) <i>via</i> formation of (dippe)Ni(η^2 -N≡CAr) intermediate. ^{58(a),(i)}	10
Scheme 1.5 Activation of C–CN bond in a <i>C</i> -bound cyanomethyl complex of Ni(II). ..	11
Scheme 1.6 A general overview for transfer hydrogenation of ketones. ⁵	12
Scheme 2.1 Synthesis of 2,6-bis(<i>ortho</i> -carborane)pyridine (C ₅ H ₃ N)(C ₂ B ₁₀ H ₁₁) ₂ (1).	25
Scheme 2.2 Synthesis of {(C ₅ H ₃ N)(C ₂ B ₁₀ H ₁₀) ₂ }Ni(CH ₃ CN) (2).....	28
Scheme 2.3 Addition of piperidine to acetonitrile promoted by 2. The catalyst loading was 1 mol % relative to the amount of piperidine. Acetonitrile served as both the reagent and the solvent.	31
Scheme 3.1 Synthesis of {(C ₅ H ₃ N)(C ₂ B ₁₀ H ₁₀) ₂ }Ni(CH ₃ CN) (2).....	46
Scheme 3.2 Base assisted C–H activation of labile acetonitrile ligand.....	47
Scheme 3.3 Synthesis of ¹³ C labeled cyanomethyl (¹³ CH ₂ –CN) bearing complex 2a from 1a followed by O ₂ assisted C–CN bond activation. Red carbon atoms represents 99 % enriched ¹³ C.	52
Scheme 3.4 Oxidation of triphenylphosphine by O ₂ in the presence of 2.	55
Scheme 3.5 Activation of I ₂ by 3 to afford <i>N</i> -bound iodoacetonitrile complex 5.	55
Scheme 4.1 Cyanomethylation of aldehyde to yield β -hydroxy nitrile.	69

Scheme 4.2 <i>Mechanism A</i> : Base (DBU) initiated catalytic cycle proposed by Fan and Ozerov for cyanomethylation of aldehyde. ⁷ <i>Mechanism B</i> : Base-free cyanomethylation of aldehyde proposed by Guan <i>et. al.</i> ¹	70
Scheme 4.3 Deprotonation of acetonitrile followed by ligand flip to afford C-bound cyanomethyl containing anionic CNC Ni(II) pincer complex (2) from N-bound acetonitrile bearing neutral CNC Ni(II) pincer complex (1).	72
Scheme 4.4 Reaction of 1, aldehyde, and KO ^t Bu in benzene at room temperature.	73
Scheme 4.5 Alternative synthetic route of 5 from 1.	75
Scheme 4.6 Proposed mechanism for the formation of N-bound acrylamide bearing anionic complex (6). (<i>Cis</i> -acrylonitrile is omitted for clarity)	76
Scheme 4.7 Proposed pathway for the synthesis of deuterated C-bound cyanomethyl complex 2c from 2 <i>via</i> formation of an unstable N-bound cyanomethyl isomer 2a.	77
Scheme 4.8 Proposed mechanism for the synthesis of 1a and 6a.	79
Scheme 5.1 Removal of B3/B6 atom by using methanolic KOH to yield <i>nido</i> -carborane anion 7,8-C ₂ B ₉ H ₁₂	90
Scheme 5.2 Synthesis of [2,6-bis{ <i>nido</i> -(<i>ortho</i> -carborane)}pyridine](NBu ₄) ₂ (2).	92
Scheme 6.1 Transfer hydrogenation of ketone to yield secondary alcohol.	106
Scheme 6.2 Synthesis of (<i>ortho</i> -carboranyl)pyridine (C ₅ H ₃ N)(C ₂ B ₁₀ H ₁₁) (1).	108
Scheme 6.3 Synthesis of RuCl(C ₁₀ H ₁₄)(C ₇ H ₁₄ B ₁₀ N) (Ru-C) (2).	109
Scheme 6.4 Mercury test: transfer hydrogenation of acetophenone by complex 3 in the presence of excess Hg ⁰	115
Scheme 7.1 Synthesis of {(<i>ortho</i> -carboranyl)pyridine} ₂ nickel(II) (2).	130

LIST OF FIGURES

- Figure 1.1 Numbering scheme and three isomers of carborane based on the relative positions of the CH vertices.3
- Figure 1.2 [2 + 2 + 2] Cycloaddition of carboryne with alkynes *via* the Ni–carboryne intermediate (η^2 -C₂B₁₀H₁₀)Ni(PPh₃)₂.²⁵5
- Figure 1.3 Metal complexes of derivatized *ortho*–carborane ligands. (a) pyridine-backbone *ortho*–carborane donor arms pincer complex of Ni(II),³¹ (b) Ir(III) complexes bearing a cyclometallated NHC–*ortho*–carborane ligand,³⁵ (c) boron/phosphorus-bridged carboranyl ligands containing constrained-geometry group 4 complexes,^{20,21} (d) constrained-geometry ruthenium complex of carboranyl ligand which undergoes C–C bond coupling ((d) to (e)) and Ru–C to Ru–B conversion ((d) to (f)).²²6
- Figure 1.4 Rh and Hf metallacarboranes as catalysts: (a) Hydrogenation catalyst for prochiral ketones,⁴⁷ (b) terminal alkynes dimerization catalyst.⁴⁸ and (c, d) hydrogenation catalyst for alkynes.⁴⁹8
- Figure 1.5 NHCs bearing Ru and Ir complexes for transfer hydrogenation of ketones. (a) CNC bis(carbenes) Ru pincer complex,¹⁸ (b) NNC (pyrazol–3–yl)–*N*–heterocyclic carbene Ru(II) complex,¹⁹ (c) Ru(II) complex with imidazol–2–ylidene (ImNHC) and 1,2,3–traizol–5–ylidene (tzNHC) donors,²⁰ and (d) *N*–heterocyclic carbene–carborane containing Ir(III) complex.²¹14
- Figure 2.1 Displacement ellipsoid plot (50 % probability) of the proligand (C₅H₃N)(C₂B₁₀H₁₁)₂ (1). (a): a view perpendicular to the (C3–N1–C3A) plane (b): a view along the (C3–N1–C3A) plane.27
- Figure 2.2 Displacement ellipsoid plot (50 % probability) of the {(C₅H₃N)(C₂B₁₀H₁₀)₂}Ni(CH₃CN) complex (2). (a): a view perpendicular to the (C3–N1–Ni1–C3A) plane (b): a general view (c): space-filling diagram of 2 with the acetonitrile ligand omitted.29
- Figure 3.1 (a) Cyclic voltammogram of 1 mM of 1 in 0.1 M TBAPF₆ in THF, glassy carbon (GC) as working electrode, Pt as counter electrode, scan rate 60 mVs⁻¹. (b) Cyclic voltammogram of 1 mM of complex 2 in 0.1 M TBAPF₆ in THF, GC as working electrode, Pt as counter electrode, scan rate 60 mVs⁻¹..46

- Figure 3.2 (a) Displacement ellipsoids of **3** drawn at the 50% probability level (expanded by symmetry). (b) Crystal structure of **3**, highlighting locations of two C₆D₆ molecules, and environment of K atom. In both figures, superscripts denote symmetry-equivalent atoms.49
- Figure 3.3 (a) Displacement ellipsoids of **4** drawn at the 50 % probability level. The C28–C27, N3–Ni2 bond distances are 1.483(5) Å and 1.892(3) Å. (b) Coordination of K atoms of the pseudocubane K₄N₄ core, no C₆D₆ is coordinated to K4. The N4–K2, K3–N6, K4–N8 and K1–N2 distances are 2.819(3) Å, 2.843(3) Å, 2.794(3) Å and 2.781(3) Å, respectively. The K4–N4, K1–N6, K3–N2 and K2–N8 distances are 2.766(3) Å, 2.778(3) Å, 2.955(3) Å and 2.803(3) Å, respectively. In both images, hydrogen atoms are omitted for clarity.50
- Figure 3.4 (a) UV-vis absorption spectrum of 0.05 mM **3** in dichloromethane. (b) UV-vis absorption spectrum of 0.05 mM **4** in dichloromethane. (c) UV-vis spectral changes after addition of O₂ in a solution 0.05 mM **3** in dichloromethane. Curves: green line, pure **3**; dashed blue line, **3** + O₂ after 5 minutes (first intermediate); dashed red line, **3** + O₂ after 10 minutes (second intermediate); black line, formation of **4** after 2 hours. (d) Decay of the second intermediate over time at the absorption maximum of 286 nm.53
- Figure 3.5 EPR studies of oxygenated **3** in CD₂Cl₂ using DMPO as radical trapping agent. Curves: black line, spectra of **3** and DMPO solution before oxygenation; green line, spectra of DMPO–free radical adduct after 20 minutes of oxygenation.54
- Figure 4.1 Crystal structure of Ni(N≡C–CH=CHC₁₂H₉)(C₉H₂₃B₂₀N) (**4**). The Ni1–N2–C10 bond angle is slightly deviated from linearity (174.69°).74
- Figure 4.2 Crystal structure of K[{(C₅H₃N)(C₂B₁₀H₁₀)₂}Ni(OH)] (**5**)74
- Figure 4.3 Crystal structure of K[{(C₅H₃N)(C₂B₁₀H₁₀)₂}Ni(C₁₅H₁₂NO)] (**6**). The Ni1–N2, N2–C10, C10–C11 bond distances are 1.867(2) Å, 1.323(4) Å, 1.473(4) Å, respectively.75
- Figure 5.1 (A) Two orientations of **2** which are superimposed to each other. The hydrogen atoms are omitted for clarity. (B) Depiction of **2** showing the bridged protons based on the NMR spectroscopy and the single crystal X–ray crystallography.93
- Figure 5.2 (a) The 40 % probability displacement ellipsoid plot of **3**. (b) The comparison of the relevant bond distances of the two ruthenacarborane clusters. The complex is located on an idealized C₂ rotational axis. The two *p*-cymene ligands and the cluster hydrogen atoms are omitted for clarity.95

Figure 5.3 The 30 % probability displacement ellipsoid plot of 4 where the C1/B1(A/B) sites are scrambled (shown in pink color). The hydrogen atoms of <i>p</i> -cymene moieties are omitted for clarity. The C3–C2, B1–Ru1 and C1–Ru1 bond distances are 1.597(5) Å, 2.180(4) Å and 2.182(4) Å, respectively. The C2–C1 and C2–B1 bond distances are 1.665(6) Å and 1.691(6) Å, respectively.	96
Figure 6.1 (a) 1,3-Bis(2,4,6-trimethylphenyl)imidazol-2-ylidene, a general example of <i>N</i> -heterocyclic carbene. (b) (<i>ortho</i> -carboranyl)pyridine ligand, used in this work.	107
Figure 6.2 Displacement ellipsoid plot (50 % probability) of the RuCl(C ₁₀ H ₁₄)(C ₇ H ₁₄ B ₁₀ N) complex (2).....	109
Figure 6.3 Displacement ellipsoid plot (50 % probability) of the [Ru(CH ₃ CN)(C ₁₀ H ₁₄)(C ₇ H ₁₄ B ₁₀ N)](BF ₄) complex (3).....	110
Figure 6.4 Displacement ellipsoid plot (50 % probability) of the RuCl(C ₁₀ H ₁₄)(C ₇ H ₁₄ B ₁₀ N) (Ru–B) complex (4).	111
Figure 6.5 Displacement ellipsoid plot (50 % probability) of the Ru(C ₂₀ H ₂₅)(C ₇ H ₁₄ B ₁₀ N) complex (5).	113
Figure 7.1 (a) Cyclic voltammogram of 1 mM of (<i>ortho</i> -carboranyl)pyridine (1) in 0.1 M TBAPF ₆ in acetonitrile, glassy carbon (GC) as working electrode, Pt as counter electrode, scan rate 100 mVs ⁻¹ . (b) Cyclic voltammogram of 1 mM of complex 2 in 0.1 M TBAPF ₆ in acetonitrile, GC as working electrode, Pt as counter electrode, scan rate 100 mVs ⁻¹	131
Figure 7.2 (a) 30 % probability displacement ellipsoid plot of 2. (b) Skeletal view highlighting the <i>C,N</i> - coordination of the ligand 1 to the nickel(II) center to form a five-membered ring. (c) A space-filling diagram of 2.....	132

Chapter 1

Carboranes in the Realm of Organometallic Chemistry

1.1.1 INTRODUCTION

Carboranes are of topical interest due to their unique structures and applications in the fields of catalysis,¹ polymers,² material sciences,³ and supramolecular chemistry.⁴ In medicinal chemistry, carboranes have been used in boron neutron capture therapy (BNCT)⁵ and boron neutron capture synovectomy (BNCS).⁶ In addition, they are also used as pharmacophores in drug delivery systems.⁷ Among the carboranes, icosahedral *closo*-dicarbadodecaboranes ($C_2B_{10}H_{12}$) are remarkably robust electron-deficient three-dimensional boron-carbon clusters which are derived from $B_{12}H_{12}^{2-}$ dianion by replacing two BH vertices with two CH vertices.⁸ In this introduction, icosahedral *closo*-dicarbadodecaboranes will be referred simply as carboranes.

In organometallic chemistry carboranes are an extraordinary candidate as ligands due to their desirable properties, such as thermal and redox stability, chemical inertness, low nucleophilicity, and high hydrophobicity.⁸ The cluster properties of carboranes depend on the geometry and electron-deficient nature of the boron atoms. Based on the relative positions of the two CH vertices, carboranes are constructed of three different isomers - known as *ortho*-, *meta*- and *para*- carboranes (**Figure 1.1**). The *ortho*- and *meta*- carboranes exhibit C_{2v} symmetry, and *meta*-carborane possesses D_{5d} symmetry.⁹ Based on van der Waals volume, the steric bulk of carboranes (148 \AA^3 for *ortho*-carborane) is almost twice as large as benzene (79 \AA^3) and similar to that of adamantane (136 \AA^3). The low electron density of the carborane clusters is revealed by the total electron count of 26 (26 skeletal electrons for 12 vertices). In addition, the cluster atoms of carboranes adopt nonclassical bonding interactions manifested by unusual three-center two-electron bonds. Each cluster atom is connected to five

neighboring atoms by this three-center two-electron bonds, and one hydrogen atom by exohedral classical two-center two-electron bond.¹⁰

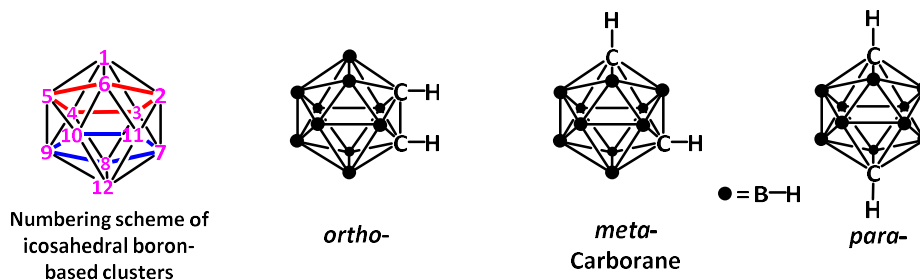


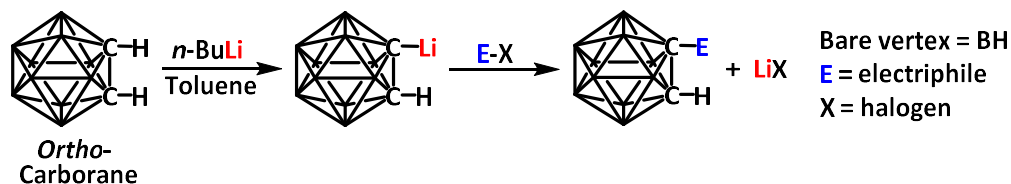
Figure 1.1: Numbering scheme and three isomers of carborane based on the relative positions of the CH vertices.

Similar to an aromatic compound, the bonding electron density of carborane is delocalized over the cluster, hence in literature carboranes are sometimes named as “three-dimensional benzene”.¹⁰ However, the delocalized electron density is not uniformly distributed among the cluster atoms, which results in significantly different electronic effects experienced by exohedral substituents attached to the cage carbon or boron atoms.¹¹ In addition, the electronegativity differences of the carbon and boron atoms, and icosahedral geometry of carborane cage is responsible for large dipole moment for *ortho-*, and *meta-* isomers (4.53 (5) D and, 2.85 (5) D, respectively). Due to the higher electronegativity of the carbon atoms compared to boron atoms, carbon atoms withdraw electron density from C-functionalized substituents^{12,13} and boron atoms donate electron density to B-functionalized substituents.^{14,15} The carbon atoms of the carborane cage favor nonadjacent sites due to the stronger B-C bonds in comparison with C-C bonds, which stabilizes *para*-carborane more than the other two isomers.¹⁶ The hydride-like behavior of the ten hydrogen atoms attached exohedrally to the boron atoms makes the carborane cage very hydrophobic.¹⁷ In contrast to the BH hydrogen atoms, the

hydrogens attached to the cage carbons are slightly acidic ($pK_a = 23$ for *ortho*-carborane), due to the higher electronegativity of carbon atoms.¹¹

1.1.2 FUNCTIONALIZATION OF CARBORANES

The higher acidity of CH bonds allows a high degree of control for the reactivity and functionalization of the carborane cage.¹⁰ One or both of the acidic CH protons of a carborane cluster can be removed by using an equivalent amount of organometallic base, such as *n*-butyllithium¹⁸ or lithium bis(trimethylsilyl)amide¹⁹ to generate carboranyl nucleophile. The C-functionalization of a carborane cage is accomplished by reacting the carboranyl group with an electrophile in an organic solvent such as *n*-pentane, *n*-hexane, toluene, or ethers (diethyl ether, dimethoxyethane, THF) (**Scheme 1.1**). Most of the electrophiles employed to date are halides, which react with lithiated nucleophilic carboranes to yield corresponding lithium salt along with substituted carboranes. The reactions for carborane functionalization are performed under air-free conditions due to the moisture sensitivity of organic bases; however, the substituted carboranes are air-stable and can be purified and stored in air.¹⁰ Upon installation of a substituent on a cluster carbon atom, the acidity of the remaining cluster protons is influenced by the substituent, and the acidity of the substituent is dominated by the cluster.¹⁰



Scheme 1.1: A general overview to afford C-functionalized *ortho*-carborane. The second deprotonation can be done by employing another equivalent of base.¹⁰

1.1.3 TRANSITION METAL COMPLEXES OF CARBORANES IN CATALYSIS

The incorporation of carborane clusters in transition-metal based catalysts offers significant advantages for chemical bond transformations. For example, the bulkiness of a carborane moiety provides substantial stabilization of high and low oxidation states of an active transition metal center. In addition, catalysts for specific applications can be designed by tailoring steric properties and functional versatility of carborane clusters.²⁰⁻²²

The di-anionic 1,2-dehydro-*ortho*-carborane ligand ($\eta^2\text{-C}_2\text{B}_{10}\text{H}_{10}^{2-}$) is regarded as the three-dimensional analogue of benzyne, and are designated as “carboryne”.²³ The *C,C*-coordinated transition metal complexes of carboryne have drawn tremendous attention in recent years because of their fascinating chemistry and applications in chemical bond activation.²⁴⁻²⁹ For example, Xie and co-workers reported a novel method for the regioselective [2 + 2 + 2] cycloaddition of carboryne with unsaturated substrates mediated by Ni-carboryne complex (**1**), *via* formation of an intermediate ($\eta^2\text{-C}_2\text{B}_{10}\text{H}_{10}$)Ni(PPh₃)₂ (**2**). In this case, the high regioselectivity is attribute to the presence of the bulky carborane moiety (**Figure 1.2**).²⁵

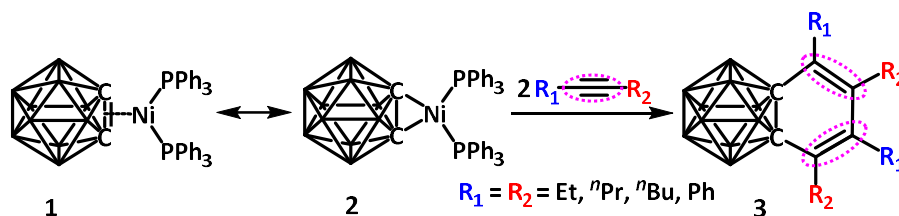


Figure 1.2: [2 + 2 + 2] Cycloaddition of carboryne with alkynes *via* the Ni-carboryne intermediate ($\eta^2\text{-C}_2\text{B}_{10}\text{H}_{10}$)Ni(PPh₃)₂.²⁵

In recent years, *C*-functionalized *ortho*-carborane derivatives have been extensively studied to explore their potential applications as ligands in transition-metal mediated catalysis.^{18,30-36} In 2018, we reported the synthesis of a pyridine-backbone

pincer complex $\{(C_5H_3N)(C_2B_{10}H_{10})_2\}Ni(CH_3CN)$ (**Figure 1.3, (a)**) in which two *ortho*-carborane clusters act as the arms of the pincer framework. The complex (**a**) was found to be a competent catalyst for nucleophilic addition of piperidine to acetonitrile.³¹ Willans and co-workers demonstrated the transfer hydrogenation of acetophenone by a series of Ir(III) complexes bearing a cyclometallated NHC-*(ortho*-carborane) ligand (such as, (**b**) in **Figure 1.3**).³⁵ Xie and co-workers developed constrained-geometry group 4 metal complexes by utilizing boron/phosphorus-bridged carboranyl ligands ((**c**) in **Figure 1.3**) which are excellent ethylene polymerization catalysts.^{20,21} Intriguingly, the constrained-geometry facilitates unique chemical transformations, such as C–C coupling reaction, and conversion of a Ru–C(cage) to a Ru–B(cage) by ruthenium carboranyl complexes as depicted in **Figure 1.3** ((**d**) to (**e**), and (**d**) to (**f**), respectively).²²

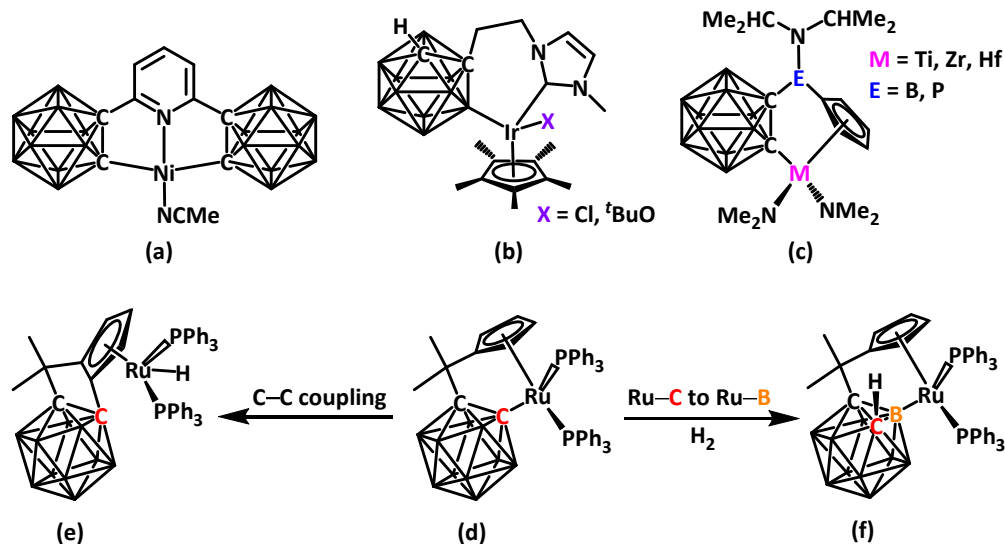
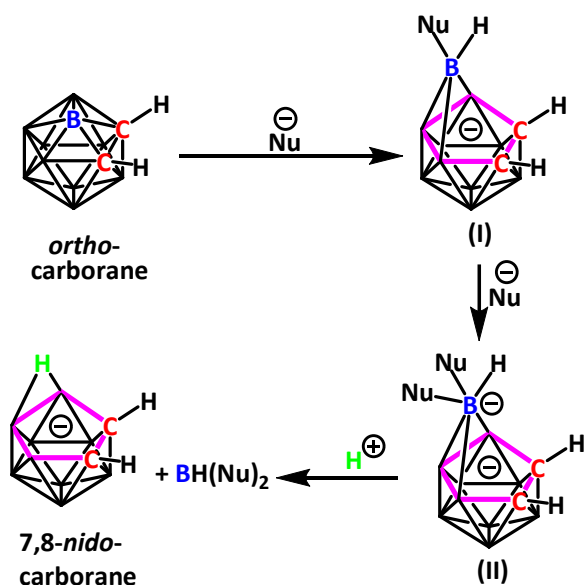


Figure 1.3: Metal complexes of derivatized *ortho*-carborane ligands. (**a**) pyridine-backbone *ortho*-carborane donor arms pincer complex of Ni(II),³¹ (**b**) Ir(III) complexes bearing a cyclometallated NHC-*ortho*-carborane ligand,³⁵ (**c**) boron/phosphorus-bridged carboranyl ligands containing constrained-geometry group 4 complexes,^{20,21} (**d**) constrained-geometry ruthenium complex of carboranyl ligand which undergoes C–C bond coupling ((**d**) to (**e**)) and Ru–C to Ru–B conversion ((**d**) to (**f**)).²²

1.1.4 METALLACARBORANES AND THEIR APPLICATIONS IN CATALYSIS

Removal of a boron vertex to afford *nido*-carborane is one of the most common reactivities of boron atoms within a carborane cluster.^{10,37,38} The decapitation of a boron vertex is performed by employing strong Lewis bases such as alkoxides,³⁷ amines,³⁹ fluorides,^{40,41} and *N*-heterocyclic carbenes.⁴² The most electropositive boron atom (B3 or B6) of a carborane cluster is prone to attack by a nucleophile (Nu^-) to form (I), as shown in **Scheme 1.2**. The anionic *nido*-7,8-carborane (*nido*-7,8- $\text{C}_2\text{B}_9\text{H}_{12}^-$) is afforded by the attack of a second nucleophile to the same boron atom followed by the formal removal of $\text{BH}(\text{Nu})_2$ and addition of H^+ (**Scheme 1.2**).^{10,43}



Scheme 1.2: Deboronation of *ortho*-carborane by anionic nucleophile (Nu^-) to yield 7,8-*nido*-carborane.^{10,43}

The *nido*-7,8- $\text{C}_2\text{B}_9\text{H}_{12}$ anion is a precursor for a large number of 12 vertex metallocarboranes of general formula $\text{C}_2\text{B}_9\text{H}_{11}\text{M}$ (M = metal). In contrast to exo-metal complexes, in metallocarborane a metal is incorporated into the cluster framework upon

removal of the bridging proton (B–H–B).⁴⁴ The role of exo-metal complexes of carboranes in catalysis is well explored, and that for metallocarboranes is still underexplored. However, metallocarboranes are considered as efficient candidates in homogenous catalysis due to their functional tunability, thermal and chemical stability, great solubility, and versatile reactivity.^{45,46} In literature, few examples of metallocarborane mediated catalytic transformations have been reported that includes, hydrogenation of prochiral ketones to chiral alcohols by a rhodacarborane,⁴⁷ regioselective dimerization of terminal alkynes,⁴⁸ and hydrogenation of internal alkynes to *cis*-alkenes⁴⁹ by Hf–metallocarboranes (**Figure 1.4**).

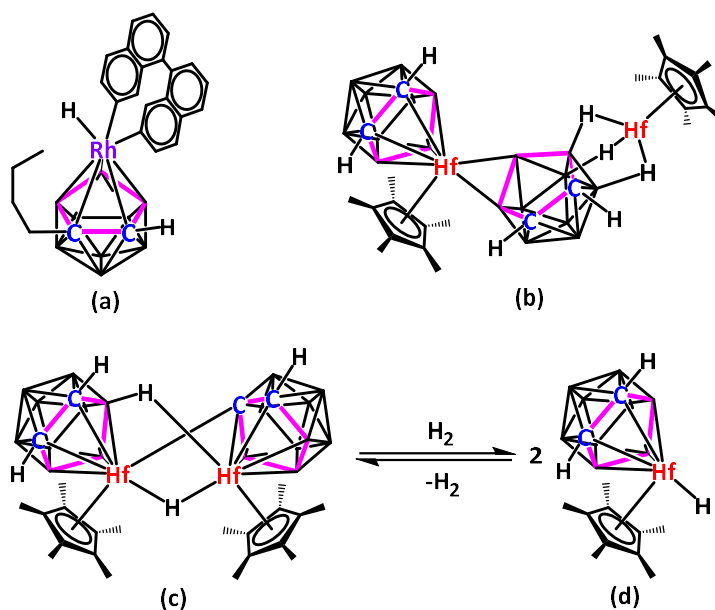
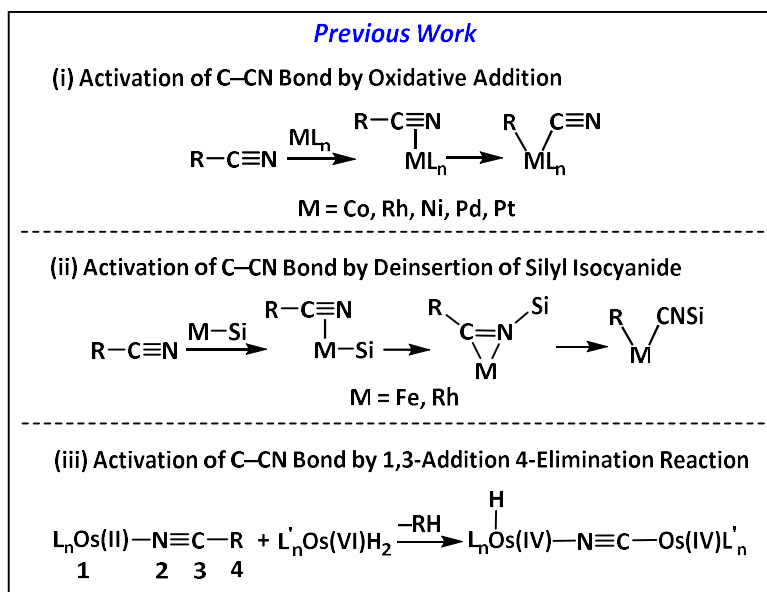


Figure 1.4: Rh and Hf metallocarboranes as catalysts: (a) Hydrogenation catalyst for prochiral ketones,⁴⁷ (b) terminal alkynes dimerization catalyst.⁴⁸ and (c, d) hydrogenation catalyst for alkynes.⁴⁹

1.2 C–CN BOND ACTIVATION OF NITRILES

The activation of C–C σ -bond is an area of great importance for chemical transformations in organic synthesis⁵⁰, for example cracking of alkanes in petroleum

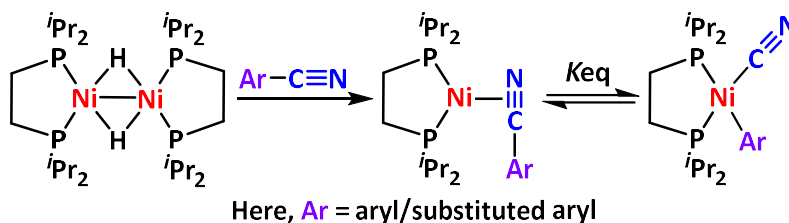
refinery.⁵¹ However, the C–C bond activation of alkanes is challenging due to the high directionality of the σ -orbital,⁵² large C–C bond energy (83 kcalmol⁻¹)⁵³ and weak coordination to metals.⁵² In this context, transition metal mediated C–CN bond cleavage of nitriles has attained some advancement, despite the higher C–CN bond energy (133 kcalmol⁻¹)⁵⁴ compared to alkanes. This is attributed to the ability of the C \equiv N functionality to interact with transition metal centers.^{50,52,56} In literature three strategies have been reported so far (**Scheme 1.3**), that include (i) oxidative addition of C–CN bond to a low valent metal center, such as Rh(–I)⁵⁵, Co(I),⁵⁶ Rh(I),⁵⁷ Ni(0),⁵⁸ Pd(0),⁵⁹ and Pt(0),⁶⁰ (ii) insertion of C \equiv N bond into a M–Si (M = Fe,⁵³ Rh⁶¹) or Rh–B⁶² bond that undergoes α -carbon elimination resulting in the rupture of C–C bond, and (iii) 1,3-addition 4-elimination of Os(II) coordinated alkylnitriles to afford C–CN bond activation.⁵² In the last two decades, few examples of Cu complex mediated heterolytic cleavage of a C–CN bond of acetonitrile to yield CN⁻ and CH₃⁺ fragments have also been reported.^{54,63}



Scheme 1.3: Strategies for activation of C–CN bond of nitriles.

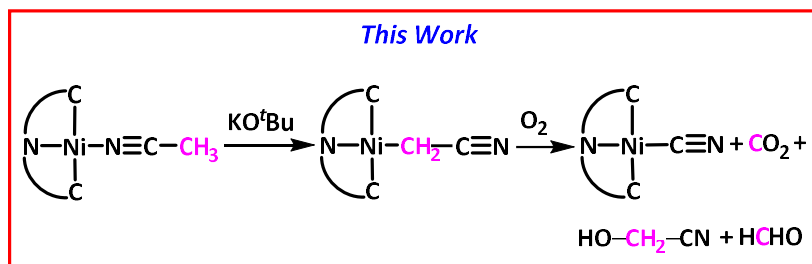
Among the transition metals, nickel complexes play a significant role for activation of nitrile C–CN bond,⁵⁸ and are known to catalyze decyanation,⁶⁴ hydrogenolysis,⁶⁵ cross-coupling,⁶⁶ and transfer hydrocyanation^{58(g)} for a wide range of nitrile substrates. Jones and co-workers demonstrated reversible C–CN bond activation of benzonitrile⁵⁸⁽ⁱ⁾ and substituted benzonitriles^{58(a)} by a [Ni(dippe)] fragment which was generated *in-situ* upon removal of H₂ from a hydrido dimer [(dippe)NiH]₂. Recently, Maiti and co-workers reported Ni(0) catalyzed decyanation of aryl and aliphatic cyanides by employing hydrosilane as a hydride donor.⁶⁴ They also developed Ni(0) mediated hydrogenolysis of nitriles using H₂ as hydrogen source.⁶⁵ Han and co-workers discovered a novel approach for P–H/C–CN cross-coupling to synthesize arylphosphines and arylphosphine oxides by employing Ni(COD)₂/8–hydroxyquinoline catalyst under mild reaction conditions.⁶⁶ In 2016, Fang and co-workers reported their pioneering strategy on Ni(0) catalyzed transfer hydrocyanation of alkenes by utilizing alkylnitriles in the presence of AlMe₂Cl as a Lewis acid.^{58(g)}

All of the above mentioned examples of catalytic transformations by zerovalent Ni complexes based on C–CN activation proceeded *via* formation of a η^2 -side-on-coordinated intermediate LNi(η^2 -N≡C–R/Ar) (L = ligand, R/Ar = alkyl/aryl) which is also supported by a recent computational mechanistic investigation (**Scheme 1.4**).^{58(h)}



Scheme 1.4: Activation of C–CN bond by Ni(0) *via* formation of (dippe)Ni(η^2 -N≡CAr) intermediate.^{58(a),(i)}

Recently, we explored the first example of di-valent Ni CNC–pincer complex ((a) in **Figure 3**) mediated C–CN bond activation of acetonitrile *via* the formation of an anionic intermediate (CNC)Ni(II)–CH₂CN[−]. The intermediate underwent C–CN bond cleavage by a free radical pathway in the presence of added O₂ to yield K[(CNC)Ni(II)(CN)] (**3**), HCHO, HO–CH₂CN and CO₂ (**Scheme 1.5**). The formation of an oxygen centered free radical was confirmed through its trapping by DMPO (DMPO = 5,5–dimethyl–1–pyrroline *N*–oxide, a free radical trapping agent) as evidenced by Electron Paramagnetic Resonance spectroscopy (EPR). A radical assisted mechanism was also corroborated by the drastic slowdown of C–CN activation reaction upon addition of DMPO.



Scheme 1.5: Activation of C–CN bond in a C–bound cyanomethyl complex of Ni(II).

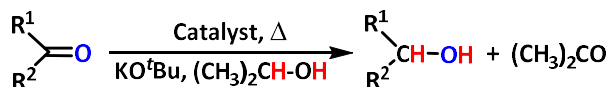
1.3 COUPLING OF NITRILE WITH ALDEHYDE

The formation of a C–C bond *via* the coupling of nucleophilic α -deprotonated nitriles with carbonyl electrophiles is an attractive route for the synthesis of pharmaceutically important β -hydroxy nitriles.⁶⁷⁻⁷² However, the selective deprotonation of the α -hydrogen atom of a nitrile to generate a nucleophile *in-situ* often requires a strong base that makes the whole process challenging due to the base sensitivity of the neighboring C \equiv N functionality.^{71,72} In this context, the Lewis acidic transition metal complexes have been proven as efficient catalysts for C–C coupling because of their

ability to lower p*K*_a of *N*-coordinated nitriles.⁷¹ Acetonitrile is a widely studied substrate for C–C coupling reactions because of its relatively acidic *sp*³ C–H bond (p*K*_a = 25 in H₂O).⁷³ In literature, three ‘pincer’ Ni(II) complexes have been found to be effective catalysts for the cyanomethylation reaction.^{71,72,74} Fan and Ozerov reported the cyanomethylation of aldehydes with acetonitrile by a diarylamido-based PNP complex of nickel in the presence of a base.⁷² Guan and co-workers demonstrated a diarylamido-based PNP pincer complex of Ni(II) with the cyanomethyl ligand that catalyzed C–C bond formation of aldehyde with acetonitrile without the addition of base.⁷¹ In 2015, Miller and co-workers explored a Ni(II) complex supported by a NCOP pincer framework which mediated aldehyde cyanomethylation reaction to afford β-hydroxy nitrile.⁷⁴ In this dissertation, we described C–C coupling of aldehyde with acetonitrile mediated by a pyridine backbone *ortho*-carboranyl arms pincer complexes of Ni(II) (Chapter 4).

1.4 TRANSFER HYDROGENATION OF KETONES

Transfer hydrogenation of unsaturated chemical bonds (such as C=O) has drawn significant attention in the last few decades because of its widespread applications in various fields, including pharmaceuticals, fine chemicals, bioactive molecules, and agricultural chemicals.⁷⁵⁻⁷⁸ As an alternative to direct hydrogenation, transfer hydrogenation is a powerful and inexpensive technique for transformation of ketones to corresponding secondary alcohols by utilizing ^tPrOH as a sacrificial hydrogen donor (Scheme 1.6).⁷⁹



Scheme 1.6: A general overview for transfer hydrogenation of ketones.⁵

A wide range of NHC ligands bearing transition metal complexes have been reported as efficient transfer hydrogenation catalysts.⁸⁰⁻⁸⁸ Among the transition metals, NHCs bearing Ru complexes have been studied extensively for C=O bond hydrogenation.^{79,89-92} In 2003, Peris and co-workers reported the transfer hydrogenation of cyclohexanone as a model substrate with TONs up to 126000 and a TOF of 15200 h⁻¹ catalyzed by a CNC bis(carbene) ligand bearing Ru pincer complex ((**a**) in **Figure 1.5**).⁹² Yu and co-workers explored “pincer”-type pyridyl based (pyrazol-3-yl)-*N*-heterocyclic carbene ligand containing Ru(II) complex as a competent transfer hydrogenation catalyst for ketones ((**b**) in **Figure 1.5**).⁹³ In 2019, Rit and co-workers described the catalytic ability of a series of Ru(II) complexes with two different carbene donors for the reduction of ketones with a broad substrate scope.⁹⁴

Although NHC based transition metal complexes have been successfully explored for the reduction of ketones, complexes containing carborane as transfer hydrogenation catalysts are still underexplored. To the best of our knowledge, the Ir(III) complex (**d**) in **Figure 1.5** that contains a carborane moiety attached with a chelating *N*-heterocyclic carbene is the only example of a transfer hydrogenation catalyst with limited substrate scope.³⁵ Recently, we explored the synthesis of a chelating (*ortho*-carboranyl)pyridine bearing Ru(II) complex, and its catalytic application for transfer hydrogenation of a wide variety of ketones which will be discussed in Chapter 6.

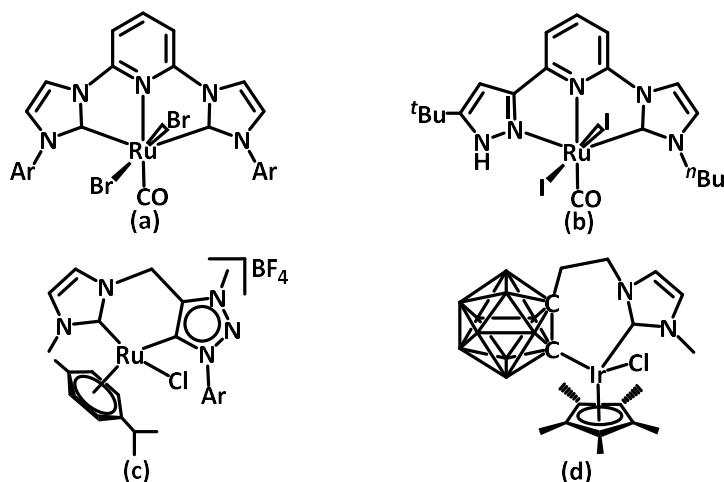


Figure 1.5: NHCs bearing Ru and Ir complexes for transfer hydrogenation of ketones. **(a)** CNC bis(carbenes) Ru pincer complex,¹⁸ **(b)** NNC (pyrazol-3-yl)-*N*-heterocyclic carbene Ru(II) complex,¹⁹ **(c)** Ru(II) complex with imidazol-2-ylidene (ImNHC) and 1,2,3-triazol-5-ylidene (tzNHC) donors,²⁰ and **(d)** *N*-heterocyclic carbene-carborane containing Ir(III) complex.²¹

1.5 A GENERAL OUTLINE OF THE DISSERTATION

In catalysis *ortho*-carborane and its *C*-functionalized derivatives are considered as attractive ligands because of the remarkable thermal and chemical stability, three-dimensional structure, and pseudo-aromatic character of the carborane moiety.^{8,30,31,95} In Chapter 2, we demonstrated the synthesis of a pyridine backbone *C*-functionalized *ortho*-carborane donor arms containing pincer complex of Ni(II), and its role on nucleophilic addition of piperidine to acetonitrile.³¹ The two *ortho*-carborane clusters of the pincer framework make the Ni(II) center highly Lewis acidic by withdrawing electron density. The activation of C-H and C-CN bonds of an acetonitrile ligand at the Lewis acidic Ni(II) center is described in Chapter 3. Deprotonation of an acidic α -hydrogen of the *N*-coordinated acetonitrile at Ni(II) by employing a base (KO^tBu) generates cyanomethyl nucleophile *in-situ*. In Chapter 4, we reported the formation of acrylonitrile

and acrylamide *via* coupling of this nucleophilic cyanomethyl group with electrophilic carbonyl moiety of an aldehyde. The Chapter 5 involves the synthesis of *nido*-bis(7,8-carborane)pyridine ligand, and its corresponding Ru-metallacarborane complex.

In addition to Ni(II) pincer complex of 2,6-bis(*ortho*-carborane)pyridine ligand, we synthesized cyclometalated Ru(II) complex with chelating (*ortho*-carboranyl)pyridine ligand. We explored this complex as an efficient catalyst for transfer hydrogenation of a wide range of ketones by employing *i*PrOH as the hydrogen donor, and the details of these finding is described in Chapter 6. Finally, we synthesized an unusual distorted square planar complex of Ni(II) bearing two chelating (*ortho*-carboranyl)pyridine ligands which is described in Chapter 7.

REFERENCES

1. Severin, K. *Curr. Org. Chem.* **2006**, *10*, 217.
2. Parrott, M. C.; Valliant, J. F.; Adronov, A. *Langmuir* **2006**, *22*, 5251.
3. Larsen, A. S.; Holbrey, J. D.; Tham, F. S.; Reed, C. A. *J. Am. Chem. Soc.* **2000**, *122*, 7264.
4. Wedge, T. J.; Hawthorne, M. F. *Coord. Chem. Rev.* **2003**, *240*, 111.
5. Soloway, A. H.; Tjarks, W.; Barnum, B. A.; Rong, F. G.; Barth, R. F.; Codogni, I. M.; Wilson, J. G. *Chem. Rev.* **1998**, *98*, 1515.
6. Watson-Clark, R. A.; Banquerigo, M. L.; Shelly, K.; Hawthorne, M. F.; Brahn, E. *Proc. Natl. Acad. Sci. U. S. A.* **1998**, *95*, 2531.
7. Fujii, S.; Goto, T.; Ohta, K.; Hashimoto, Y.; Suzuki, T.; Ohta, S.; Endo, Y. *J. Med. Chem.* **2005**, *48*, 4654.
8. Núñez, R.; Tarrés, M.; Ferrer-Ugalde, A.; de Biani, F. F.; Teixidor, F. *Chem. Rev.* **2016**, *116*, 14307.
9. Bohn, R. K.; Bohn, M. D. *Inorg. Chem.* **1971**, *10*, 350.
10. Scholz, M.; Hey-Hawkins, E. *Chem. Rev.* **2011**, *111*, 7035.
11. Hermansson, K.; Wójcik, M.; Sjöberg, S. O-, *Inorg. Chem.* **1999**, *38*, 6039.
12. Fabre, B.; Clark, J. C.; Vicente, M. G. H. *Macromolecules.* **2006**, *39*, 112.
13. Karnahl, M.; Tschierlei, S.; Erdem, Ö. F.; Pullen, S.; Santoni, M.-P.; Reijerse, E. J.; Lubitz, W.; Mixed-Valence, O. S. [Feifeii] *Dalton Trans.* **2012**, *41*, 12468.
14. Kalinin, V.; Ol'shevskaya, V. *Russ. Chem. Bull.* **2008**, *57*, 815.

15. Spokoyny, A. M.; Lewis, C. D.; Teverovskiy, G.; Buchwald, S. L. *Organometallics*. **2012**, *31*, 8478.
16. Schleyer, P. v. R.; Najafian, K. *Inorg. Chem.* **1998**, *37*, 3454.
17. Lesnikowski, Z. J. *Collect. Czech. Chem. Commun.* **2007**, *72*, 1646.
18. Axtell, J. C.; Kirlikovali, K. O.; Djurovich, P. I.; Jung, D.; Nguyen, V. T.; Munekiyo, B.; Royappa, A. T.; Rheingold, A. L.; Spokoyny, A. M. *J. Am. Chem. Soc.* **2016**, *138*, 15758.
19. Anderson, K. P.; Mills, H. A.; Mao, C.; Kirlikovali, K. O.; Axtell, J. C.; Rheingold, A. L.; Spokoyny, A. M. *Tetrahedron*. **2019**, *75*, 187.
20. Wang, H.; Chan, H.-S.; Okuda, J.; Xie, Z. *Organometallics*. **2005**, *24*, 3118.
21. Zi, G.; Li, H., -W.; Xie, Z. *Organometallics*. **2002**, *21*, 3850.
22. Shen, H.; Xie, Z. *Chem. Commun.* **2009**, 2431.
23. Qiu, Z.; Ren, S.; Xie, Z. *Acc Chem Res*. **2011**, *44*, 2999.
24. Qiu, Z.; Deng, L.; Chan, H.-S.; Xie, Z. *Organometallics*. **2010**, *29*, 4541.
25. Deng, L.; Chan, H.-S.; Xie, Z. *J. Am. Chem. Soc.* **2006**, *128*, 7728.
26. Ren, S.; Qiu, Z.; Xie, Z. *Angew. Chem. Int. Ed.* **2012**, *51*, 1010.
27. Wang, S. R.; Qiu, Z.; Xie, Z. *J. Am. Chem. Soc.* **2011**, *133*, 5760.
28. Zhao, D.; Zhang, J.; Xie, Z. *Angew. Chem.-Int. Ed.* **2014**, *53*, 12902.
29. Zhao, D.; Zhang, J.; Xie, Z. *J. Am. Chem. Soc.* **2015**, *137*, 13938.
30. Guo, S.- T.; Cui, P-, F.; Gao, Y.; Jin. G-, X. *Dalton Trans.* **2018**, *47*, 13641.
31. Islam, M. J.; Smith, M. D.; Peryshkov, D. V. *J. Organomet. Chem.* **2018**, *867*, 208.
32. Qiu, Z. *Tetrahedron Lett.* **2015**, *56*, 963.

33. Harder, R. A.; MacBride, J. A. H.; Rivers, G. P.; Yufit, D. S.; Goeta, A. E.; Howard, J. A. K.; Wade, K.; Fox, M. A. *Tetrahedron*. **2014**, *70*, 5182.
34. Bae, H. J.; Kim, H.; Lee, K. M.; Kim, T.; Eo, M.; Lee, Y. S.; Do, Y.; Lee, M. H. *Dalton Trans.* **2013**, *42*, 8549.
35. Holmes, J.; Pask, C. M.; Willans, C. E. *Dalton Trans.* **2016**, *45*, 15818.
36. R. N. Grimes, *Carboranes*, Elsevier, Amsterdam, 2nd edn, 2011.
37. Wiesboeck, R. A.; Hawthorne, M. F. *J. Am. Chem. Soc.* **1964**, *86*, 1642.
38. Hawthorne, M. F.; Young, D. C.; Garrett, P. M.; Owen, D. A.; Schwerin, S. G.; Tebbe, F. N.; Wegner, P. A. *J. Am. Chem. Soc.* **1968**, *90*, 862.
39. Zakharkin, L. I.; Kalinin, V. N. *Tetrahedron Lett.* **1965**, *6*, 407.
40. Tomita, H.; Luu, H.; Onak, T. *Inorg. Chem.* **1991**, *30*, 812.
41. Yoo, J.; Hwang, J. -W.; Do, Y. *Inorg. Chem.* **2001**, *40*, 568.
42. Willans, C. E.; Kilner, C. A.; Fox, M. A. *Chem.—Eur. J.* **2010**, *16*, 10644.
43. Taoda, Y.; Sawabe, T.; Endo, Y.; Yamaguchi, K.; Fujii, S.; Kagechika, H. *Chem. Commun.* **2008**, 2049.
44. Fox M. A.; Wade, K. *J. Organomet. Chem.* **1999**, *573*, 279.
45. Plesek, J. *Chem. Rev.* **1992**, *92*, 269.
46. Grimes, R. N. *Coord. Chem. Rev.* **2000**, 773.
47. Yinghuai, Z.; Carpenter, K.; Bun, C. C.; Bahnmuller, S.; Ke, C. P.; Srid, V. S.; Kee, L. W.; Hawthorne M. F. *Angew. Chem.* **2003**, *115*, 3922.
48. Yoshida, M.; Jordan, R. F. *Organometallics*, **1997**, *16*, 4508.
49. Yoshida, M.; Crowther, D. J.; Jordan, R. F. *Organometallics*, **1997**, *16*, 1349.
50. Tobisu, M.; Kita, Y.; Ano, Y.; Chatani, N. *J. Am. Chem. Soc.* **2008**, *130*, 15982.

51. Crabtree, R. H. *Chem. Rev.* **1985**, *85*, 245.
52. Babón, J. C.; Esteruelas, M. A.; Fernández, I.; López, A. M.; Oñate, E. *Organometallics* **2018**, *37*, 2014.
53. Nakazawa, H.; Itazaki, M.; Kamata, K.; Ueda, K. *Chem. Asian J.* **2007**, *2*, 882.
54. Kou, X.; Zhao, M.; Qiao, X.; Zhu, Y.; Tong, X.; Shen, Z. *Chem. Eur. J.* **2013**, *19*, 16880.
55. Grochowski, M. R.; Morris, J.; Brennessel, W. W.; Jones, W. D. *Organometallics*. **2011**, *30*, 5604.
56. Xu, H. W.; Williard, P. G.; Bernskoetter, W. H. *Organometallics*. **2012**, *31*, 1588.
57. (a) Evans, M. E.; Li, T.; Jones, W. D. *J. Am. Chem. Soc.* **2010**, *132*, 16278. (b) Evans, M. E.; Jones, W. D. *Organometallics*. **2011**, *30*, 3371.
58. (a) Garcia, J. J.; Brunkan, N. M.; Jones, W. D. *J. Am. Chem. Soc.* **2002**, *124*, 9547. (b) Brunkan, N. M.; Brestensky, D. M.; Jones, W. D. *J. Am. Chem. Soc.* **2004**, *126*, 3627. (c) Atesin, T. A.; Li, T.; Lachaize, S.; Brennessel, W. W.; García, J. J.; Jones, W. D. *J. Am. Chem. Soc.* **2007**, *129*, 7562. (d) Schaub, T.; Döring, C.; Radius, U. *Dalton Trans.* **2007**, 1993. (e) Swartz, B. D.; Reinartz, N. M.; Brennessel, W. W.; García, J. J.; Jones, W. D. *J. Am. Chem. Soc.* **2008**, *130*, 8548. (f) Li, T.; García, J. J.; Brennessel, W. W.; Jones, W. D. *Organometallics*. **2010**, *29*, 2430. (g) Fang, X. J.; Yu, P.; Morandi, B. *Science*. **2016**, *351*, 832. (h) Ni, S.-F.; Yang, T.-L.; Dang, L. *Organometallics*. **2017**, *36*, 2746. (i) J. Garcia, J. J.; W. D. *Organometallics*. **2000**, *19*, 5544.
59. Munjanja, L.; Torres-López, C.; Brennessel, W. W.; Jones, W. D. *Organometallics*. **2016**, *35*, 2010.
60. Swartz, B. D.; Brennessel, W. W.; Jones, W. D. *Organometallics*. **2011**, *30*, 1523.

61. Taw, F. L.; Mueller, A. H.; Bergman, R. G.; Brookhart, M. *J. Am. Chem. Soc.* **2003**, *125*, 9808.
62. Esteruelas, M. A.; Oliván, M.; Vélez, A. *J. Am. Chem. Soc.* **2015**, *137*, 12321.
63. (a) Marlin, D. S.; Olmstead, M. M.; Mascharak, P. K. *Angew. Chem. Int. Ed.* **2001**, *40*, 4752. (b) Lu, T.; Zhuang, X.; Li, Y.; Chen, S. *J. Am. Chem. Soc.* **2004**, *126*, 4760. (c) Yang, L.-Z.; Li, Y.; Zhuang, X.-M.; Jiang, L.; Chen, J.-M.; Luck, R. L.; Lu, T.-B. *Chem. Eur. J.* **2009**, *15*, 12399. (d) Jin, J.; Wen, Q.; Lu, P.; Wang, Y. *Chem. Commun.* **2012**, *48*, 9933. (e) Zhu, Y.; Li, L.; Shen, Z. *Chem. Eur. J.* **2015**, *21*, 13246.
64. Patra, T.; Agasti, S.; Akanksha.; Maiti, D. *Chem. Commun.* **2013**, *49*, 69.
65. Patra, T.; Agasti, S.; Modak, A.; Maiti, D. *Chem. Commun.* **2013**, *49*, 8362.
66. Zhang, J.-S.; Chen, T.; Yanga, J.; Han, L.-B. *Chem. Commun.* **2015**, *51*, 7540.
67. Kumagai, N.; Matsunaga, S.; Shibasaki, M. *J. Am. Chem. Soc.* **2004**, *126*, 13632.
68. Suto, Y.; Kumagai, N.; Matsunaga, S.; Kanai, M.; Shibasaki, M. *Org. Lett.* **2003**, *5*, 3147.
69. Kisanga, P.; McLeod, D.; D'Sa, B.; Verkade, J. *J. Org. Chem.* **1999**, *64*, 3090.
70. a) Kamal, A.; Khanna, G. B. R.; Ramu, R. *Tetrahedron: Asymmetry* **2002**, *13*, 2039.; b) Fukuda, Y.; Okamoto, Y.; *Tetrahedron* **2002**, *58*, 2513.; c) Kamila, S.; Zhu, D.; Biehl, E. R.; Hua, L. *Org. Lett.* **2006**, *8*, 4429.; d) Ankati, H.; Zhu, D.; Yang, Y.; Biehl, E. R.; Hua, L. *J. Org. Chem.* **2009**, *74*, 1658.
71. Chakraborty, S.; Patel, Y. J.; Krause, J. A.; Guan, H. *Angew. Chem. Int. Ed.* **2013**, *52*, 7523.
72. Fan, L.; Ozerov, O. V. *Chem. Commun.* **2005**, 4450.

73. Anslyn, E. V.; Dougherty, D. A. *Modern Physical Organic Chemistry*; University Science Books: Sausalito, CA, 2006.
74. Smith, J. B.; Miller, A. J. M. *Organometallics* **2015**, *34*, 4669.
75. a) Gladiali, S.; Alberico, E. *Chem. Soc. Rev.* **2006**, *35*, 226; b) Samec, J. S. M.; BGckvall, J.-E.; Andersson, P. G.; Brandt, P. *Chem. Soc. Rev.* **2006**, *35*, 237; c) Clapham, S. E.; Hadzovic, A.; Morris, R. H. *Coord. Chem. Rev.* **2004**, *248*, 2201.
76. Cervený, L. Ed. *Catalytic Hydrogenation*; Elsevier: Amsterdam, 1986.
77. de Vries, J. G., Elsevier, C. J. Eds. *The Handbook of Homogeneous Hydrogenation*; Wiley-VCH: Weinheim, 2007.
78. Andersson, P. G., Munslow, I. J. Eds. *Modern Reduction Methods*; Wiley-VCH Verlag GmbH & Co. KGaA: Weinheim, 2008.
79. Wang, D.; Astruc, D. *Chem. Rev.* **2015**, *115*, 6621.
80. Strassberger, Z.; Mooijman, M.; Ruijter, E.; Alberts, A. H.; de Graaff, C.; Orru, R. V. A.; Rothenberg, G. *Appl. Organometal. Chem.* **2010**, *24*, 142.
81. Monney, A.; Venkatachalam, G.; Albrecht, M. *Dalton Trans.* **2011**, *40*, 2716.
82. Akta, A.; Gök, Y. *Transition Met. Chem.* **2014**, *39*, 925.
83. Yasar, S.; Çekirdek, S.; Özdemir, I. *J. Coord. Chem.* **2014**, *67*, 1236.
84. DePasquale, J.; White, N. J.; Ennis, E. J.; Zeller, M.; Foley, J. P.; Papish, E. T. *Polyhedron* **2013**, *58*, 162.
85. Wdowik, T.; Samojłowicz, C.; Jawiczuk, M.; Malińska, M.; Woźniak, K.; Grela, K. *Chem. Commun.* **2013**, *49*, 674.
86. Yigit, B.; Yigit, M.; Özdemir, I.; Çetinkaya, E. *Transition Met. Chem.* **2012**, *37*, 297.
87. Witt, J.; Pöthig, A.; Kühn, F. E.; Baratta, W. *Organometallics* **2013**, *32*, 4042.

88. Aktas, A.; Gok, Y. *Catal. Lett.* **2015**, *145*, 631.
89. Dragutan, V.; Dragutan, I.; Delaude, L.; Demonceau, A. *Coord. Chem. Rev.* **2007**, *251*, 765.
90. Enthaler, S.; Jackstell, R.; Hagemann, B.; Junge, K.; Erre, G.; Beller, M. *J. Organomet. Chem.* **2006**, *691*, 4652.
91. Danopoulos, A. A.; Winston, S.; Motherwell, W. B. *Chem. Commun.* **2002**, 1376.
92. Poyatos, M.; Mata, J. A.; Falomir, E.; Crabtree, R. H.; Peris, E. *Organometallics* **2003**, *22*, 1110.
93. Zeng, F.; Yu, Z. *Organometallics* **2008**, *27*, 6025.
94. Illam, P. M.; Donthireddy, S. N. R.; Chakrabartty, S.; Rit, A. *Organometallics* **2019**, *38*, 2610.
95. Grimes, R. N. *Dalton Trans.* **2015**, *44*, 5939.

Chapter 2

Sterically Encumbered Dianionic Dicarboranyl Pincer Ligand

$(C_5H_3N)(C_2B_{10}H_{11})_2$ and its CNC Nickel (II) Complex¹

¹ Islam, M. J.; Smith, M. D.; Peryshkov, D. V. *J. Organomet. Chem.* **2018**, 867, 208.

Reprinted here with permission of publisher.

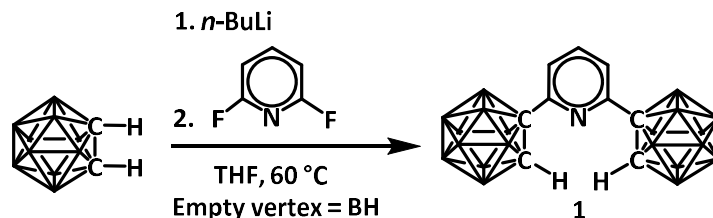
2.1 INTRODUCTION

Pincer-type frameworks, which are tridentate ligands that enforce meridional coordination to a metal center, attracted significant attention in last 20 years.¹ Pincer complexes of transition metals often exhibit a favorable combination of both stability and reactivity, which made them invaluable for fundamental studies of reaction mechanisms and for catalysis. As originally devised by Moulton and Shaw, pincer ligands contain an anionic carbon center between two pendant phosphine donors “arms”.² This arrangement type has been broadened to include other monoanionic moieties with two neutral sterically hindered arms and it is the most studied subclass of pincer ligands.³ Related dianionic and trianionic pincer-type ligands and their complexes with both early and late transition metals have recently attracted increased attention.⁴⁻⁸

Icosahedral boron clusters, such as neutral *closo*-carboranes $C_2B_{10}H_{12}$ and their monoanionic counterparts $CB_{11}H_{12}^-$ possess an unusual delocalized electronic structure as well as an extreme steric hindrance profile that make them interesting building blocks in ligand design, catalysis, polymer and material chemistry.⁹⁻¹⁶ Carboranes have been used as auxiliary groups attached to phosphines, amines, amides, cyclopentadienyls, and heterocyclic carbene systems.¹⁷⁻²³

A number of tridentate complexes containing carboranes has recently emerged.²⁴⁻²⁷ The utilization of the pincer-type geometry with boron cages serving as central “backbones” allowed, for example, an isolation of an unusual three-membered (BB)>Ru carboryne metalacycle²⁸ as well as a development of an efficient, water-tolerant Pd-based catalyst for Suzuki coupling reactions²⁶ and an air-tolerant Ru-based catalyst for alkane transfer dehydrogenation.²⁹

In general, carborane clusters can be exohedrally metalated at carbon or boron vertices. The C–H bonds of carboranes are relatively acidic ($pK_a = 22$ for *ortho*-carborane), and these C atoms can be lithiated and subsequently transmetalated by transition metal salt metathesis.³⁰⁻³⁵ In contrast, unsupported metal-boron bonds of carboranes are rare.³⁶⁻³⁹ However, there are numerous examples of successful metalation of carborane B–H bonds, primarily by late transition metals, with the use of donor directing groups attached to the cage. These cyclometalated products are intermediates in direct selective B–H bond functionalization of boron clusters and often are isolable.⁴⁰⁻⁴⁶



Scheme 2.1: Synthesis of 2,6-bis(*ortho*-carborane)pyridine (C_5H_3N)($C_2B_{10}H_{11}$)₂ (**1**).

In this contribution, we report the synthesis of the novel type of the chelating pincer ligand precursor containing two sterically hindered icosahedral carborane cages as “arms” and a pyridine “backbone”. Deprotonation of C–H bonds of both carborane clusters afforded a dianionic ligand that was successfully metalated to yield a nickel(II) complex.

2.2 RESULTS AND DISCUSSION

The use of carborane clusters as “arms” of a pincer ligand prompts the use of a neutral donor as a central “backbone”. The rigidity of the target pincer ligand was an important consideration, therefore, we chose not to use carborane picolyl derivatives where a boron cluster is connected to a pyridine ring through the methylene linker.⁴⁷⁻⁴⁹

Instead, we elected to use a rigid planar pyridine fragment as its direct functionalization with two carborane cages in 2- and 6- positions would lead to meridional geometry of the target ligand. Several synthetic routes to carboranyl pyridines have been reported in literature, including reactions of decaborane and pyridyl acetylenes and copper-promoted coupling of 2-bromopyridine and lithiated carborane.⁵⁰⁻⁵² These synthetic methods, while successful, have been plagued by relatively low yields. Recently, a simpler alternative method, involving nucleophilic aromatic substitution of 2-fluoropyridine by lithiated carborane, has been developed.⁵³ Notably, all these previously reported synthetic routes led to pyridine derivatives containing one carborane cage. We surmised that the S_NAr reaction of 2,6-difluoropyridine with two equivalents of lithiated carborane would lead to efficient formation of the dicarboranyl pyridine. Gratifyingly, heating the mixture of 2,6-difluoropyridine with LiC₂B₁₀H₁₁ in THF at 80°C under nitrogen atmosphere overnight led, after aqueous workup and extraction to dichloromethane, to the target 2,6-dicarboranyl pyridine (C₅H₃N)(C₂B₁₀H₁₁)₂ (**1**) (**Scheme 2.1**). The product was characterized by the array of multinuclear NMR spectrometry techniques, mass-spectrometry, and the single crystal X-ray diffraction. The ¹¹B and ¹¹B{¹H} NMR spectra of **1** exhibited a set partially overlapping signals in the range from -2.6 to -13.1 ppm. The ¹H NMR resonance corresponding to the remaining C-H bond of the carborane cage was found at 4.49 ppm in CDCl₃, which is shifted downfield in comparison with the related signal of the starting C₂B₁₀H₁₂ cluster at 3.56 ppm.

Single crystals of **1** were grown from dichloromethane/hexanes solvent mixture by slow evaporation on air. The structure determination confirmed the expected geometry of the proligand with crystallographically-required C₂ and idealized C_{2v} symmetry

(**Figure 2.1**). The central pyridine fragment is connected to carborane cages through unstrained bonds with the C2–C3 bond length of 1.496(3) Å, the N1–C3–C2 angle of 116.6(2)° and the C3–C2–C1 angle of 117.5(2)°. The C1–C2 bond in the carborane cluster is 1.629(2) Å. The separation between two boron cages is substantial as indicated by the C1····C1A distance of 4.554(3) Å.

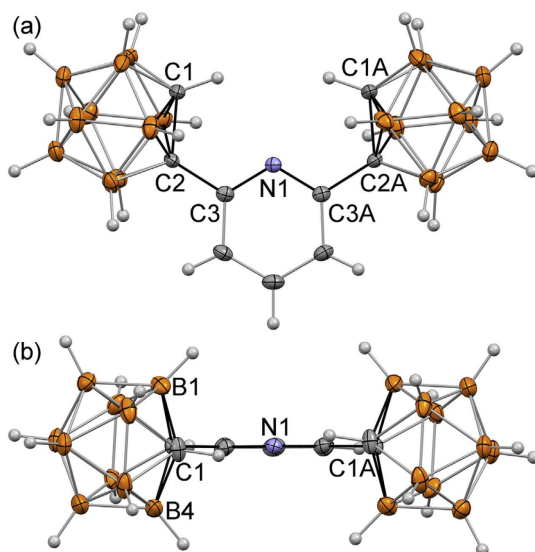
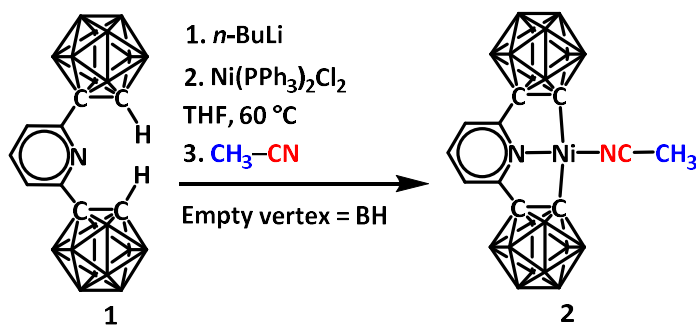


Figure 2.1: Displacement ellipsoid plot (50 % probability) of the proligand $(C_5H_3N)(C_2B_{10}H_{11})_2$ (**1**). (a): a view perpendicular to the (C3–N1–C3A) plane (b): a view along the (C3–N1–C3A) plane.

Interestingly, the molecular structure of **1** in the solid state revealed a conformation that features C–H bonds of carborane clusters pointing inwards the cavity of the ligand, in other words, towards the nitrogen atom of the pyridine ring. This arrangement is likely stabilized by the intramolecular C–H···N hydrogen bonding which has been found in the related 2–carboranylpyridine.⁵⁴ Similarly, existence of relatively strong hydrogen bonds between aryl C–H bonds and nitrogen atoms of pyridines have been demonstrated.⁵⁵

The ligand precursor **1** possesses two relatively acidic C–H bonds on two carborane cages. Deprotonation of the ligand was done using 2.1 equiv *n*-BuLi in THF at room temperature. The lithiated ligand was not isolated but used *in-situ* in the reaction with 1.1 equivalent of Ni(PPh₃)₂Cl₂ at 60 °C for 6 h (**Scheme 2.2**). The target complex {(C₅H₃N)(C₂B₁₀H₁₀)₂}Ni(CH₃CN) (**2**) was isolated as a yellow powder.



Scheme 2.2: Synthesis of {(C₅H₃N)(C₂B₁₀H₁₀)₂}Ni(CH₃CN) (**2**).

Single crystals of **2**·C₆H₆ were grown from benzene by slow evaporation. The structure determination revealed the expected square-planar geometry around the nickel center that is coordinated to two carboranyl arms through carbon atoms, the pyridine ring, and acetonitrile. The complex adopted crystallographically required C_{2v} symmetry, however, elongated displacement ellipsoids of boron atoms suggested mild cluster disorder through their displacement from the mirror plane. The Ni1–C1 bond length in **2** is 1.929(2) Å. This value is within the typical range for nickel C–carboranyl compounds (1.880(6)–2.01(1) Å).⁵⁶ The Ni1–N2(C₆H₃) bond length is 1.882(2) Å and the Ni1–N2(CCH₃) bond length is 1.841(2) Å. The C2≡N6 bond length of the coordinated acetonitrile ligand is 1.134(5) Å. The coordination of the metal center led to the increased strain of the complex which is indicated by the decreased intraligand angles N1–C3–C2 (113.4(2)°) and C3–C2–C1 (110.6(2)°). This is also manifested in the decreased

separation between boron cages in **2** with the C1...C1A distance of 3.853(3) Å. The C1–Ni1–C1A bite angle is close to linearity at 173.7(1)°.

The diamagnetic complex **2** was characterized by ^1H , ^{13}C , and ^{11}B NMR, and FTIR spectroscopies. The FTIR spectrum of the solid sample exhibited characteristic absorption bands $\nu(\text{B–H})$ at 2586 cm^{-1} as well as $\nu(\text{C}\equiv\text{N})$ at 2332 cm^{-1} . The ^{11}B NMR spectrum contained a set of partially overlapping signals in the range from -3.4 ppm to -11.3 ppm (**Figure 2.2**).

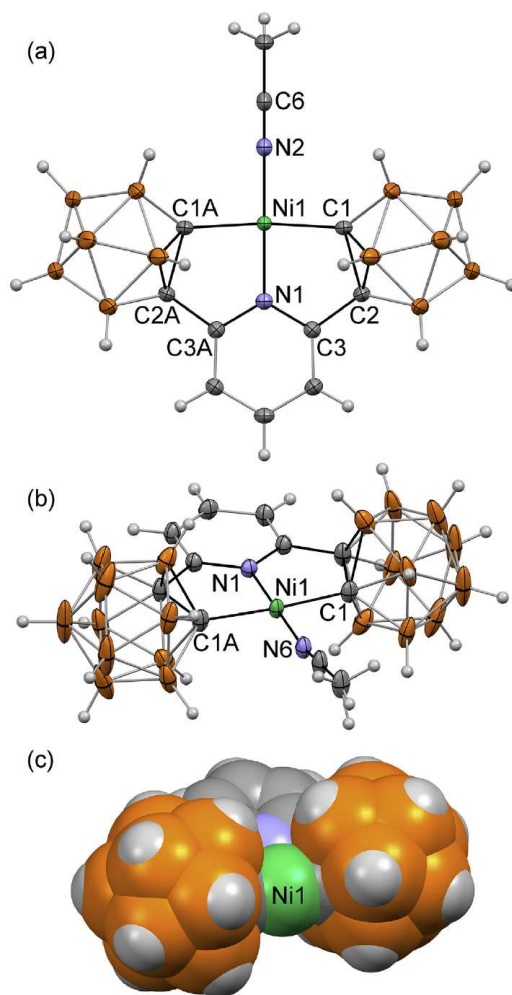


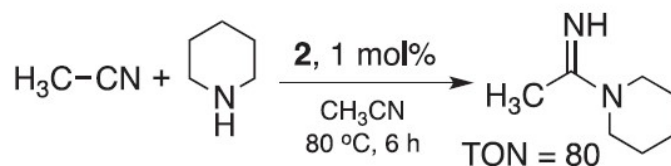
Figure 2.2: Displacement ellipsoid plot (50 % probability) of the $\{(\text{C}_5\text{H}_3\text{N})(\text{C}_2\text{B}_{10}\text{H}_{10})_2\}\text{Ni}(\text{CH}_3\text{CN})$ complex (**2**). **(a)**: a view perpendicular to the (C3–N1–Ni1–C3A) plane **(b)**: a general view **(c)**: space-filling diagram of **2** with the acetonitrile ligand omitted.

Carborane clusters as ligands exert an unusually high degree of steric hindrance due to their icosahedral shape. For example, each of the metal-carbon bonds in **2** is surrounded by five neighboring cluster atoms. A space-filling diagram of the complex **2** with acetonitrile ligand omitted is shown in **Figure 2.2 (c)** to highlight steric requirements of 2,6-bis(carborane)pyridine. Ligand buried volume ($\% V_{\text{bur}}$) has been recently introduced as a quantitative descriptor of steric congestion around the metal center.⁵⁷ We found that the $(\text{C}_5\text{H}_3\text{N})(\text{C}_2\text{B}_{10}\text{H}_{10})_2$ ligand in the complex **2** exhibited a high value of $\% V_{\text{bur}} = 70.6 \%$, which indicates a high degree of steric hindrance imposed by the dicarboranyl pincer ligand. This value can be compared to that for the recently reported complex of gold featuring two anionic carborane $\{\text{CB}_{11}\}$ cages connected to the *N*-heterocyclic carbene backbone.⁵⁸ The presence of five-membered ring NHC backbone as well as two weakly coordinating anionic boron cages in that complex have resulted in the value of $\% V_{\text{bur}}$ of 47.2 %. The neutral $(\text{C}_5\text{H}_3\text{N})(\text{C}_2\text{B}_{10}\text{H}_{10})_2$ ligand reported herein is pyridine-based, which enforces two neutral $\{\text{C}_2\text{B}_{10}\}$ carborane cages closer to each other leading to the coordination to the metal center and the increase in $\% V_{\text{bur}}$.

The electron density distribution in the carborane cluster is not uniform and gives rise to significant differences in the electronic effects of the carborane cage on an exohedral substituent when attached to either carbon or boron atoms.⁵⁹ A carborane cluster is usually regarded as an electron-withdrawing group when it is bound through its carbon atom.⁶⁰ The high value of the $\nu(\text{CN})$ in **2** indicates the electron-deficient environment of the nitrile group which is likely due to coordination to relatively electron-poor *C*-carboranyl bound metal center. A significant positive charge on the carbon atom of the nitrile group would assist a nucleophilic attack, for example, by an amine. Notably,

there have been reports of cationic nickel(II) complexes catalyzing hydroamination of nitriles *via* an outer-sphere mechanism.^{61,62}

We found that the complex **2** efficiently catalyzes the addition of piperidine to acetonitrile with the formation of the amidine $\text{HN}=\text{C}(\text{CH}_3)\text{NC}_5\text{H}_{10}$. In a typical reaction, a mixture of piperidine and acetonitrile containing **2** (1 mol % relative to the amount of piperidine) was heated at 80 °C for 6 h (**Scheme 2.3**). A relatively high value of the turnover number (TON = 80) was observed, thus demonstrating that the complex **2** is a competent catalyst of this reaction.



Scheme 2.3: Addition of piperidine to acetonitrile promoted by **2**. The catalyst loading was 1 mol % relative to the amount of piperidine. Acetonitrile served as both the reagent and the solvent.

2.3 CONCLUSION

The novel pincer ligand framework containing two carborane clusters and a central pyridine backbone was synthesized. The CNC-type pincer complex 2,6-bis(carboranyl)pyridine nickel(II)(acetonitrile) was prepared in the reaction of the lithiated ligand $\text{Li}_2(\text{C}_5\text{H}_3\text{N})(\text{C}_2\text{B}_{10}\text{H}_{10})_2$ and $\text{Ni}(\text{PPh}_3)_2\text{Cl}_2$. The molecular structure of the nickel complex featured high degree of steric hindrance imposed by coordination of two icosahedral carborane clusters. The title complex was found to be a competent catalyst for hydroamination of acetonitrile with piperidine.

2.4 EXPERIMENTAL SECTION

All synthetic manipulations, unless stated otherwise, were carried out either in a nitrogen-filled VAC drybox or on a dual manifold Schlenk-style vacuum line.⁶³ The solvents were sparged with nitrogen, passed through activated alumina, and stored over activated 4 Å Linde-type molecular sieves. CD₂Cl₂, CDCl₃, and (CD₃)₂SO were degassed and stored over activated 4 Å Linde-type molecular sieves. NMR spectra were recorded using Varian spectrometers at 400 (¹H), 100 (¹³C), 128 (¹¹B) MHz, reported in δ (parts per million) and referenced to the residual ¹H/¹³C signals of the deuterated solvent or an external BF₃(Et₂O) (¹¹B(δ): 0.0 ppm) standard.

2.4.1 Synthesis of 2,6-bis(carborane)pyridine (C₅H₃N)(C₂B₁₀H₁₁)₂ (1)

A solution of *n*-butyllithium in hexanes (1.6 M, 3.5 mL, 5.6 mmol) was added to a solution of *ortho*-carborane (400 mg, 2.77 mmol) in 10 mL of anhydrous tetrahydrofuran at room temperature under nitrogen atmosphere. The mixture was stirred at room temperature for 12 h. 2,6-difluoropyridine (0.13 mL, 1.43 mmol) was added to the reaction mixture and stirred at 60 °C for 6 h, after which time tetrahydrofuran was removed under vacuum. Dichloromethane (50 mL) and water (50 mL) were added, and products were extracted to the organic layer. The organic portion was passed through a silica gel column using dichloromethane as an eluent. Volatiles were removed under vacuum and the unreacted *ortho*-carborane was sublimed out to obtain pure 2,6-bis(carborane)pyridine with 28% yield (140 mg, 0.385 mmol).

¹H NMR (CDCl₃): δ 7.78 (t, 1H, C₅H₃N), 7.63 (d, 2H, C₅H₃N), 4.49 (s, 2H, (C–H, C₂B₁₀H₁₁), 3.10–1.50 (overlapping, 20H, B–H, C₂B₁₀H₁₁). ¹¹B{¹H} NMR (CDCl₃): δ -2.6, -3.4, -8.3, -11.4, -13.1 (br). ¹³C NMR (CDCl₃): δ 150.5 (C₅H₃N),

139.2 (C_5H_3N), 122.8 (C_5H_3N), 74.0 (C–C, $C_2B_{10}H_{11}$), 56.6 (C–H, $C_2B_{10}H_{11}$). Calcd for $C_9H_{27}B_{20}N$: C, 29.57; H, 7.45; N, 3.83. Found: C, 29.38; H, 7.11, N, 3.61.

2.4.2 Synthesis of 2,6-bis(carboranyl)pyridine nickel(II)(acetonitrile) complex $\{(C_5H_3N)(C_2B_{10}H_{10})_2\}Ni(CH_3CN)$ (2)

A solution of *n*-butyllithium in hexanes (1.6 M, 0.72 mL, 1.16 mmol) was added to a solution of 2,6-bis(carborane)pyridine (200 mg, 0.55 mmol) in 10 mL of dry tetrahydrofuran at room temperature under nitrogen. The mixture was stirred at room temperature for 12 h. Bis(triphenylphosphine)nickel(II) dichloride (395.77 mg, 0.61 mmol) was added and the mixture was stirred at 60 °C for 6 h, after which time volatiles were removed under vacuum. Hydrochloric acid (3 M, 20 mL) and acetonitrile (20 mL) were added. The mixture was filtered and the resulting precipitate was washed with hexanes (10 mL) and diethyl ether (10 mL) to obtain 2,6-bis(carboranyl)pyridine nickel(II)(acetonitrile) complex as a yellow powder (89 mg, 0.19 mmol, 35% yield).

1H NMR (CD_2Cl_2): δ 7.79 (t, 1H, C_5H_3N), 7.22 (δ , 2H, C_5H_3N), 3.50–1.20 (overlapping, B–H, $C_2B_{10}H_{10}$), 2.38 (s, 3H, CH_3CN). $^{11}B\{^1H\}$ NMR (CD_2Cl_2): δ –3.4, –6.7, –7.5, –11.3. ^{13}C NMR ($(CD_3)_2SO$): δ 159.7 (C_5H_3N), 143.1 (C_5H_3N), 122.3 (C_5H_3N), 118.7 (CH_3CN), 79.7 ($C_2H_{11}B_{10}$), 71.9 ($C_2H_{11}B_{10}$), 1.7 (CH_3CN). Calcd for $C_{11}H_{26}B_{20}N_2Ni$: C, 28.64; H, 5.68; N, 6.07 Found: C, 28.71; H, 5.80, N, 5.72.

2.4.3 Hydroamination of acetonitrile promoted by 2

Piperidine (0.1 mL, 1.0 mmol) was added to a solution of 2,6-bis(carboranyl)pyridine nickel(II)(acetonitrile) complex (2) (4.62 mg, 0.01 mmol) in 5 mL of acetonitrile and the reaction mixture was stirred at 80 °C for 6 h. A solution of naphthalene (12.82 mg, 1.0 mmol) in 10 mL of ether was added to the mixture as an

internal ^1H NMR spectroscopy standard. The volatiles were removed under vacuum at room temperature. The turnover number (TON = 80) was determined by integration of signals corresponding to the imine product relative to signals of the internal standard (naphthalene) in the ^1H NMR spectrum of the reaction mixture.

2.4.4 Crystal Structure Determination Details

The calculations of the buried volume $\%V_{\text{bur}}$ were carried out for the atomic coordinates from the crystal structure of **2** using SambVca2 program (<https://www.molnac.unisa.it/OMtools/sambvca2.0/>)⁵⁷ with the following (default) parameters: sphere radius 3.5 Å, distance from the center of the sphere: 2.1 Å, mesh spacing: 0.05 Å, H atoms not included, and Bondi radii scaled by 1.17.

X-ray intensity data from a colorless, almond-shaped plate were collected at 100(2) K using a Bruker D8 QUEST diffractometer equipped with a PHOTON-100 CMOS area detector and an Incoatec microfocus source (Mo $K\alpha$ radiation, $\lambda = 0.71073$ Å). The raw area detector data frames were reduced and corrected for absorption effects using the Bruker APEX3, SAINT+ and SADABS programs.⁶⁴⁻⁶⁶ Final unit cell parameters were determined by least-squares refinement of large sets of reflections from the data sets. The structure was solved with SHELXT.^{67,68} Subsequent difference Fourier calculations and full-matrix least-squares refinement against F^2 were performed with SHELXL-2016 using OLEX2.⁶⁹

2.4.4.1 Crystal structure determination of $(\text{C}_5\text{H}_3\text{N})(\text{C}_2\text{B}_{10}\text{H}_{11})_2$ (**1**)

The compound crystallized in the tetragonal system. The pattern of systematic absences in the intensity data was consistent with the space groups $I-42d$ and $I4_1md$. Space group $I-42d$ (No. 122) was confirmed by structure solution. The asymmetric unit

consists of half of one molecule, which is located on a crystallographic twofold axis of rotation. All non-hydrogen atoms were refined with anisotropic displacement parameters. All hydrogen atoms were located in Fourier difference maps and refined freely, resulting in normal bond distances and displacement parameters. The largest residual electron density peak in the final difference map is $0.23 \text{ e } \text{\AA}^{-3}$, located 0.72 \AA from C1. Because of the absence of heavy atoms in the crystal, the absolute structure could not be determined.

Crystal Data for $\text{C}_9\text{H}_{25}\text{B}_{20}\text{N}$ (CCDC 1583707): tetragonal, space group I-42d (no. 122), $a = 14.9477(5) \text{ \AA}$, $c = 19.0491(7) \text{ \AA}$, $V = 4256.2(3) \text{ \AA}^3$, $Z = 8$, $T = 100(2) \text{ K}$, $\mu(\text{MoK}\alpha) = 0.051 \text{ mm}^{-1}$, $M = 363.50 \text{ g/mol}$, $D_{\text{calc}} = 1.135 \text{ g/cm}^3$, 47566 reflections measured ($5.45^\circ \leq 2\Theta \leq 52.806^\circ$), 2188 unique ($R_{\text{int}} = 0.0700$, $R_{\text{sigma}} = 0.0185$) which were used in all calculations. The final R_1 was 0.0401 ($I > 2\sigma(I)$) and wR_2 was 0.1047 (all data).

2.4.4.2 Crystal structure determination of $\{(\text{C}_5\text{H}_3\text{N})(\text{C}_2\text{B}_{10}\text{H}_{10})_2\}\text{Ni}(\text{CH}_3\text{CN})(\text{C}_6\text{H}_6)_2$ ($2 \cdot (\text{C}_6\text{H}_6)_2$)

The compound crystallized in the orthorhombic system. The pattern of systematic absences in the intensity data was consistent with the space groups *Imma* and *Ima2*. The centrosymmetric group *Imma* was eventually confirmed as the best description of the structure. The asymmetric unit consists of $\frac{1}{4}$ of one Ni complex with crystallographic mm (C_{2v}) point symmetry, and half of one benzene molecule located on a mirror plane. Atoms Ni1, N1, C5, N2, C1, C2, B5 and B6 are located in the mirror plane perpendicular to the crystallographic *a* axis; Ni1, N1, C5, N2, C6 and C7 are also located in the mirror perpendicular to the *b* axis. The carbon and hydrogen atoms of the acetonitrile ligand (C6

and C7) are disordered across the mirror perpendicular to the a axis and were refined with half-occupancy. The benzene solvent guest disorder consists of two independent half-benzene molecules per asymmetric unit, both located on the mirror plane perpendicular to the b axis. All nonhydrogen atoms were refined with anisotropic displacement parameters.

The anisotropic displacement parameters (*adps*) of the disordered benzene carbon atoms were restrained to be approximately spherical using an ISOR restraint. Some elongated *adps* for boron atoms in the carborane cage (e.g. $U_3/U_1 = 11.4$ for B6) suggest some atoms in the cage part of the structure are displaced away from the mirror plane bisecting the cage. A refinement in space group *Ima2*, which still retains this mirror plane, also showed strongly prolate boron *adps* and was unstable. Refinements in lower space groups without mirror symmetry (e.g. *I212121*) also gave highly prolate boron ellipsoids and unstable refinements. Disorder modeling in *Imma* of the carborane cage part was not successful owing to the small displacements of the B atoms from their average positions. The best refinement was therefore judged to be in space group *Imma* with prolate boron ellipsoids suggesting mild cage disorder. Hydrogen atoms bonded to carbon were placed in geometrically idealized positions and included as riding atoms with $d(\text{C-H}) = 0.95 \text{ \AA}$ and $U_{\text{iso}}(\text{H}) = 1.2U_{\text{eq}}(\text{C})$ for aromatic hydrogen atoms. The acetonitrile methyl hydrogens were located in a difference map, adjusted to $d(\text{C-H}) = 0.98 \text{ \AA}$ and $U_{\text{iso}}(\text{H}) = 1.5U_{\text{eq}}(\text{C})$ included as riding on C7. Hydrogen atoms bonded to boron atoms were located in difference maps and refined freely. The largest residual electron density peak in the final difference map is 0.28 e \AA^{-3} , located 0.45 \AA from B6.

Crystal Data for $C_{23}H_{38}B_{20}N_2Ni$ (CCDC 1583707): orthorhombic, space group *Imma* (no. 74), $a = 14.4701(8) \text{ \AA}$, $b = 16.2302(8) \text{ \AA}$, $c = 14.0240(7) \text{ \AA}$, $V = 3293.6(3) \text{ \AA}^3$, $Z = 4$, $T = 100(2) \text{ K}$, $\mu(\text{MoK}\alpha) = 0.611 \text{ mm}^{-1}$, $M = 617.46 \text{ g/mol}$, $D_{calc} = 1.245 \text{ g/cm}^3$, 66111 reflections measured ($5.02^\circ \leq 2\Theta \leq 55.472$), 2080 unique ($R_{int} = 0.0390$, $R_{sigma} = 0.0109$) which were used in all calculations. The final R_1 was 0.0309 ($I > 2\sigma(I)$) and wR_2 was 0.0815 (all data).

Acknowledgments

This material is based in part upon work supported by the National Science Foundation under Award CHE-1654301.

REFERENCES

1. van Koten, G.; Gossage R. A. (Eds.), *The Privileged Pincer-metal Platform: Coordination Chemistry & Applications*, first ed., Springer, 2015, 2016 edition.
2. Moulton, C. J.; Shaw, B. L. *J. Chem. Soc. Dalton Trans.* 1976 1020.
3. van Koten, G. *Pure Appl. Chem.* **2009**, *61*, 1681.
4. O'Reilly, M. E.; Veige, A. S. *Chem. Soc. Rev.* **2014**, *43*, 6325.
5. Nguyen, A. I.; Blackmore, K. J.; Carter, S. M.; Zarkesh, R. A.; Heyduk, A. F. *J. Am. Chem. Soc.* **2009**, *131*, 3307.
6. S. Sarkar, S.; McGowan, K. P.; Culver, J. A.; Carlson, A. R.; Koller, J.; Peloquin, A. J.; Veige, M. K.; Abboud, K. A.; Veige, A. S. *Inorg. Chem.* **2010**, *49*, 5143.
7. Sarkar, S.; McGowan, K. P.; Kuppuswamy, S.; Ghiviriga, I.; Abboud, K. A.; Veige, A. S. *J. Am. Chem. Soc.* **2012**, *134*, 4509.
8. Sattler, A.; Parkin, G. *J. Am. Chem. Soc.* **2012**, *134*, 2355.
9. Hawthorne, M. F. *J. Chem. Educ.* **2009**, *86*, 1131.
10. Grimes, R. N. *Dalton Trans.* **2015**, *44*, 5939.
11. Hosmane N. S. (Ed.), *Boron Science: New Technologies and Applications*, 1 edition, CRC Press, Boca Raton. FL, 2011.
12. Grimes, R. N. *Carboranes*, third ed., Academic Press, Amsterdam; Boston, **2016**, 3rd edition.
13. Dash, B. P.; Satapathy, R.; Maguire, J. A.; Hosmane, N. S. *New J. Chem.* **2011**, *35*, 1955.
14. Douvris, C.; Michl, J. *Chem. Rev.* 2013, *113*, PR179.

15. Chen, G.; Yang, J.; Lu, G.; Liu, P. C.; Chen, Q.; Xie, Z.; Wu, C. *Mol. Pharm.* **2014**, *11*, 3291.
16. R. Núñez, R.; Romero, I.; Teixidor, F.; Vinas, C. *Chem. Soc. Rev.* **2016**, *45*, 5147.
17. Popescu, A. R.; Teixidor, F.; Vinas C. *Coord. Chem. Rev.* **2014**, *269*, 54.
18. Yao, Z, -J.; Jin, G. -X. *Coord. Chem. Rev.* **2013**, *257*, 2522.
19. Fey, N.; Haddow, M. F.; Mistry, R.; Norman, N. C.; Orpen, A. G.; Reynolds, T. J.; Pringle, P. G. *Organometallics* **2012**, *31*, 2907.
20. Spokoyny, A. M. Lewis, C. D.; Teverovskiy, G.; Buchwald, S. L. *Organometallics* **2012**, *31*, 8478.
21. El-Hellani, A.; Lavallo, V. *Angew. Chem. Int. Ed.* **2014**, *53*, 4489.
22. Estrada, J.; Lavallo, V. *Angew. Chem. Int. Ed.* **2017**, *56*, 9906.
23. Holmes, J.; Pask, C. M.; Fox, M. A.; Willans, C. E. *Chem. Commun.* **2016**, *52*, 6443.
24. Spokoyny, A. M.; Reuter, M. G.; Stern, C. L.; Ratner, M. A.; Seideman, T.; Mirkin, C. A. *J. Am. Chem. Soc.* **2009**, *131*, 9482.
25. El-Zaria, M. E.; Aarii, H.; Nakamura, H. *Inorg. Chem.* **2011**, *50*, 4149.
26. Tsang, M. Y.; Vinas, C.; Teixidor, F.; Planas, J. G.; Conde, N.; SanMartin, R.; Herrero, M. T.; Domínguez, E.; Lledos, A.; Vidossich, P.; Choquesillo-Lazarte, D. *Inorg. Chem.* **2014**, *53*, 9284.
27. Eleazer, B. J.; Smith, M. D.; Peryshkov, D. V. *Organometallics* **2016**, *35*, 106.
28. Eleazer, B. J.; Smith, M. D.; Popov, A. A.; Peryshkov D. V. *J. Am. Chem. Soc.* **2016**, *138*, 10531.
29. Eleazer, B. J.; Smith, M. D.; Popov, A. A.; Peryshkov D. V. *Chem. Sci.* **2017**, *8*, 5399.

30. Smart, J. C.; Garrett, P. M.; Hawthorne, M. F. *J. Am. Chem. Soc.* **1969**, *91*, 1031.
31. Hawthorne, M. F.; Owen, D. A. *J. Am. Chem. Soc.* **1971**, *93*, 873.
32. Shen, H.; Xie Z. *Chem. Commun.* **2009**, 2431.
33. Qiu, Z.; Xie, Z. *Dalton Trans.* **2014**, *43*, 4925.
34. Riley, L. E.; Chan, A. P. Y.; Taylor, J.; Man, W. Y.; Ellis, D.; Rosair, G. M.; Welch, A. J.; Sivaev, I. B. *Dalton Trans.* **2016**, *45*, 1127.
35. Kirlikovali, K. O.; Axtell, J. C.; Gonzalez, A.; Phung, A. C.; Khan, S. I.; Spokoyny, A. M. *Chem. Sci.* **2016**, *7*, 5132.
36. Hoel, E. L.; Hawthorne, M. F. *J. Am. Chem. Soc.* **1975**, *97*, 6388.
37. Bregadze, V. I.; Usiatinsky, A. Y.; Godovikov, N. N. *J. Organomet. Chem.* **1985**, *292*, 75.
38. Saleh, L. M. A.; Dziedzic, R. M.; Khan, S. I.; Spokoyny, A. M. *Chem. Eur. J.* **2016**, *22*, 8466.
39. Adams, R. D.; Kiprotich, J.; Peryshkov, D. V.; Wong, Y. O. *Chem. Eur. J.* **2016**, *22*, 6501.
40. Yu, W. -B.; Cui, P. -F.; Gao, W. -X.; Jin, G. -X. *Coord. Chem. Rev.* **2017**, *350*, 300.
41. Yao, Z. -J.; Yu, W. -B.; Lin, Y. -J.; Huang, S. -L.; Li, Z.-H.; Jin, G. -X. *J. Am. Chem. Soc.* **2014**, *136*, 2825.
42. Quan, Y.; Xie, Z. *J. Am. Chem. Soc.* **2014**, *136*, 15513.
43. Quan, Y.; Xie, Z. *Angew. Chem. Int. Ed.* **2016**, *55*, 1295.
44. Lyu, H.; Quan, Y.; Xie, Z. *Angew. Chem. Int. Ed.* **2016**, *55*, 11840.
45. Adams, R. D.; Kiprotich, J.; Peryshkov, D. V.; Wong, Y. O. *Inorg. Chem.* **2016**, *55*, 8207.

46. Quan, Y.; Lyu, H.; Xie, Z. *Chem. Commun.* **2017**, *53*, 4818.
47. Wang, X.; Jin, G.-X. *Organometallics* **2004**, *23*, 6319.
48. Wang, X.; Jin, G.-X. *Chem. Eur. J.* **2005**, *11*, 5758.
49. Terrasson, V.; Planas, J. G.; Vinas, C.; Teixidor, F.; Prim, D.; Light, M. E.; Hursthouse, M. B. *Organometallics*, **2010**, *29*, 4130.
50. Coult, R.; Fox, M. A.; Gill, W. R.; Herbertson, P. L.; MacBride, J. A. H.; Wade, K. J. *Organomet. Chem.* **1993**, *462*, 19.
51. Teixidor, F.; Laromaine, A.; Kivekas, R.; Sillanpaa, R.; Vinas, C.; Vespalec, R.; Horakova, H. *Dalton Trans.* **2008**, *3*, 345.
52. El-Zaria, M. E.; Keskar, K.; Genady, A. R.; Ioppolo, J. A.; McNulty, J.; Valliant, J. F. *Angew. Chem. Int. Ed.* **2014**, *53*, 5156.
53. Axtell, J. C.; Kirlikovali, K. O.; Djurovich, P. I.; Jung, D.; Nguyen, V. T.; Munekiyo, B.; Royappa, A. T.; Rheingold, A. L.; Spokoyny, A. M. *J. Am. Chem. Soc.* **2016**, *138*, 15758.
54. Alekseyeva, E. S.; Batsanov, A. S.; Boyd, L. A.; Fox, M. A.; Hibbert, T. G.; Howard, J. A. K.; MacBride, J. A. H.; Mackinnon, A.; Wade, K. *Dalton Trans.* **2003**, 475.
55. Bosch, E.; Bowling, N. P.; Darko, J. *Cryst. Growth Des.* **2015**, *15*, 1634.
56. Martin, M. J.; Man, W. Y.; Rosair, G. M.; Welch, A. J. *J. Organomet. Chem.* **2015** *798* (1), 36.
57. Falivene, L.; Credendino, R.; Poater, A.; Petta, A.; Serra, L.; Oliva, R.; Scarano, V.; Cavallo, L. *Organometallics* **2016**, *35*, 2286.
58. Fisher, S. P.; El-Hellani, A.; Tham, F. S.; Lavallo, V. *Dalton Trans.* **2016**, *45*, 9762.
59. Hermansson, K.; Wojcik, M.; Sjoberg, S. *Inorg. Chem.* **1999**, *38*, 6039.

60. Kalinin, V.; Ol'shevskaya, V. *Russ. Chem. Bull.* **2008**, *57*, 815.
61. Rozenel, S. S.; Kerr, J. B.; Arnold, J. *Dalton Trans.* **2011**, *40*, 10397.
62. Vabre, B.; Canac, Y.; Lepetit, C.; Duhayon, C.; Chauvin, R.; Zargarian, D. *Chem. – Eur. J.* **2015**, *21*, 17403.
63. Shriver, D. F.; Drezdson, M. A. *The Manipulation of Air-sensitive Compounds*, second ed., Wiley-Interscience, New York, **1986**, 2 edition.
64. APEX3, Bruker AXS, Inc., Madison, Wisconsin, USA, **2016**.
65. SAINTp, Bruker AXS, Inc., Madison, Wisconsin, USA, **2016**.
66. Krause, L.; Herbst-Irmer, R.; Sheldrick, G. M.; Stalke, D. *J. Appl. Crystallogr.* **2015**, *48*, 3.
67. Sheldrick, G. M. *Acta Crystallogr. A* **2008**, *64*, 112.
68. Sheldrick, G. M.; *Acta Crystallogr. Sect. Found. Adv.* **2015**, *71*, 3.
69. Dolomanov, O. V.; Bourhis, L. J.; Gildea, R. J.; Howard, J. A. K.; Puschmann, H. *J. Appl. Crystallogr.* **2009**, *42*, 339.

Chapter 3

Activation of C–H and C–CN Bonds of Acetonitrile by a Dianionic Dicarboranyl Pincer Ligand $(C_5H_3N)(C_2B_{10}H_{11})_2$ Bearing CNC Nickel(II) Complex

3.1 INTRODUCTION

The activation of C–C bond of nitriles is an area of great importance for chemical transformations, such as, decyanation,¹ hydrogenolysis,² cross-coupling³ and transfer hydrocyanation⁴ of a wide range of substrates in organic synthesis. Acetonitrile is the most widely used organonitrile; however, the activation of the C–C bond of acetonitrile has rarely been explored due to its strong C–C bond (133 kcalmol⁻¹) and weak interaction with transition metal centers, compared to aromatic nitriles.⁵ Low valent metal centers, such as Co(I),⁶ Rh(I),⁷ Ni(0),⁸ Pd(0)⁹ promoted oxidative addition of the C–C bond of acetonitrile is the most common activation strategy reported in literature. Presumably, this type of activation is attained *via* formation of a η^2 -side-on-coordinated intermediate, LM(η^2 -N≡C-CH₃) (L = ligand, M = metal), which is further supported by recent computational mechanistic investigation.¹⁰

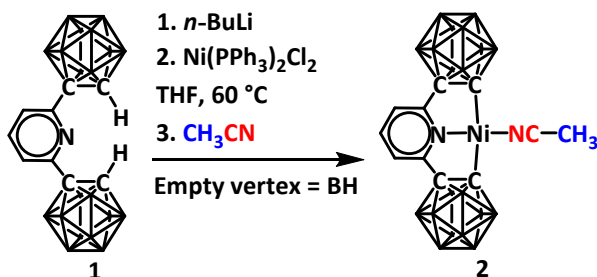
To date, few examples of copper promoted C–C bond cleavage of acetonitrile have been reported in literature. In 2001, Mascharak and co-workers discovered the cleavage of the C–C bond of acetonitrile by a mononuclear copper complex [Cu(dmppy)(en)] (dmppy = *N,N'*-dimethylpyridine-2,6-dicarboxamide anion; en = ethylenediamine).¹¹ However, the fate of all of the CH₃ fragments, and a mechanism for this bond breaking process were not described. In 2004, Lu and co-workers explored the activation of the C–C bond of acetonitrile by a dinuclear Cu(II) cryptate complex to afford a cyanide-bridged dinuclear copper cryptate complex and methanol.¹² However, Nelson and co-workers were unable to replicate the activation of acetonitrile under similar reaction conditions.¹³ Recently, Shen and co-workers reported copper-mediated cyanation of aromatic C–H bond with a wide substrate scope by utilizing acetonitrile as a

cyanide source upon activation of the C–C bond.¹⁴ Notably, all of these copper assisted activations of the typically inert C–C bond of acetonitrile followed the heterolytic cleavage pathway.

Among the transition metals, nickel plays a significant role for the activation of the C–C bond of nitriles. All of the nickel complexes reported to date for the C–C activation of nitriles contain only zero valent nickel center, and follow an oxidative addition pathway.⁸ Recently, we reported the synthesis and characterization of a pyridine-backbone *ortho*-carborane donor arms containing pincer ligand (C₅H₃N)(C₂B₁₀H₁₁)₂ (**1**), and its CNC Ni(II) complex {(C₅H₃N)(C₂B₁₀H₁₀)₂}Ni(CH₃CN) (**2**).¹⁵ Herein, we report the first example of a divalent Ni center (of **2**) mediated C–C bond activation of acetonitrile *via* formation of a C–H activated cationic intermediate K[{(C₅H₃N)(C₂B₁₀H₁₀)₂}Ni(CH₂CN)] (**3**). According to UV-visible and multinuclear NMR spectroscopic studies, upon oxygenation, the C–C bond activation of C-bound cyanomethyl group of complex **3** proceeded *via* formation of a short-lived and then a relatively long-lived intermediate. The slow decomposition of the second intermediate afforded mono-cyano complex K[{(C₅H₃N)(C₂B₁₀H₁₀)₂}Ni(CN)] (**4**), cyano-bridged complex K[Ni₂(CN)(C₉H₂₃B₂₀N)₂] (**5**), HCHO, HO–CH₂CN and CO₂ as the final products. Based on ¹H NMR spectroscopy, in the presence of a free radical trapping agent DMPO (5,5-dimethyl-1-pyrroline *N*-oxide), the complete cessation of the C–C bond breaking reaction was observed, suggesting the generation of an oxygen centered free radical *in-situ* under aerobic conditions.

3.2 RESULTS AND DISCUSSION

The pincer ligand **1**, and its Ni(II) complex **2** were synthesized by following our previously reported procedure (Scheme 3.1).¹⁵



Scheme 3.1: Synthesis of $\{(C_5H_3N)(C_2B_{10}H_{10})_2\}Ni(CH_3CN)$ (**2**).

The cyclic voltammogram (CV) of **1** in 0.1 M TBAPF₆ in THF showed a reduction event at -1.192 mV, which is expected to occur on carborane clusters. The events in the range from -2.0 mV to -3.1 are attributed to the reduction of THF (Figure 3.1 (a)). Compared to the free ligand **1**, the reduction of the carborane clusters in complex **2** in 0.1 M TBAPF₆ in THF exhibited a peak at a higher value of -1.397 mV, presumably due to the stabilization of both of the carborane clusters upon coordination with the Ni(II) center *via* C-atoms. An oxidation event was also observed at -0.561 mV (Figure 3.1 (b)).

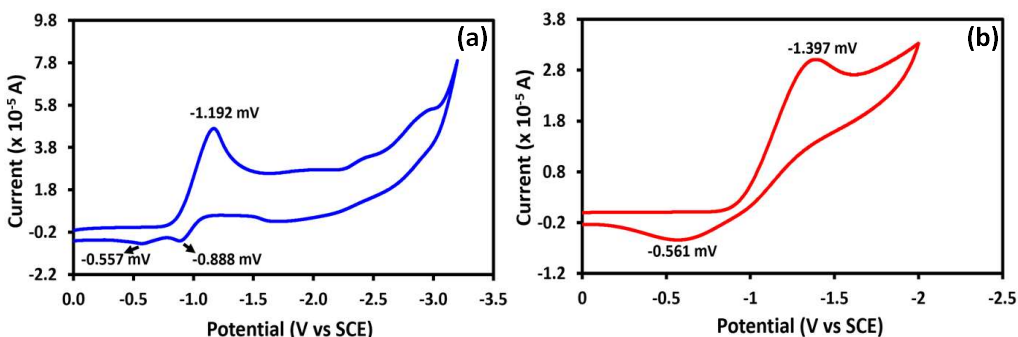
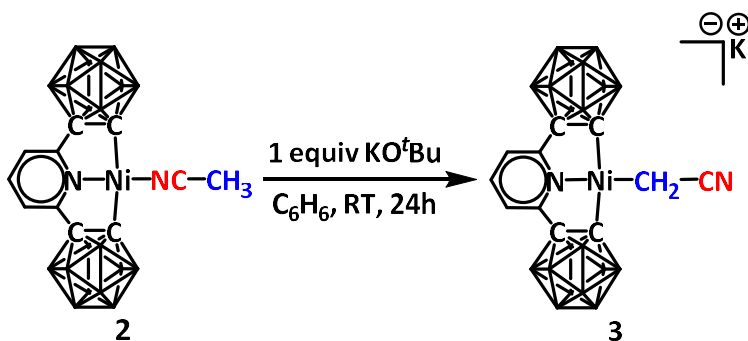


Figure 3.1: (a) Cyclic voltammogram of 1 mM of **1** in 0.1 M TBAPF₆ in THF, glassy carbon (GC) as working electrode, Pt as counter electrode, scan rate 60 mVs⁻¹. (b) Cyclic voltammogram of 1 mM of complex **2** in 0.1 M TBAPF₆ in THF, GC as working electrode, Pt as counter electrode, scan rate 60 mVs⁻¹.

As a C-carboranyl functionality, carborane arms act as electron withdrawing group¹⁶ and make the nickel center in **2** electron deficient, which is manifested by the high value of the $\nu(\text{C}\equiv\text{N})$ of 2332 cm^{-1} of the coordinated acetonitrile ligand in the FT-IR spectrum.¹⁵ The electron poor environment of the nickel center was also supported by the high value of $\nu(\text{CO})$ (2123 cm^{-1}) of the Ni(II)-bound CO complex, $\{(\text{C}_5\text{H}_3\text{N})(\text{C}_2\text{B}_{10}\text{H}_{10})_2\}\text{Ni}(\text{CO})$ due to weak Ni(II) to CO back donation. The *N*-heterocyclic carbene (NHC) ligands bearing electron deficient nickel complexes are known to activate the α -CH bonds of nitriles.¹⁷ In this context, we hypothesized that the C-H bond of the acetonitrile ligand in **2** is acidic enough to be deprotonated by a moderate base, such as KO^tBu. Upon treatment of a solution of **2** in benzene with KO^tBu under nitrogen, we observed fast and quantitative deprotonation of the labile *N*-bound acetonitrile ligand leading to the formation of a cyanomethyl group. The resulting cyanomethyl group flipped and coordinated at the nickel center *via* the C atom to afford yellow powder of $\text{K}[\{(\text{C}_5\text{H}_3\text{N})(\text{C}_2\text{B}_{10}\text{H}_{10})_2\}\text{Ni}(\text{CH}_2\text{CN})]$ (**3**) (**Scheme 3.2**), confirmed after air-free workup by an array of multinuclear NMR spectroscopic techniques, mass-spectrometry and single crystal X-ray crystallography.



Scheme 3.2: Base assisted C-H activation of labile acetonitrile ligand.

In the ^1H NMR of **3** in CD_2Cl_2 , a characteristic resonance for the C-bound cyanomethyl protons was observed at 0.63 ppm. The ^{13}C NMR spectrum contained a resonance at -12.89 ppm which corresponds to the methylene carbon atom of the cyanomethyl group. The ^{11}B and $^{11}\text{B}\{^1\text{H}\}$ NMR spectra revealed a set of partially overlapping signals in the range from -3.53 ppm to -11.27 ppm. The FT-IR spectrum of a solution of **3** in dry and degassed methylene chloride exhibited characteristic absorption bands $\nu(\text{B-H})$ at 2580 cm^{-1} as well as $\nu(\text{C}\equiv\text{N})$ at 2188 cm^{-1} .

Single crystals of **3-C₆D₆** were grown by slow evaporation of benzene inside the inert atmosphere of a nitrogen filled glovebox. The compound crystallizes in the space group $C2/m$ (No. 12) of the monoclinic system. The anion $[\text{Ni}(\text{C}_9\text{B}_{20}\text{H}_{23}\text{N})(\text{CH}_2\text{CN})]$ possesses a crystallographic mirror symmetry, in which the mirror plane passes through the C5, N1, Ni1, C6, C7 and N2 atoms (**Figure 3.2 (a)**). The pyridine backbone of the pincer framework is sandwiched between two independent C_6D_6 molecules. The potassium ion is connected with the N2 atom of the pendant cyanomethyl group, and interacts weakly with the H3, H7, and H8 protons of the two adjacent carborane clusters of two independent molecules of **3** (**Figure 3.2 (b)**).

The formation of a C-bound CH_2CN group from N-bound CH_3CN ligand resulted in the Ni1-C6-C7 angle of $100.3(2)^\circ$. The N1-Ni1-C6 bond angle ($174.67(15)^\circ$) also deviates from linearity to afford a slightly distorted square planar geometry around the N(II) center (defined by C1, N1, C1ⁱ, C6 plane). The C1-Ni1-N1 and C1-Ni1-C1ⁱ bond angles are $86.83(7)^\circ$ and $173.50(15)^\circ$, respectively. Interestingly, the C1-C2, C1-Ni1 and N1-Ni1 bond distances in **3** ($1.683(3)\text{ \AA}$, $1.930(2)\text{ \AA}$ and $1.917(3)\text{ \AA}$, respectively) are elongated than those in the complex **2** ($1.659(2)\text{ \AA}$,

1.9292(19) Å and 1.882(2) Å, respectively).¹⁵ The C2–C3 and C3–N1 bond distances are 1.483(3) Å and 1.345(3) Å, respectively (**Figure 3.2**).

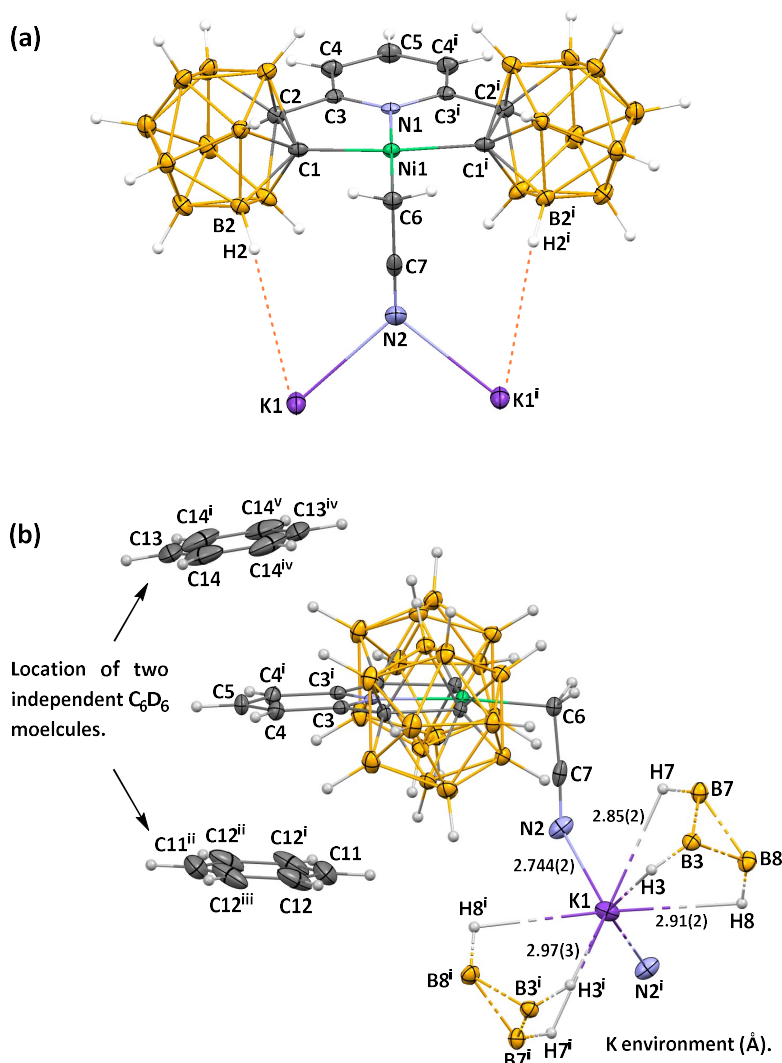


Figure 3.2: (a) Displacement ellipsoids of **3** drawn at the 50% probability level (expanded by symmetry). (b) Crystal structure of **3**, highlighting locations of two C₆D₆ molecules, and environment of K atom. In both figures, superscripts denote symmetry-equivalent atoms.

Notably, when a solution of **3** in benzene was exposed to air, within one hour a gradual decrease in intensity of yellow color was observed, suggesting its possible air instability. After slow evaporation of volatiles, the ¹H NMR spectrum of light yellow crystals was recorded in CD₂Cl₂, which revealed complete disappearance of the

methylene protons resonance at 0.63 ppm of the cyanomethyl group, and significant downfield chemical shifts of the pyridine protons.

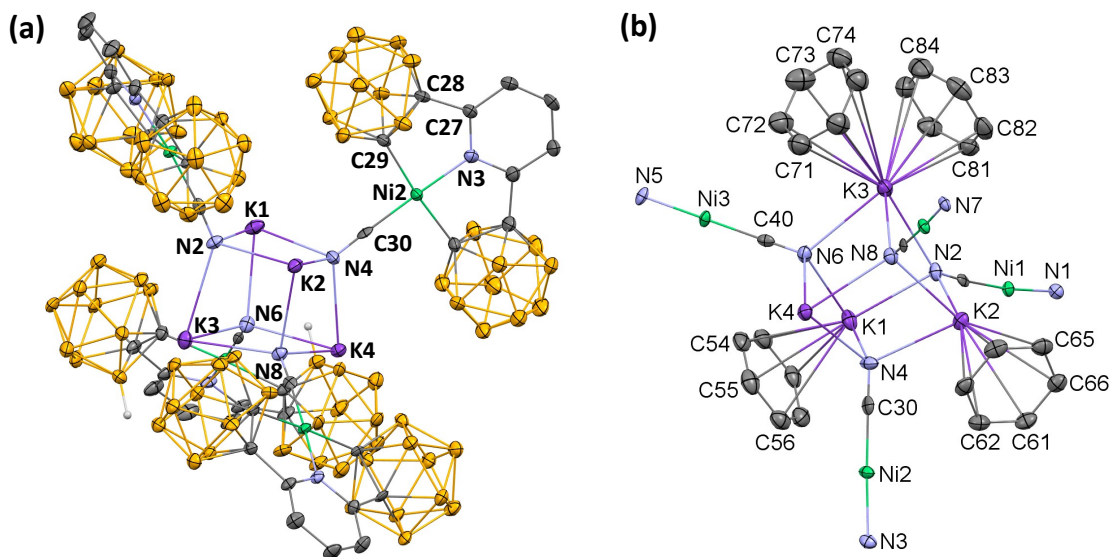


Figure 3.3: (a) Displacement ellipsoids of **4** drawn at the 50 % probability level. The C28–C27, N3–Ni2 bond distances are 1.483(5) Å and 1.892(3) Å. (b) Coordination of K atoms of the pseudocubane K_4N_4 core, no C_6D_6 is coordinated to K4. The N4–K2, K3–N6, K4–N8 and K1–N2 distances are 2.819(3) Å, 2.843(3) Å, 2.794(3) Å and 2.781(3) Å, respectively. The K4–N4, K1–N6, K3–N2 and K2–N8 distances are 2.766(3) Å, 2.778(3) Å, 2.955(3) Å and 2.803(3) Å, respectively. In both images, hydrogen atoms are omitted for clarity.

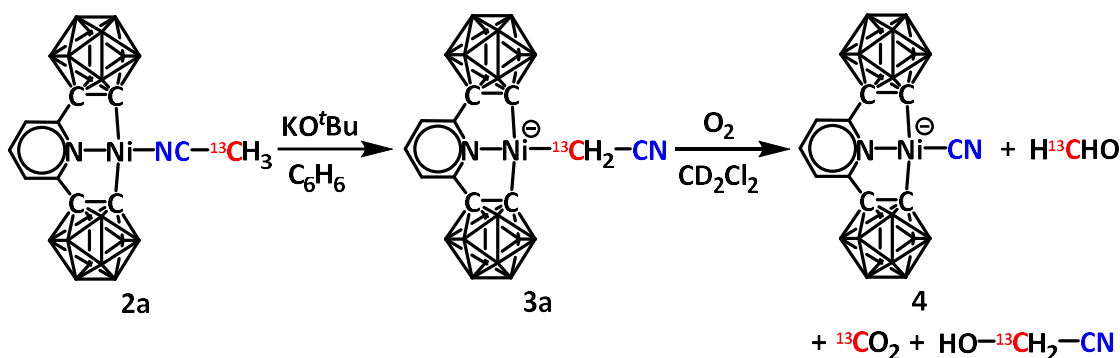
Intriguingly, the single crystal X-ray diffraction studies revealed the formation of a cyano ($C\equiv N$) group coordinated nickel complex $K[\{(C_5H_3N)(C_2B_{10}H_{10})_2\}Ni(CN)]$ (**4**). The complex **4** is crystallized as a novel K_4Ni_4 pseudocubane complex, in which four $[\{(C_5H_3N)(C_2B_{10}H_{10})_2\}Ni(CN)]$ anions are coordinated to four potassium ions forming a distorted K_4N_4 cube (**Figure 3.3 (a)**). Three of the four K ions are also coordinated to either one or two C_6D_6 molecules, and the fourth K ion is surrounded by three carborane clusters (**Figure 3.3 (b)**). In addition, these crystals contain a large number of C_6D_6 solvent molecules, 8.5 C_6D_6 per formula unit. Upon coordination of $C\equiv N$ group, the N3–Ni2–C30 and Ni2–C30–N4 bond angles are slightly deviated from linearity

(176.69(16)° and 178.1(4)°, respectively). The C29–C28, Ni2–C30 and C30–N4 bond distances are 1.666(5) Å, 1.825(4) Å and 1.156(5) Å, respectively.

The unprecedented formation of a C≡N group from a cyanomethyl moiety indicated the activation of the C–CN bond, possibly assisted by moisture or oxygen in air. Water promoted C–CN bond cleavage of acetonitrile by [Cu₂L](ClO₄)₄ (L=N[(CH₂)₂NHCH₂(C₆H₄-*p*)CH₂NH(CH₂)₂]₃N) to afford methanol and a cyano bridged complex [Cu₂L(CN)](ClO₄)₃.2CH₃CN.4H₂O is known.¹⁸ Interestingly, upon addition of water to a solution of **3** in CD₂Cl₂ in air, formation of methanol was not detected either in ¹H NMR or in the GC–MS spectra. In an attempt to determine the possible role of oxygen in C–CN bond activation, we purged oxygen through a freshly prepared solution of **3** in CD₂Cl₂ in a J–Young NMR tube. After 30 minutes, the ¹H NMR spectrum exhibited the resonance at 9.69 ppm which corresponds to formaldehyde, along with the signals of **4**. In addition, significant pressure release was noticed during opening the NMR cap, suggesting the possible formation of a gaseous product.

To further investigate the fate of the methylene moiety by ¹H and ¹³C NMR spectroscopy, we synthesized complex **3a** from a ¹³C-enriched acetonitrile ligand (¹³CH₃–CN, 99 atom % ¹³C) bearing complex **2a** (Scheme 3.3). In a time-controlled experiment, we observed the complete disappearance of the ¹H and ¹³C resonances of the methylene moiety after five minutes of oxygen addition to a solution of **3a** in CD₂Cl₂. Moreover, the ¹H and ¹³C NMR spectra exhibited new resonances at 4.50 ppm (integrated to two protons) and 62.98 ppm, respectively, which confirmed the rapid conversion of **3a** to a single short-lived intermediate. Within the next 15 minutes, the intensity of the ¹H resonance at 4.50 ppm decreased drastically, and a set of broad resonances appeared in

the range 5.01 ppm to 4.19 ppm. The solution was heated at 50 °C for 24 hours for the completion of the reaction. To our surprise, the ^1H and ^{13}C NMR spectra confirmed the formation of $^{13}\text{CO}_2$, along with H^{13}CHO , and $\text{HO}-^{13}\text{CH}_2-\text{CN}$ as the final products (**Scheme 3.3**). Intriguingly, when a solution of **3a** was treated with approximately one equivalent of oxygen, the short-lived intermediate was stable at room temperature for up to 2 hours. When this oxygenated solution was heated at 50 °C for 2 hours, only H^{13}CHO was detected, suggesting the dependency of the two intermediates formation and CO_2 generation on oxygen concentration.



Scheme 3.3: Synthesis of ^{13}C labeled cyanomethyl ($^{13}\text{CH}_2-\text{CN}$) bearing complex **2a** from **1a** followed by O_2 assisted C–CN bond activation. Red carbon atoms represents 99 % enriched ^{13}C .

Additionally, UV–visible absorption spectroscopy was employed to follow the C–CN bond breaking process. A solution of 0.05 mM of **3** in dichloromethane was prepared, and the UV–vis spectrum was recorded prior to O_2 addition (**Figure 3.4 (a)**) and green trace in **Figure 3.4 (c)**). Upon addition of O_2 , a short-lived intermediate was generated immediately (dashed green line in **Figure 3.4 (c)**), which was converted to a relatively stable second intermediate after ten minutes (dashed red line in **Figure 3.4 (c)**). The decay of the second intermediate afforded the Ni(II)–CN complex within two hours of oxygenation (black line in **Figure 3.4 (c)**), confirmed by comparing with the

absorption spectrum of 0.05 mM of **3** in dichloromethane (**Figure 3.4 (b)**). These observations further support the conclusion drawn from the NMR studies of generation of the two consecutive intermediates.

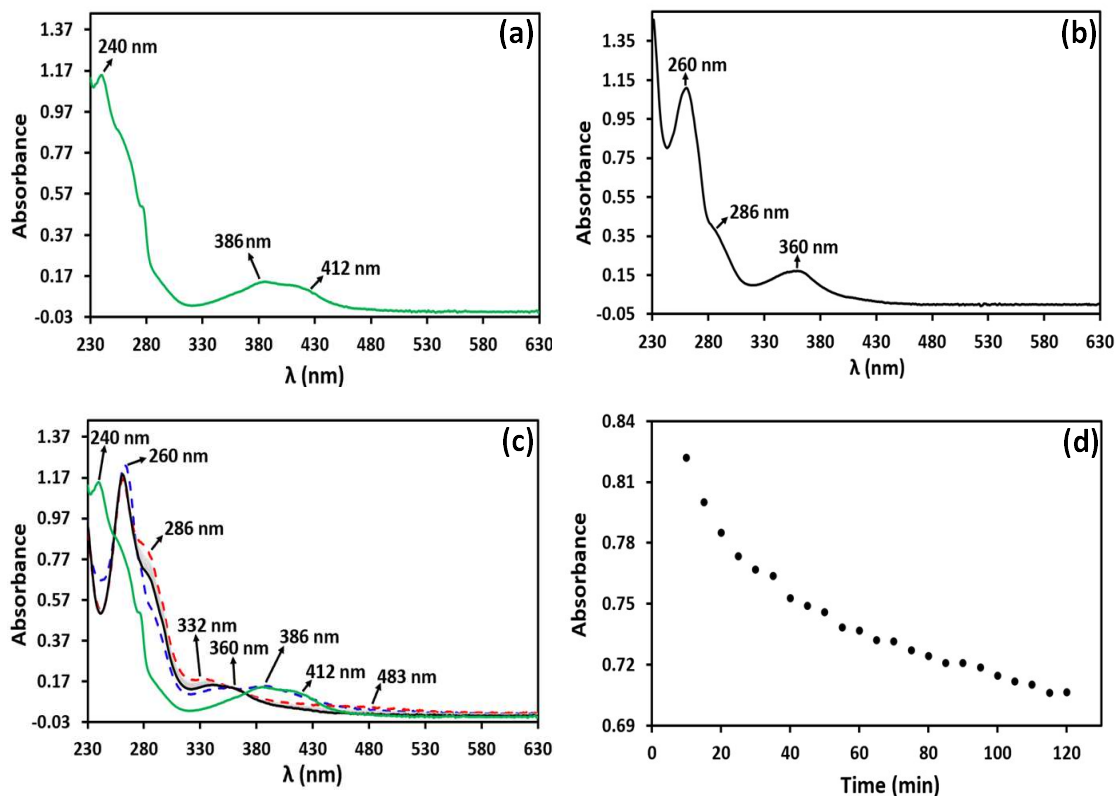


Figure 3.4: (a) UV-vis absorption spectrum of 0.05 mM **3** in dichloromethane. (b) UV-vis absorption spectrum of 0.05 mM **4** in dichloromethane. (c) UV-vis spectral changes after addition of O₂ in a solution 0.05 mM **3** in dichloromethane. Curves: green line, pure **3**; dashed blue line, **3** + O₂ after 5 minutes (first intermediate); dashed red line, **3** + O₂ after 10 minutes (second intermediate); black line, formation of **4** after 2 hours. (d) Decay of the second intermediate over time at the absorption maximum of 286 nm.

The elucidation of the reaction mechanism involving activation of dioxygen is challenging, since a variety of paths may exist depending on the reaction conditions.¹⁹ Metal mediated dioxygen activation *via* formation of a metal-superoxo (M–O–O^{•−}) species as a key intermediate has been intensively studied, and is well established.²⁰ As a reactive oxygen species (ROS), the radical anion O₂^{•−} is considered as a potential green

oxidant, however, in most cases its detection and characterization are still elusive.²¹ The broadening of the ^1H resonances upon oxygenation in a solution of **3a** during controlled NMR studies suggested the possible formation of a free radical in the reaction medium.

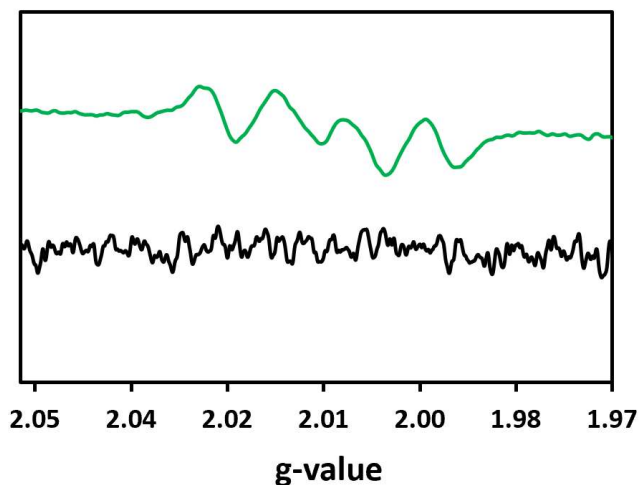
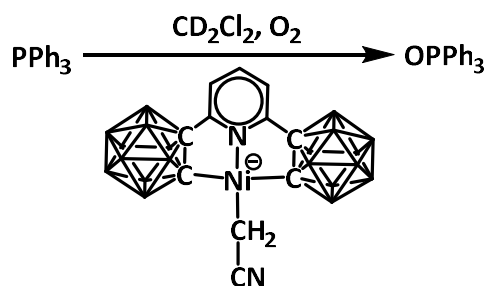


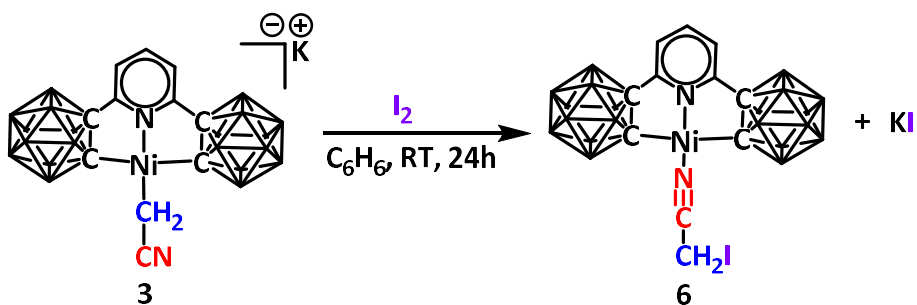
Figure 3.5: EPR studies of oxygenated **3** in CD_2Cl_2 using DMPO as radical trapping agent. Curves: black line, spectra of **3** and DMPO solution before oxygenation; green line, spectra of DMPO-free radical adduct after 20 minutes of oxygenation.

The assumption of an oxygen centered free radical generation was confirmed by employing a radical trapping reagent, 5,5-dimethyl-1-pyrroline *N*-oxide (DMPO). Upon addition of oxygen in presence of DMPO in a solution of **3a** in CD_2Cl_2 , the complete cessation of the reaction was observed, based on ^1H NMR spectroscopy. In an electron paramagnetic resonance (EPR) experiment, we explored formation of a DMPO-free radical adduct; however, full characterization of the adduct by simulation was problematic (**Figure 3.5**). The spin trap DMPO forms a less stable adduct with $\text{O}_2^{\cdot-}$ which spontaneously decays to afford the DMPO- $\cdot\text{OH}$ adduct.²² Therefore, the characterization of $\text{O}_2^{\cdot-}$ as a DMPO-OOH adduct is controversial and not reliable. However, the ^1H NMR and EPR experiments confirmed the generation of an oxygen centered free radical during the C-CN bond activation process.

Oxidation of triphenylphosphine (PPh₃) to yield triphenylphosphine oxide (O=PPh₃) is known to proceed in the presence of superoxide free radical in aerobic conditions.^{19,23} Recently, MacBeth and co-workers demonstrated stoichiometric oxidation of PPh₃ by a monometallic cobalt complex Co(II)-O₂^{•-}.²⁴ In an attempt to detect the generation of O₂^{•-}, we added oxygen in a PPh₃ containing solution of **3** in CD₂Cl₂. The ³¹P NMR spectrum exhibited a characteristic resonance at 29.30 ppm for O=PPh₃ after 5 minutes of oxygen addition. The oxidation of PPh₃ further supports the conclusion drawn from ¹H NMR and EPR spectroscopy studies for evidence of O₂^{•-} generation at the nickel center (**Scheme 3.4**).



Scheme 3.4: Oxidation of triphenylphosphine by O₂ in the presence of **2**.



Scheme 3.5: Activation of I₂ by **3** to afford *N*-bound iodoacetonitrile complex **5**.

In addition to dioxygen activation, **3** is also proved effective for the cleavage of the I-I bond of I₂ at room temperature (**Scheme 3.5**). The reaction of I₂ with *C*-bound

cyanomethyl group of **3** afforded iodoacetonitrile, which flipped and coordinated with the Ni(II) center *via* N-atom (**6**).

3.3 CONCLUSION

In conclusion, the activation of C–H bond of N-bound acetonitrile of **2** by KO^tBu, followed by ligand flip afforded the C-bound cyanomethyl containing Ni(II) complex **3**. Upon oxygenation, the complex **3** afforded a short-lived intermediate, followed by a relatively long-lived second intermediate. The slow decay of the second intermediate yielded a mono-cyano complex $K[\{(C_5H_3N)(C_2B_{10}H_{10})_2\}Ni(CN)]$ (**4**), a cyano-bridged complex $K[Ni_2(CN)(C_9H_{23}B_{20}N)_2]$ (**5**), HCHO, HO–CH₂CN and CO₂. An oxygen centered free radical chain mechanism was manifested by oxidation of PPh₃ as well as, EPR experiment. Currently, we are working on elucidation of a detailed reaction mechanism for the activation reaction of the C–C bond of acetonitrile.

3.4 EXPERIMENTAL SECTION

All synthetic manipulations, unless stated otherwise, were carried out either in a nitrogen-filled VAC drybox or on a dual manifold Schlenk-style vacuum line.²⁵ The solvents were sparged with nitrogen, passed through activated alumina, and stored over activated 4 Å Linde-type molecular sieves. C₆D₆ and CD₂Cl₂ were degassed and stored over activated 4 Å Linde-type molecular sieves. NMR spectra were recorded using Varian spectrometers at 400 (¹H), 100 (¹³C), 128 (¹¹B) MHz, reported in δ (parts per million) and referenced to the residual ¹H/¹³C signals of the deuterated solvent or an external BF₃(Et₂O) (¹¹B(δ): 0.0 ppm) standard.

3.4.1 Synthesis of $\text{K}\{(\text{C}_5\text{H}_3\text{N})(\text{C}_2\text{B}_{10}\text{H}_{10})_2\}\text{Ni}(\text{CH}_2\text{CN})$ (3)

Potassium *tert*-butoxide (26 mg, 0.23 mmol) was added to a solution of 2,6-bis(carboranyl)pyridine nickel(II)(acetonitrile) (100 mg, 0.22 mmol) in benzene (5 mL) under nitrogen atmosphere. Dissolution of the complex was observed in 30 min, thus leading to a light yellow solution containing a yellow salt. The mixture was stirred at room temperature for 12 h, after which time volatiles were removed under vacuum. The air sensitive solid was washed with dry hexane (3×3 mL) and dried under vacuum (101 mg, 93% yield).

^1H NMR (CD_2Cl_2): δ 7.71 (t, 1H, $\text{C}_5\text{H}_3\text{N}$), 7.21 (d, 2H, $\text{C}_5\text{H}_3\text{N}$), 3.10–1.30 (overlapping, 20H, B–H, $\text{C}_2\text{B}_{10}\text{H}_{10}$), 0.63 (s, 2H, CH_2CN). $^{10}\text{B}\{^1\text{H}\}$ NMR (CD_2Cl_2): δ –3.85, –6.63, –10.86. ^{13}C NMR (CD_2Cl_2): δ 158.0 ($\text{C}_5\text{H}_3\text{N}$), 138.4 ($\text{C}_5\text{H}_3\text{N}$), 120.4 ($\text{C}_5\text{H}_3\text{N}$), 133.2 (CH_2CN), 82.9 ($\text{C}_2\text{H}_{10}\text{B}_{10}$), 81.42 ($\text{C}_2\text{H}_{10}\text{B}_{10}$), –12.89 (CH_2CN).

3.4.2 Synthesis of $\text{K}\{(\text{C}_5\text{H}_3\text{N})(\text{C}_2\text{B}_{10}\text{H}_{10})_2\}\text{Ni}(\text{CN})$ (4)

Oxygen was bubbled through a solution of $\text{K}\{(\text{C}_5\text{H}_3\text{N})(\text{C}_2\text{B}_{10}\text{H}_{10})_2\}\text{Ni}(\text{CH}_2\text{CN})$ (50 mg, 0.20 mmol) in benzene (10 mL) for 5 minutes. The mixture was stirred at 65 °C for 24 h, after which time volatiles were removed under vacuum. The pale yellow solid was washed with hexane (3×3 mL) and dried under vacuum (40 mg, 82% yield).

^1H NMR (C_6D_6): δ 6.24 (d, 2H, $\text{C}_5\text{H}_3\text{N}$), 6.15 (t, 1H, $\text{C}_5\text{H}_3\text{N}$), 3.80–1.90 (overlapping, 20H, B–H, $\text{C}_2\text{B}_{10}\text{H}_{10}$). $^{10}\text{B}\{^1\text{H}\}$ NMR (CD_2Cl_2): δ –3.14, –6.47, –9.82. ^{13}C NMR (CD_2Cl_2): δ 159.5 ($\text{C}_5\text{H}_3\text{N}$), 140.5 ($\text{C}_5\text{H}_3\text{N}$), 120.9 ($\text{C}_5\text{H}_3\text{N}$), 82.0 ($\text{C}_2\text{H}_{10}\text{B}_{10}$), 76.0 ($\text{C}_2\text{H}_{10}\text{B}_{10}$).

3.4.3 Synthesis of $\{(C_5H_3N)(C_2B_{10}H_{10})_2\}Ni(ICH_2CN)$ (6)

To a solution of $K\{(C_5H_3N)(C_2B_{10}H_{10})_2\}Ni(CH_2CN)$ (100 mg, 0.20 mmol) in benzene (10 mL) under nitrogen atmosphere, iodine (80 mg, 0.32 mmol) was added and stirred at room temperature overnight. The formed yellow precipitate was separated by filtration and washed with hexane (3×3 mL). The solid was dried under vacuum (112 mg, 96% yield).

1H NMR (CD_2Cl_2): δ 7.81 (t, 1H, C_5H_3N), 7.23 (d, 2H, C_5H_3N), 3.84 (s, 2H, ICH_2CN) 3.00–1.45 (overlapping, 20H, B–H, $C_2B_{10}H_{10}$). $^{11}B\{^1H\}$ NMR (CD_2Cl_2): δ -3.04, -6.67, -10.94. ^{13}C NMR (CD_2Cl_2): δ 161.4 (C_5H_3N), 141.6 (C_5H_3N), 124.8 (ICH_2CN), 121.8 (C_5H_3N), 80.0 ($C_2H_{10}B_{10}$), 73.4 ($C_2H_{10}B_{10}$), -33.1 (ICH_2CN).

3.4.4 Synthesis of $\{(C_5H_3N)(C_2B_{10}H_{10})_2\}Ni(^{13}CH_3CN)$ (2a)

^{13}C labeled acetonitrile (*CH_3CN , 2- ^{13}C 99%) (0.068 mL, 1.30 mmol) was added to a solution of 2,6-bis(carboranyl)pyridine nickel(II)(acetonitrile) (30 mg, 0.065 mmol) in methylene chloride (5 mL). The mixture was stirred at 65 °C for 6 h, after which time volatiles were removed under vacuum.

1H NMR (CD_2Cl_2): δ 7.79 (t, 1H, C_5H_3N), 7.21 (d, 2H, C_5H_3N), 2.38 (t, 3H, CH_3CN). ^{13}C NMR (CD_2Cl_2): δ 3.99 (CH_3CN).

3.4.5 Synthesis of $K[\{(C_5H_3N)(C_2B_{10}H_{10})_2\}Ni(^{13}CH_2CN)]$ (3a)

Potassium *tert*-butoxide (2.6 mg, 0.023 mmol) was added to a solution of $\{(C_5H_3N)(C_2B_{10}H_{10})_2\}Ni(^*CH_3CN)$ (10 mg, 0.022 mmol) in benzene (5 mL) under nitrogen atmosphere. Dissolution of the complex was observed in 30 min, thus leading to a light yellow solution containing a yellow salt. The mixture was stirred at room

temperature for 12 h, after which time volatiles were removed under vacuum. The air sensitive solid was washed with dry hexane (3 × 3 mL) and dried under vacuum.

^1H NMR (CD_2Cl_2): δ 7.71 (t, 1H, $\text{C}_5\text{H}_3\text{N}$), 7.23 (d, 2H, $\text{C}_5\text{H}_3\text{N}$), 3.10–1.30 (overlapping, 20H, B–H, $\text{C}_2\text{B}_{10}\text{H}_{10}$), 0.62 (t, 2H, CH_2CN). ^{13}C NMR (CD_2Cl_2): δ –12.58 (CH_2CN).

3.4.6 Reaction of $\text{K}\{(\text{C}_5\text{H}_3\text{N})(\text{C}_2\text{B}_{10}\text{H}_{10})_2\}\text{Ni}(^{13}\text{CH}_2\text{CN})$ with Oxygen

A portion of $\text{K}\{(\text{C}_5\text{H}_3\text{N})(\text{C}_2\text{B}_{10}\text{H}_{10})_2\}\text{Ni}(^{13}\text{CH}_2\text{CN})$ (2 mg, 0.004 mmol) was dissolved in CD_2Cl_2 (2 mL) in a vial under nitrogen atmosphere. The solution was transferred to a J-Young valve NMR tube and oxygen was added through a long glass pipette. The reaction mixture was capped and heated at 75 °C for 48 h.

^1H NMR (CD_2Cl_2): δ 9.68 (2, CH_2O), 7.77 (t, $\text{C}_5\text{H}_3\text{N}$), 7.24 (d, $\text{C}_5\text{H}_3\text{N}$). ^{13}C NMR (CD_2Cl_2): δ 195.54 (CH_2O), 125.20 (CO_2).

3.4.7 OXYGENATION OF $\text{K}\{(\text{C}_5\text{H}_3\text{N})(\text{C}_2\text{B}_{10}\text{H}_{10})_2\}\text{Ni}(\text{CH}_2\text{CN})$ (3) IN PRESENCE OF DMPO (5,5-DIMETHYL-1-PYRROLINE N-OXIDE)

3.4.7.1 Preparation of Stock Solution of 3 and DMPO for EPR and NMR Studies

DMPO (2.4 μL , 0.022 mmol) was transferred to a storage flask *via* a micropipette. CD_2Cl_2 (4 mL) was added to the flask and freeze-pump-thaw was performed four times to degas the mixture. The flask was transferred into a nitrogen-filled VAC drybox, and the solution was stored over activated 4 Å Linde-type molecular sieves overnight. Complex 3 (5 mg, 0.01 mmol) was added to the flask and stirred for 30 minutes to dissolve completely. This stock solution was utilized for EPR and ^1H NMR studies.

3.4.7.2 EPR Study: Superoxide Spin Trapping Experiment

All EPR spectra were recorded using a Bruker EMX plus equipped with a Bruker X-band microwave bridgehead and Xenon software (v 1.1b.66). At a power of 1.589 mW and modulation amplitude of 2.0 G, similar parameters were used to perform all the EPR experiments.

A small portion of the stock solution was transferred to a Norell Suprasil Quartz EPR tube, and was sealed under the inert atmosphere of a nitrogen-filled VAC drybox to record the pre-O₂ EPR data. Oxygen was bubbled into the solution of the EPR tube *via* a long glass pipette for 2 minutes, and the EPR data was recorded again.

3.4.7.3 Monitoring Reaction Progress in the Presence of DMPO

Inside the inert atmosphere of a nitrogen-filled VAC drybox, a small portion of the stock solution of the DMPO and **3** mixture was transferred in a J-Young NMR tube and sealed. Prior to the addition of oxygen, the ¹H NMR spectrum of this mixture was recorded. Oxygen was bubbled into the solution of the NMR tube *via* a long glass pipette for 2 minutes. According to the ¹H NMR spectrum, no formation of HCHO and K{(C₅H₃N)(C₂B₁₀H₁₀)₂}Ni(CN) was observed at room temperature even after 1 hour.

3.4.8 CRYSTAL STRUCTURE DETERMINATION DETAILS

X-ray intensity data were collected at 100(2) K using a Bruker D8 QUEST diffractometer equipped with a PHOTON-100 CMOS area detector and an Incoatec microfocus source (Mo K α radiation, $\lambda = 0.71073$ Å). The raw area detector data frames were reduced, scaled and corrected for absorption effects using the Bruker APEX3, SAINT+ and SADABS programs.²⁶⁻²⁷ Final unit cell parameters were determined by least-squares refinement of 9990 reflections taken from the data set. The structure was

solved with SHELXT.²⁸ Subsequent difference Fourier calculations and full-matrix least-squares refinement against F^2 were performed with SHELXL-2018²⁸ using OLEX2.²⁹

3.4.8.1 X-ray Structure Determination of $\text{K}\{(\text{C}_5\text{H}_3\text{N})(\text{C}_2\text{B}_{10}\text{H}_{10})_2\}\text{Ni}(\text{CH}_2\text{CN})\cdot\text{C}_6\text{D}_6$ (3)

Crystals formed as yellow rectangular plates. All crystals examined, intact or cleaved and of various sizes, persistently gave a pattern with diffraction spots grouped into pairs, along with difficulty in indexing the diffraction pattern to a reasonable unit cell. An apparent *C*-centered orthorhombic cell with dimensions $\mathbf{a} \sim 14.0 \text{ \AA}$, $\mathbf{b} \sim 14.9 \text{ \AA}$, $\mathbf{c} \sim 86.3 \text{ \AA}$ could be indexed, fitting most reflections. The occurrence of the unusually long axis suggested twinning. The Bruker Cell_Now program³⁰ confirmed that the crystals are twinned by non-merohedry. A set of 424 reflections from the data crystal was indexed entirely to two domains having the reported *C*-centered monoclinic unit cell parameters. The derived twin law, relating indices of one domain to those of the other, is $(-1 \ 0 \ 0 / 0 \ -1 \ 0 / 0.344 \ 0 \ 1)$. The twin law corresponds to a 180° rotation about the reciprocal-space $[001]$ axis. The major twin domain volume fraction refined to 0.553(1).

The compound crystallizes in the space group $C2/m$ (No. 12) of the monoclinic system. The asymmetric unit consists of (formally) half of one $\text{K}[\text{Ni}(\text{C}_9\text{B}_{20}\text{H}_{23}\text{N})(\text{CH}_2\text{CN})]$ complex and $\frac{1}{4}$ each of two independent benzene- d_6 molecules. The $[\text{Ni}(\text{C}_9\text{B}_{20}\text{H}_{23}\text{N})(\text{CH}_2\text{CN})]^-$ anion has crystallographic mirror symmetry; atoms Ni1, N1, N2, and C5 – C7 are located on the mirror plane. The potassium cation is located on a C_2 rotational axis. Both d_6 -benzene molecules are located on sites of local $2/m$ (C_{2h}) point symmetry and only $\frac{1}{4}$ of each is present per asymmetric unit. All non-hydrogen atoms were refined with anisotropic displacement parameters. Hydrogen atoms

bonded to carbon were located in Fourier difference maps before being placed in geometrically idealized positions and included as riding atoms with $d(\text{C-H/D}) = 0.95 \text{ \AA}$ and $U_{\text{iso}}(\text{H/D}) = 1.2U_{\text{eq}}(\text{C})$ for aromatic hydrogen/deuterium atoms and $d(\text{C-H}) = 0.99 \text{ \AA}$ and $U_{\text{iso}}(\text{H}) = 1.2U_{\text{eq}}(\text{C})$ for the unique methylene hydrogen. Hydrogen atoms bonded to boron atoms of the carborane cage were located in a difference Fourier maps and refined freely. The largest residual electron density peak in the final difference map is $0.4 \text{ e}^-/\text{\AA}^3$, located 2.39 \AA from N2.

Crystal Data for $\text{C}_{17}\text{H}_{25}\text{B}_{20}\text{D}_6\text{KN}_2\text{Ni}$ ($M = 583.48 \text{ g/mol}$): monoclinic, space group $C2/m$ (no. 12), $a = 14.0198(7) \text{ \AA}$, $b = 14.9567(6) \text{ \AA}$, $c = 14.6019(6) \text{ \AA}$, $\beta = 99.507(2)^\circ$, $V = 3019.8(2) \text{ \AA}^3$, $Z = 4$, $T = 100(2) \text{ K}$, $\mu(\text{MoK}\alpha) = 0.796 \text{ mm}^{-1}$, $D_{\text{calc}} = 1.283 \text{ g/cm}^3$, 6124 reflections measured ($4.62^\circ \leq 2\theta \leq 55.052^\circ$), 6124 unique ($R_{\text{int}} = ?$, $R_{\text{sigma}} = 0.0538$) which were used in all calculations. The final R_1 was 0.0442 ($I > 2\sigma(I)$) and wR_2 was 0.0781 (all data).

3.4.8.2 X-ray Structure Determination of

$\text{K}_4(\text{C}_6\text{D}_6)_4[\{(\text{C}_5\text{H}_3\text{N})(\text{C}_2\text{B}_{10}\text{H}_{10})_2\}\text{Ni}(\text{CN})].8.5(\text{C}_6\text{D}_6)$ (4)

The compound crystallizes in the monoclinic system. The pattern of systematic absences in the intensity data was consistent with the space group $P2_1/n$, which was verified by structure solution. The asymmetric unit consists of one $\text{K}_4(\text{C}_6\text{D}_6)_4[\text{Ni}(\text{CN})(\text{C}_9\text{H}_{23}\text{B}_{20}\text{N})]_4$ complex and 8.5 independent d_6 -benzene molecules. One C_6D_6 molecule is located on a crystallographic inversion center and only half is present per asymmetric unit. Two are disordered and were modeled with two closely separated components (C161-C166/C261-C266 and C171-C176/C271-C276). C-C distance restraints (DFIX and SADI) and anisotropic displacement parameter restraints

(EADP and RIGU) were used in modeling the C₆D₆ disorder, and also to improve the refinement of non-disordered C₆D₆ molecules. All non-hydrogen atoms were refined with anisotropic displacement parameters. Hydrogen and deuterium atoms of the K₄(C₆D₆)₄[Ni(CN)(C₉H₂₃B₂₀N)]₄ complex (carborane B-H, pyridyl C-H and C₆D₆ D atoms) were clearly located in difference Fourier maps before being placed in geometrically idealized positions and included as riding atoms with $d(\text{B-H}) = 1.12 \text{ \AA}$ and $U_{\text{iso}}(\text{H}) = 1.2U_{\text{eq}}(\text{B})$ for carborane H atoms and $d(\text{C-H/D}) = 0.95 \text{ \AA}$ and $U_{\text{iso}}(\text{H/D}) = 1.2U_{\text{eq}}(\text{C})$ for aromatic hydrogen and deuterium atoms. Deuterium atoms of the non-coordinated *d*₆-benzene molecules were idealized and included as riding atoms with $U_{\text{iso}}(\text{D}) = 1.2U_{\text{eq}}(\text{C})$. The largest residual electron density peak in the final difference map is $0.43 \text{ e}^-/\text{\AA}^3$, located 0.64 \AA from H42.

Crystal Data for C₁₁₅H₉₂B₈₀D₇₅K₄N₈Ni₄ ($M = 2993.06 \text{ g/mol}$): monoclinic, space group $P2_1/n$ (no. 14), $a = 18.9131(9) \text{ \AA}$, $b = 27.3096(14) \text{ \AA}$, $c = 30.7941(15) \text{ \AA}$, $\beta = 90.8187(19)^\circ$, $V = 15903.8(14) \text{ \AA}^3$, $Z = 4$, $T = 100(2) \text{ K}$, $\mu(\text{MoK}\alpha) = 0.619 \text{ mm}^{-1}$, $D_{\text{calc}} = 1.250 \text{ g/cm}^3$, 255325 reflections measured ($4.24^\circ \leq 2\theta \leq 50.342^\circ$), 28373 unique ($R_{\text{int}} = 0.1431$, $R_{\text{sigma}} = 0.0967$) which were used in all calculations. The final R_1 was 0.0633 ($I > 2\sigma(I)$) and wR_2 was 0.1196 (all data).

3.4.8.2 X-ray Structure Determination of

[K(C₆D₆)₂(H₂O)][Ni₂(CN)(C₉H₂₃B₂₀N)]₂·C₆D₆ (5)

The compound crystallizes in the monoclinic system. The pattern of systematic absences in the intensity data was consistent with the space groups Cc and $C2/c$. The centrosymmetric group $C2/c$ was confirmed by structure solution. The asymmetric unit consists of half of one [Ni₂(CN)(C₉H₂₃B₂₀N)]⁻ anion and half of one K(C₆D₆)₂(H₂O)⁺

cation, both of which are located on crystallographic two-fold axes of rotation, and half of one C₆D₆ molecule, which is located on a crystallographic inversion center. The potassium and oxygen atoms are located on the two-fold. The bridging CN group of the nickel anion is disordered across the two-fold axis, scrambling the C and N positions. The one unique CN group atomic site was refined as 50% N2 / 50% C10. All non-hydrogen atoms were refined with anisotropic displacement parameters. Hydrogen (deuterium) atoms bonded to carbon and boron were located in difference Fourier maps. Those of the nickel anion were refined freely. The *d*₆-benzene hydrogens were treated as riding on the parent C atom with $d(\text{C-D}) = 0.95 \text{ \AA}$ and $U_{\text{iso}}(\text{D}) = 1.2U_{\text{eq}}(\text{C})$. The unique water hydrogen was located in a difference map but could not be refined freely. It was adjusted to give $d(\text{O-H}) = 0.85 \text{ \AA}$ and was subsequently treated as riding with $U_{\text{iso}}(\text{H}) = 1.5U_{\text{eq}}(\text{O})$. The largest residual electron density peak in the final difference map is $0.57 \text{ e}^-/\text{\AA}^3$, located 1.17 \AA from K1.

Crystal Data for C₃₇H₄₈B₄₀D₁₈KN₃Ni₂O ($M = 1175.95 \text{ g/mol}$): monoclinic, space group *C2/c* (no. 15), $a = 11.0171(5) \text{ \AA}$, $b = 23.1189(12) \text{ \AA}$, $c = 23.9349(12) \text{ \AA}$, $\beta = 93.859(2)^\circ$, $V = 6082.5(5) \text{ \AA}^3$, $Z = 4$, $T = 100(2) \text{ K}$, $\mu(\text{MoK}\alpha) = 0.724 \text{ mm}^{-1}$, $D_{\text{calc}} = 1.284 \text{ g/cm}^3$, 50773 reflections measured ($4.346^\circ \leq 2\theta \leq 52.784^\circ$), 6216 unique ($R_{\text{int}} = 0.0549$, $R_{\text{sigma}} = 0.0391$) which were used in all calculations. The final R_1 was 0.0399 ($I > 2\sigma(I)$) and wR_2 was 0.0883 (all data).

REFERENCES

1. Patra, T.; Agasti, S.; Akanksha.; Maiti, D. *Chem. Commun.* **2013**, *49*, 69.
2. Patra, T.; Agasti, S.; Modak, A.; Maiti, D. *Chem. Commun.* **2013**, *49*, 8362.
3. Zhang, J.-S.; Chen, T.; Yanga, J.; Han, L.-B. *Chem. Commun.* **2015**, *51*, 7540.
4. Fang, X. J.; Yu, P.; Morandi, B. *Science* **2016**, *351*, 832.
5. Kou, X.; Zhao, M.; Qiao, X.; Zhu, Y.; Tong, X.; Shen, Z. *Chem. Eur. J.* **2013**, *19*, 16880.
6. Xu, H. W.; Williard, P. G.; Bernskoetter, W. H. *Organometallics* **2012**, *31*, 1588.
7. (a) Evans, M. E.; Li, T.; Jones, W. D. *J. Am. Chem. Soc.* **2010**, *132*, 16278. (b) Evans, M. E.; Jones, W. D. *Organometallics* **2011**, *30*, 3371.
8. (a) Garcia, J. J.; Arevalo, A.; Brunkan, N. M.; Jones W. D. *Organometallics* **2004**, *23*, 3997. (b) Atesin, T. A.; Li, T.; Lachaize, S.; Brennessel, W. W.; García, J. J.; Jones, W. D. *J. Am. Chem. Soc.* **2007**, *129*, 7562.
9. Munjanja, L.; Torres-López, C.; Brennessel, W. W.; Jones, W. D. *Organometallics* **2016**, *35*, 2010.
10. Ni, S.-F.; Yang, T.-L.; Dang, L. *Organometallics* **2017**, *36*, 2746.
11. Marlin, D. S.; Olmstead, M. M.; Mascharak, P. K. *Angew. Chem. Int. Ed.* **2001**, *40*, 4752.
12. Lu, T.; Zhuang, X.; Li, Y.; Chen, S. *J. Am. Chem. Soc.* **2004**, *126*, 4760.
13. Bond, A. D.; Derossi, S.; Jensen, F.; Larsen, F. B.; McKenzie, C. J.; Nelson, J. *Inorg. Chem.* **2005**, *44*, 5987.
14. Kou, X.; Zhao, M.; Qiao, X.; Zhu, Y.; Tong, X.; Shen, Z. *Chem. Eur. J.* **2013**, *19*, 16880.

15. Islam, M. J.; Smith, M. D.; Peryshkov, D. V. *J. of Organomet. Chem.* **2018**, *867*, 208.
16. Kalinin, V.; Ol'shevskaya, V. *Russ. Chem. Bull.* **2008**, *57*, 815.
17. Oertel, A. M.; Ritleng, V.; Chetcuti, M. J.; Veiros, L. F. *J. Am. Chem. Soc.* **2010**, *132*, 13588.
18. Lu, T.; Zhuang, X.; Li, Y.; Chen, S. *J. Am. Chem. Soc.* **2004**, *126*, 4760.
19. Bonesi, S. M.; Protti, S.; Albin, A. *J. Org. Chem.* **2016**, *81*, 11678.
20. Cho, J.; Kang, H. Y.; Liu, L. V.; Ritimukta Sarangi, Edward I. Solomon and Wonwoo Nam *Chem. Sci.* **2013**, *4*, 1502.
21. Hayyan, M.; Hashim, M. A.; AlNashef, I. M. *Chem. Rev.* **2016**, *116*, 3029.
22. Zhao, H.; Joseph, J.; Zhang, H.; Karoui, H.; Kalyanaraman, B. *Free Radical Biol. Med.* **2001**, *31*, 599.
23. Zeitler, H. E.; Kaminsky, W. A.; Goldberg, K. I. *Organometallics* **2018**, *37*, 3644.
24. Corcos, A. R.; Villanueva, O.; Walroth, R. C.; Sharma, S. K.; Bacsa, J.; Lancaster, K. M.; MacBeth, C. E.; Berry, J. F. *J. Am. Chem. Soc.* **2016**, *138*, 1796.
25. Shriver, D. F.; Drezdson, M. A. *The Manipulation of Air-sensitive Compounds, second ed.*, Wiley-Interscience, New York, **1986**, 2 edition.
26. APEX3 Version 2016.5-0 and SAINT+ Version 8.37A. Bruker AXS, Inc., Madison, Wisconsin, USA, **2016**.
27. Krause, L.; Herbst-Irmer, R.; Sheldrick G. M.; Stalke D. *J. Appl. Cryst.* **2015**, *48*, 3.
28. (a) Sheldrick, G. M. *Acta Cryst.* **2015**, *A71*, 3. (b) Sheldrick, G. M. *Acta Cryst.* **2015**, *C71*, 3.
29. Dolomanov, O. V., Bourhis, L. J., Gildea, R. J., Howard J. A. K.; Puschmann, H. *J. Appl. Cryst.* **2009**, *42*, 339.

30. APEX3 Version 2017.3-0, SAINT+ Version 8.38A, TWINABS Version 2012/1, Cell_Now Version 2008/4. Bruker Analytical X-ray Systems, Inc., Madison, Wisconsin, USA, 2016.

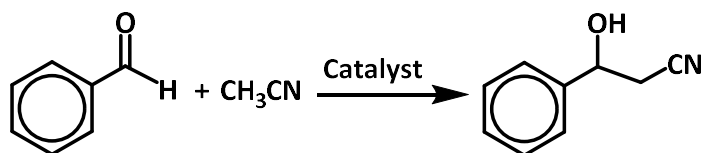
Chapter 4

Formation of Acrylamide *via* Coupling of Acetonitrile with Aldehyde,

Mediated by a CNC Ni(II) Complex: A Mechanistic Study

4.1 INTRODUCTION

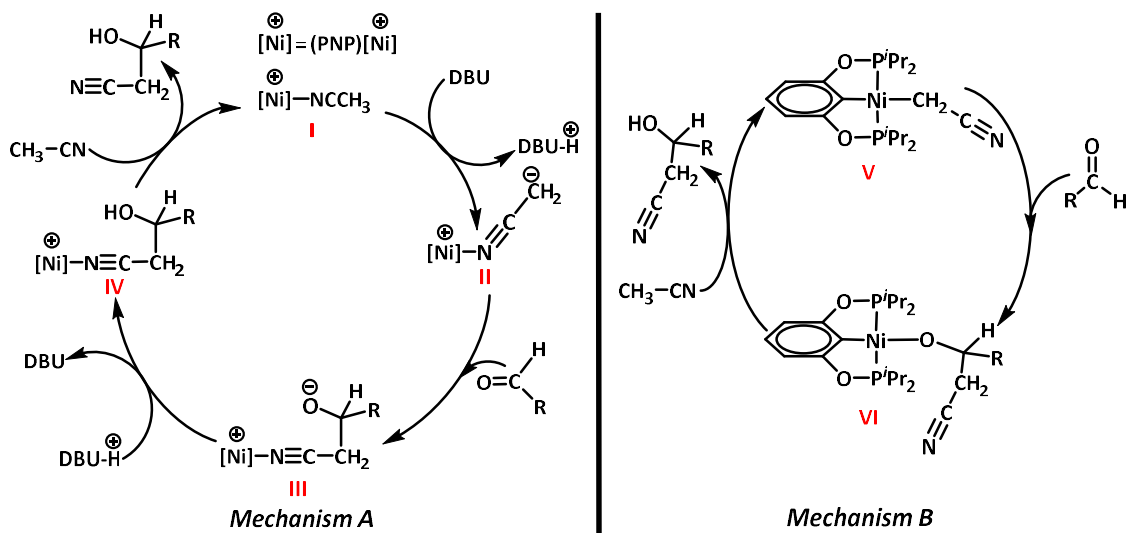
The formation of a C–C bond *via* nucleophilic addition of cyanoalkyl group with an aldehyde is an important route for synthesis of valuable commodities, such as β -hydroxy nitrile (**Scheme 4.1**),¹ an important intermediate in pharmaceuticals.² This synthetic pathway does not require highly toxic cyanide salts, and can be accessed through deprotonation of α C–H proton of nitrile. However, activation of a nitrile to render the essential carbanion is limited to the acidity of the α C–H proton, therefore, a strong base is often necessary for deprotonation.³⁻⁴ Among the nitriles, acetonitrile has been explored extensively because of its relatively acidic sp^3 C–H bond ($pK_a = 25$ in H_2O).⁵⁻⁶ Base assisted direct deprotonation of acetonitrile is often challenging due to the incompatibility of strong bases with base sensitive neighboring nitrile functionality.⁷ Lewis acidic transition metal complexes have offered a viable solution to address this issue by increasing α C–H acidity of *N*-bound acetonitrile.²



Scheme 4.1: Cyanomethylation of aldehyde to yield β -hydroxy nitrile.

Recently, Shibasaki and co-workers developed a soft Lewis acidic ruthenium complex that catalyzed nucleophilic addition of a cyanoalkyl group to an aldehyde by deprotonating a nitrile α C–H proton.⁸ Fan and Ozerov explored a PNP-type pincer ligand bearing a cationic Ni complex that used stoichiometric amount of base for the coupling of alkylnitrile with aldehyde (*Mechanism A*, **Scheme 4.2**).⁷ Guan and co-workers reported base free cyanomethylation of aldehyde by a nucleophilic cyanomethyl

Ni complex with a highest TON of 82000 (*Mechanism B*, **Scheme 4.2**).¹ These two Ni pincer complexes followed two distinct catalytic pathways for the coupling of the C–C bond. According to *Mechanism A*, the deprotonation of the coordinated acetonitrile by DBU (1,8-diazabicyclo[5.4.0]undec-7-ene) generated a nucleophilic *N*-bound cyanomethyl group which coupled with an electrophilic aldehyde to afford a β -hydroxy nitrile. In contrast, *Mechanism B* proposed the *C*-bound cyanomethyl Ni complex as the active catalyst that promoted the insertion of an aldehyde into the Ni–C bond to generate a Ni-alkoxide intermediate (**VI**). In the following step, the intermediate **VI** activated the C–H bond of acetonitrile by a “concerted metalation–deprotonation”-type pathway to yield β -hydroxy nitrile.⁹



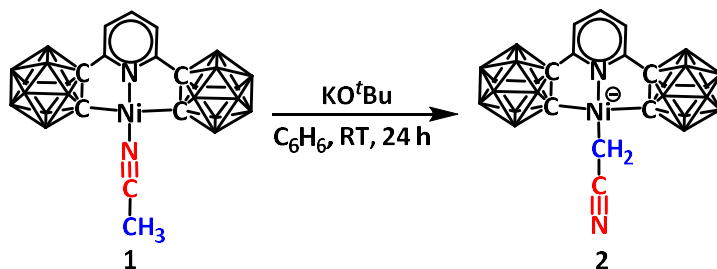
Scheme 4.2: *Mechanism A*: Base (DBU) initiated catalytic cycle proposed by Fan and Ozerov for cyanomethylation of aldehyde.⁷ *Mechanism B*: Base-free cyanomethylation of aldehyde proposed by Guan *et. al.*¹

In 2016, Canty and co-workers studied the mechanism of the nickel pincer complexes catalyzed cyanomethylation of aldehydes by density functional theory (DFT) calculations.² They explored the *N*-bound cyanomethyl Ni complex (**II**, *Mechanism A*),

not the *C*-bound isomer (**V**, *Mechanism B*), as the active catalyst for the C–C bond coupling reaction in both cases. The isomer **V** acts as a pre-catalyst, and has to convert to the less stable *N*-bound cyanomethyl complex (like **II**, in *Mechanism A*) to couple with aldehyde. Moreover, the insertion of an aldehyde to form *O*-bound isomer (**VI**, *Mechanism B*) is energetically less favorable compared to the formation of the pendant alkoxide function bearing zwitterionic intermediate (**III**, *Mechanism A*). The intermediate **III** is responsible for the activation of acetonitrile in the case of a base-free environment to yield β -hydroxy nitrile. However, the experimental evidence of this computational study is still elusive.

Recently, we reported a CNC pincer ligand featuring Ni(II) complex $\{(C_5H_3N)(C_2B_{10}H_{10})_2\}Ni(NCCH_3)$ (**1**) in which two electron deficient *ortho*-carborane clusters were employed as the donor arms of the pincer framework.¹⁰ The deprotonation of the acetonitrile ligand of **1** by KO^tBu followed by ligand flip resulted in the formation of the *C*-bound cyanomethyl complex $K[\{(C_5H_3N)(C_2B_{10}H_{10})_2\}Ni(CH_2NC)]$ (**2**) (**Scheme 4.3**) (see Chapter 3 for details). Herein, we report the experimental evidence that the *N*-bound cyanomethyl Ni complex as the active catalyst for the C–C bond coupling reactions, not the *C*-bound isomer, based on comparative studies on complexes **1** and **2**. When the nucleophilic *N*-bound cyanomethyl group was generated *in-situ* upon treatment of **1** by KO^tBu, it coupled with biphenyl-4-carboxaldehyde present in the reaction medium at room temperature before flipping to the *C*-coordination mode at the Ni(II) center. In contrast, the C–C coupling reaction proceeded slowly, even at higher temperature (105 °C) when the *C*-bound cyanomethyl complex **2** was employed under base free conditions. Presumably, heating at higher temperatures is essential to convert

the C-bound isomer to a N-bound active cyanomethyl group. These findings are in well agreement with the existing computational studies reported by Canty and co-workers.²



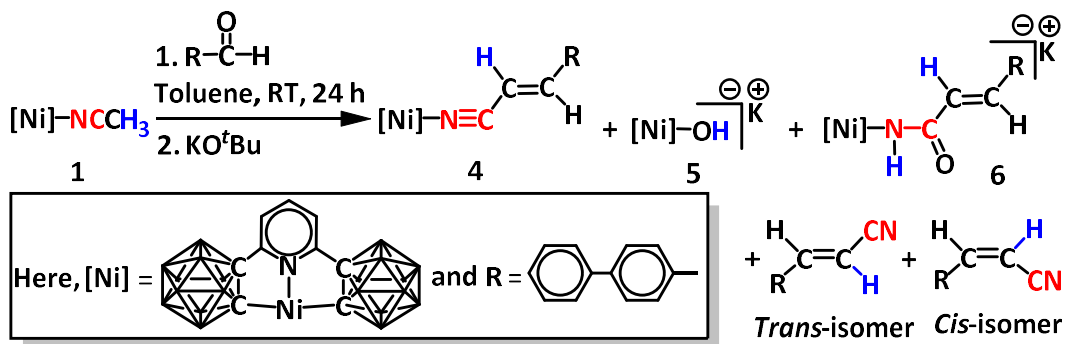
Scheme 4.3: Deprotonation of acetonitrile followed by ligand flip to afford C-bound cyanomethyl containing anionic CNC Ni(II) pincer complex (**2**) from N-bound acetonitrile bearing neutral CNC Ni(II) pincer complex (**1**).

In addition, we explored the formation of an unusual N-bound acrylamide Ni(II) complex $\text{K}[\{(\text{C}_5\text{H}_3\text{N})(\text{C}_2\text{B}_{10}\text{H}_{10})_2\}\text{Ni}(\text{C}_{15}\text{H}_{12}\text{NO})]$ (**6**), resulting from the dehydration of cyanoalcohol, followed by the hydration of the nitrile moiety promoted by an *in-situ* generated cationic Ni(II)–hydroxide complex $\text{K}[\{(\text{C}_5\text{H}_3\text{N})(\text{C}_2\text{B}_{10}\text{H}_{10})_2\}\text{Ni}(\text{OH})]$ (**5**). To the best of our knowledge, **6** is the first example where an acrylamide as a ligand is coordinated to a nickel(II) center *via* the nitrogen atom. The complexes **5** and **6** were isolated and characterized by an array of multinuclear NMR spectroscopic techniques and single crystal X-ray crystallography. Moreover, two isomers of free acrylonitrile were obtained from the same reaction mixture, and characterized by an array of multinuclear NMR spectroscopic techniques and mass spectrometry.

4.2 RESULTS AND DISCUSSION

The complexes, **1** and **2**, were synthesized by following our previously reported procedures (see Chapters 2 and 3). To explore the C–C bond coupling of acetonitrile with an aldehyde, one equivalent of KO^tBu was added in a solution of one equivalent of **1** and one equivalent of biphenyl–4–carboxaldehyde in toluene. The resulting mixture was

stirred at room temperature for 24 hours. The complex **5** was isolated as a yellow solid upon filtration, and the filtrate was collected and dried. The complex **6**, acrylonitrile coordinated Ni(II) complex Ni(N≡C–CH=CHC₁₂H₉)(C₉H₂₃B₂₀N) (**4**) and two isomers of biphenyl-4-acrylonitrile were purified from the filtrate by employing preparative TLC (Scheme 4.4).



Scheme 4.4: Reaction of **1**, aldehyde, and KO^tBu in benzene at room temperature.

The acrylonitrile coordinated neutral complex of Ni(II) (**4**) was isolated as a minor product during purification of **6** by TLC. Single crystals of **4** were obtained by slow diffusion of hexane into a saturated solution in dichloromethane inside a glovebox (Figure 4.1). The Ni1–N2 bond length is 1.827(2) Å in **4** is shorter than the Ni1–N2 bond of **6** (1.867(2) Å) and the N2–C10 bond is also shortened in **4** (1.141(3) Å) in comparison with **6** (1.323(4) Å). Slow hydrolysis of the nitrile moiety in **4** in air afforded free biphenyl-4-acrylamide that was characterized by ¹H and ¹³C NMR spectroscopy and mass spectrometry.

In the ¹H NMR spectrum of **5**, the resonance of the hydroxyl proton was observed as a broad singlet at –3.31 ppm. The ¹¹B and ¹¹B{¹H} NMR spectra exhibited a set of partially overlapping signals in the range from –3.45 ppm to –11.85 ppm.

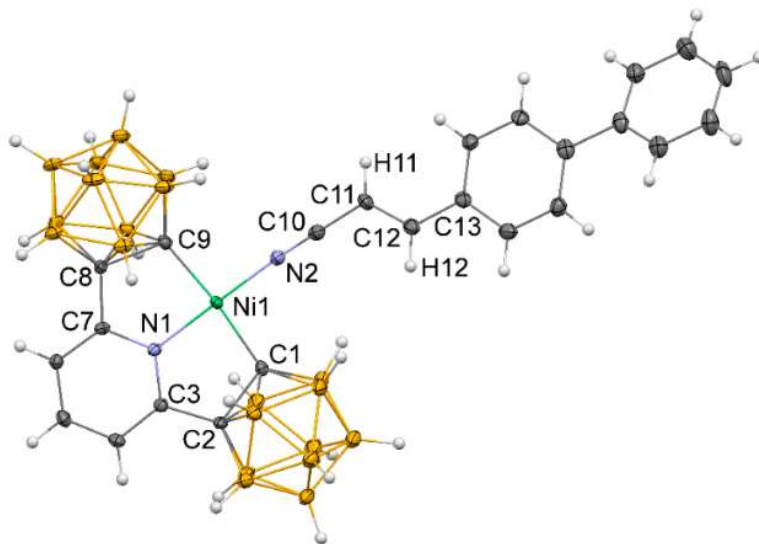


Figure 4.1: Crystal structure of $\text{Ni}(\text{N}\equiv\text{C}-\text{CH}=\text{CHC}_{12}\text{H}_9)(\text{C}_9\text{H}_{23}\text{B}_{20}\text{N})$ (**4**). The $\text{Ni1}-\text{N2}-\text{C10}$ bond angle is slightly deviated from linearity (174.69°).

The single crystals of air sensitive complex **5** were obtained by slow evaporation from dichloromethane/hexanes solvent mixture in the inert atmosphere of a nitrogen filled glovebox (**Figure 4.2**). The $\text{Ni1}-\text{O1}$, $\text{O1}-\text{H1}$ bond distances are $1.839(18)$ Å, 0.812 Å, respectively, and the $\text{Ni1}-\text{O1}-\text{H1}$ angle is 106.85° .

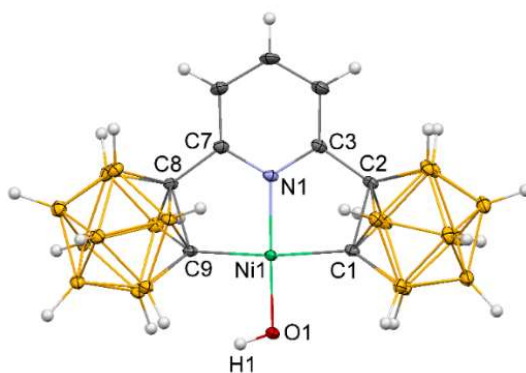
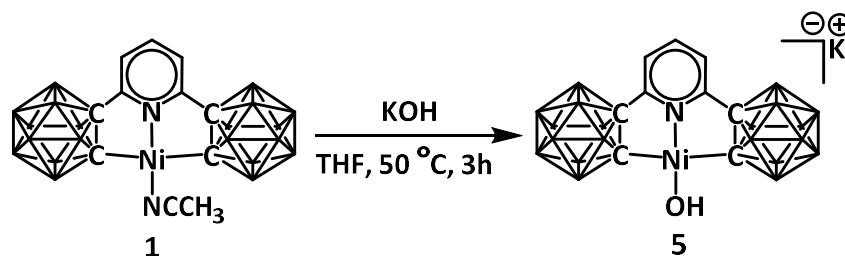


Figure 4.2: Crystal structure of $\text{K}[\{(\text{C}_5\text{H}_3\text{N})(\text{C}_2\text{B}_{10}\text{H}_{10})_2\}\text{Ni}(\text{OH})]$ (**5**).

The compound **5** can be synthesized alternatively *via* direct addition of KOH in a solution of **1** in THF under nitrogen atmosphere (**Scheme 4.5**).



Scheme 4.5: Alternative synthetic route of **5** from **1**.

The ^1H NMR spectrum of **6** in CD_2Cl_2 exhibited two coupled doublets at 6.15 ppm (integrated to one proton) and 7.66 ppm (integrated to one proton) for the two *trans*-olefinic protons. The *NH* resonance of the coordinated amide moiety was found as a broad singlet at 7.62 ppm. In the ^{11}B and $^{11}\text{B}\{^1\text{H}\}$ NMR spectra of **6**, a set of partially overlapping signals was observed in the range from -3.57 ppm to -11.13 ppm.

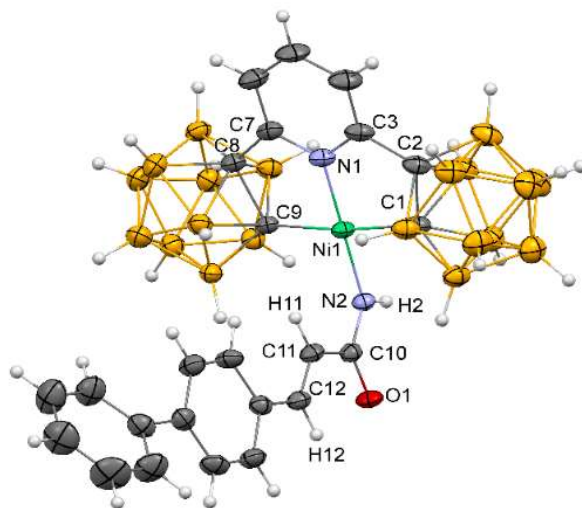
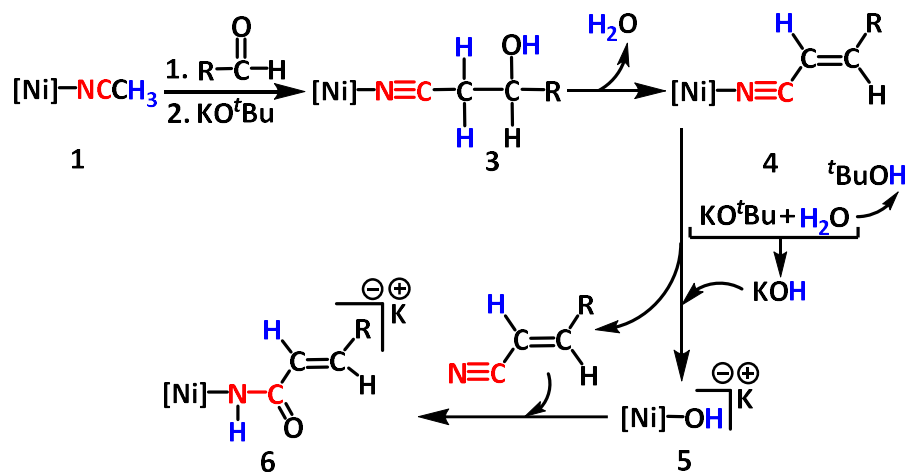


Figure 4.3: Crystal structure of $\text{K}\{[(\text{C}_5\text{H}_3\text{N})(\text{C}_2\text{B}_{10}\text{H}_{10})_2]\text{Ni}(\text{C}_{15}\text{H}_{12}\text{NO})\}$ (**6**). The Ni1–N2, N2–C10, C10–C11 bond distances are 1.867(2) Å, 1.323(4) Å, 1.473(4) Å, respectively.

Single crystals of **6** were grown from THF/hexanes solvent mixture by slow evaporation inside a nitrogen filled glovebox. The compound crystallizes in the space group *P*-1 of the triclinic system (**Figure 4.3**). The acrylamide ligand is coordinated with

the Ni1 atom *via* N2 atom with the Ni1–N2 bond length of 1.867(2) Å. The Ni1–N2–C10 angle is 128.4(2)° and C1–Ni1–C9 angle is 173.09(12)°.

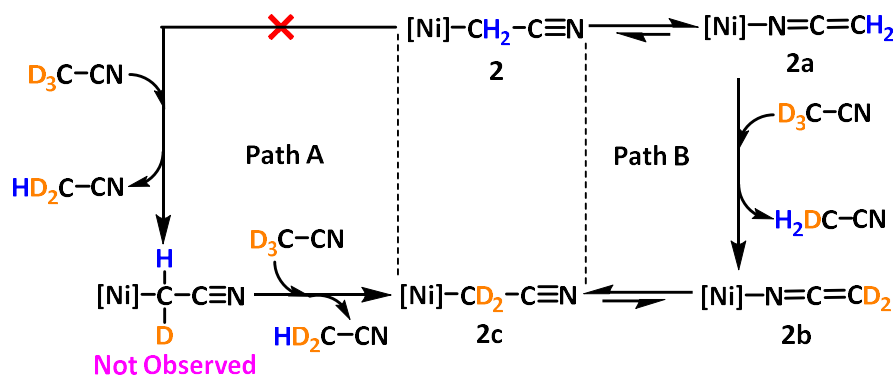


Scheme 4.6: Proposed mechanism for the formation of *N*-bound acrylamide bearing anionic complex (**6**). (*Cis*-acrylonitrile is omitted for clarity)

Typically, transition metal mediated coupling of a nucleophilic cyanomethyl group with an aldehyde yields β -hydroxy nitrile.^{1,2,6,7} However, as mentioned above we observed the formation of a *N*-bound acrylamide and two isomers of acrylonitrile as the C–C coupled products. We hypothesized that β -hydroxy nitrile bearing Ni (II) complex (**3**) was formed as an intermediate *via* the coupling of *N*-bound isomer with the aldehyde, which underwent α,β -dehydration to produce acrylonitrile containing intermediate **4** (**Scheme 4.6**). In the following step, **4** reacted with KOH (generated in the reaction $\text{KO}^t\text{Bu} + \text{H}_2\text{O} = \text{KOH}$) to afford Ni(II)-OH complex **5** and free acrylonitrile, by following a similar pathway as shown in **Scheme 4.5**. A number of pincer type Ni(II)-OH complexes have been reported as efficient catalysts for the hydration of nitriles to amides.^{11,17} We surmised that intermediate **5** mediated the selective hydration of nitrile moiety of the acrylonitrile ligand to yield *N*-bound acrylamide complex **6**. In a control experiment, when the reaction of **1**, biphenyl-4-carboxaldehyde and KO^tBu was

allowed to occur in the presence of molecular sieve as a dehydrating agent, we observed the formation of only **4** as a mixture of *cis*- and *trans*- acrylonitrile adducts. Therefore, *in-situ* formation of **5**, and its consecutive role on hydration of nitrile depends on the presence of water, which further supports the proposed mechanism as depicted in **Scheme 4.6**.

Intriguingly, the coupling of the *C*-bound cyanomethyl group of **2** with aldehyde in the presence of acetonitrile required elevated temperature, and proceeded at a slower rate, compared to the coupling of the *in-situ* generated *N*-bound isomer with aldehyde. Upon heating of a mixture of **2**, biphenyl-4-carboxaldehyde and acetonitrile in C₆D₆ inside a high-pressure J-Young NMR tube at 105 °C for 120 hours, we separated complex **6** and *cis*- and *trans*- isomers of biphenyl-4-acrylonitrile by employing preparative TLC. In addition, the formation of complex **1** was also observed in ¹H NMR spectrum. The requirement of higher temperature was attributed to the conversion step of **2** to its active *N*-bound isomeric form.



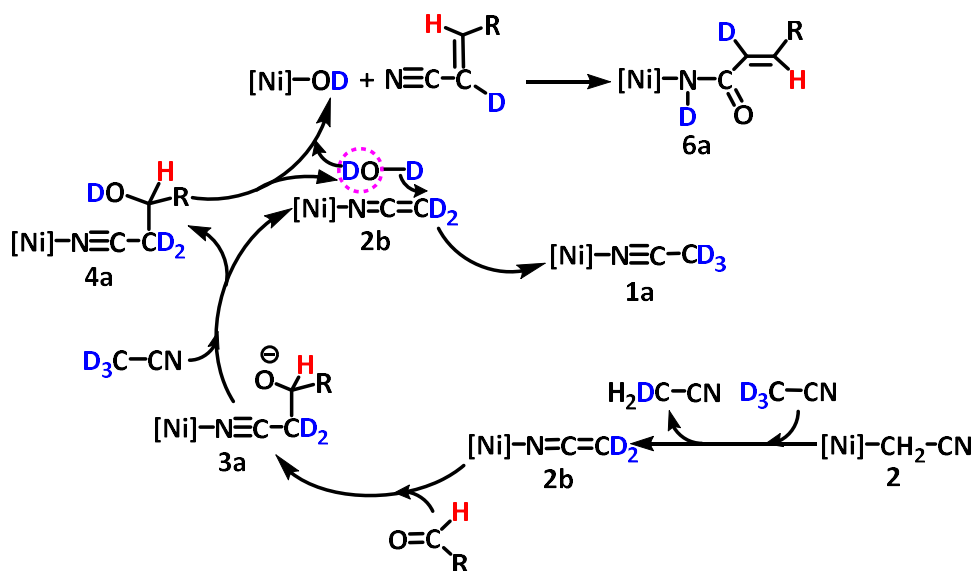
Scheme 4.7: Proposed pathway for the synthesis of deuterated *C*-bound cyanomethyl complex **2c** from **2** via formation of an unstable *N*-bound cyanomethyl isomer **2a**.

To explore the formation of an unstable *N*-bound isomer as the reactive species and reversibility of the isomerization process, we heated a mixture of **2** and CD₃CN in

C₆D₆ at 105 °C for 6 days. If the H–D exchange occurs at C–bound isomer **2**, stable mono-deuterated complex [Ni]–C(H)D–CN is expected to form as an intermediate before the formation of fully deuterated [Ni]–CD₂–CN (**Path A, Scheme 4.7**). However, after monitoring the progress of H–D exchange by ¹H NMR, we did not observe the characteristic H–D coupling which could be assigned to [Ni]–C(H)D–CN. Therefore, at elevated temperature the C–bound cyanomethyl group was converted to N–bound isomer that exchanged hydrogen with deuterium of CD₃–CN to yield NC–CD₂ anion and H₂DC–CN (**Path B, Scheme 4.7**). The anionic NC–CD₂ group immediately coordinated with the Ni(II) center *via* C–atom, manifested by the gradual disappearance of the C–bound cyanomethyl proton resonance at 1.05 ppm. In addition, the characteristic H–D coupling for H₂CD–CN was observed for its signal at 0.75 ppm in the ¹H NMR spectrum.

Surprisingly, the reaction of **2** with a biphenyl–4–carboxaldehyde in the presence of CD₃CN at 105 °C temperature after 4 days afforded deuterated acrylamide containing complex $K[\{(C_5H_3N)(C_2B_{10}H_{10})_2\}Ni(ND-CO-CD=CH-C_{12}H_9)]$, along with CD₃CN containing complex $\{(C_5H_3N)(C_2B_{10}H_{10})_2\}Ni(NCCD_3)$ (**1a**) and two isomers of deuterated acrylonitrile (**Scheme 4.8**). The formation of these final products clearly suggests the conversion of C–bound cyanomethyl group of **2** to a N–bound isomer (**2a, Scheme 4.7**) rendering active deuterated N–bound isomer **2b** (**Scheme 4.8**) and H₂DC–CN *via* H–D exchange. The isomer **2b** undergoes a C–C coupling reaction with the aldehyde to yield pendant alkoxide function which abstracts a deuterium from CD₃–CN to yield Ni(II)–bound deuterated cyanoalcohol. The α,β –elimination of D₂O from cyanoalcohol affords an acrylonitrile bearing complex, **4a**. The N–bound deuterated

cyanomethyl group accepts a deuterium from D₂O to produce **1a**, and the resulting OD⁻ group yields Ni(II)–OD complex (**2b**). The hydration of nitrile function of acrylonitrile mediated by **2b** afforded *N*-bound acrylamide complex **6a**.



Scheme 4.8: Proposed mechanism for the synthesis of **1a** and **6a**.

Under base-free conditions, the Ni–hydroxyl complex **5** was not observed, presumably due to its full conversion to *N*-bound amide complex **6** upon reaction with acrylonitrile at higher temperature. In addition, in the absence of acetonitrile no reaction was observed, thus, a proton source is required for the stabilization of an alkoxide bearing intermediate **3a** (**Scheme 4.8**) *via* formation of cyanoalcohol. In basic and base free conditions, the C–C bond coupling products were formed only in stoichiometric amount.

4.3 CONCLUSION

In conclusion, a comparative study on nucleophilic addition of a nitrile with an aldehyde was accomplished by employing a *N*-bound *in-situ* generated cyanomethyl complex (**1**) and a *C*-bound cyanomethyl complex (**2**) in basic and base-free conditions, respectively. In both conditions, we explored the *N*-bound cyanomethyl isomer as the

active species that undergoes nucleophilic attack on the carbonyl group of the aldehyde to afford β -hydroxy nitrile as an intermediate. The dehydration of cyanoalcohol generated acrylonitrile and a Ni–OH complex, **5**. The hydration of the nitrile functionality of the acrylonitrile mediated by **5** yielded unusual *N*-bound acrylamide complex, **6**.

4.4 EXPERIMENTAL SECTION

All synthetic manipulations, unless stated otherwise, were carried out either in a nitrogen-filled VAC drybox or on a dual manifold Schlenk-style vacuum line.¹² The solvents were sparged with nitrogen, passed through activated alumina, and stored over activated 4 Å Linde-type molecular sieves. C₆D₆, CDCl₃ and CD₂Cl₂ were degassed and stored over activated 4 Å Linde-type molecular sieves. NMR spectra were recorded using Varian spectrometers at 400 (¹H), 100 (¹³C), 128 (¹¹B) MHz, reported in δ (parts per million) and referenced to the residual ¹H/¹³C signals of the deuterated solvent or an external BF₃(Et₂O) (¹¹B(δ): 0.0 ppm) standard.

4.4.1 Synthesis of Biphenyl-4-acrylamide, *Cis*-biphenyl-4-acrylonitrile,

Trans-biphenyl-4-acrylonitrile, $\{(C_5H_3N)(C_2B_{10}H_{10})_2\}Ni(C_{12}H_9CH=CHCN)$ (**4**),

$K[\{(C_5H_3N)(C_2B_{10}H_{10})_2\}Ni(OH)]$ (**5**), and $K[\{(C_5H_3N)(C_2B_{10}H_{10})_2\}Ni(C_{15}H_{12}NO)]$ (**6**).

Potassium *tert*-butoxide (26 mg, 0.23 mmol) and biphenyl-4-carboxaldehyde (42 mg, 0.23 mmol) were transferred to a solution of 2,6-bis(carboranyl)pyridine nickel(II)(acetonitrile) (100 mg, 0.22 mmol) in toluene (10 mL) under nitrogen atmosphere in a glove box. The mixture was stirred at room temperature for 24 h, leading to a light yellow solution containing a yellow solid. The solution was filtered to isolate $K[\{(C_5H_3N)(C_2B_{10}H_{10})_2\}Ni(OH)]$ as a yellow solid, which was washed with benzene and dried in *vacuo* (15 mg, 0.031 mmol, 14% yield). The solvent of the yellow filtrate was

removed under vacuum, leaving a mixture of *trans*-biphenyl acrylonitrile, *cis*-biphenyl acrylonitrile, and $\text{K}[\{(\text{C}_5\text{H}_3\text{N})(\text{C}_2\text{B}_{10}\text{H}_{10})_2\}\text{Ni}(\text{C}_{15}\text{H}_{12}\text{NO})]$. The mixture was washed with hexane (3 × 3 mL) to separate *trans*-biphenyl-4-acrylonitrile and *cis*-biphenyl-4-acrylonitrile from $\text{K}[\{(\text{C}_5\text{H}_3\text{N})(\text{C}_2\text{B}_{10}\text{H}_{10})_2\}\text{Ni}(\text{C}_{15}\text{H}_{12}\text{NO})]$. Preparative TLC was performed to purify *trans*-biphenyl-4-acrylonitrile (5 mg, 0.024 mmol, 11% yield) and *cis*-biphenyl-4-acrylonitrile (3 mg, 0.015 mmol, 7% yield). The yellow powder of $\text{K}\{(\text{C}_5\text{H}_3\text{N})(\text{C}_2\text{B}_{10}\text{H}_{10})_2\}\text{Ni}(\text{C}_{15}\text{H}_{12}\text{NO})$ was washed with benzene and dried in *vacuo* (20 mg, 0.029 mmol, 13% yield). Preparative TLC (using Al_2O_3 plate) was performed to purify $\text{K}[\{(\text{C}_5\text{H}_3\text{N})(\text{C}_2\text{B}_{10}\text{H}_{10})_2\}\text{Ni}(\text{C}_{15}\text{H}_{12}\text{NO})]$ by removing an unknown impurity present in hexane, while $\{(\text{C}_5\text{H}_3\text{N})(\text{C}_2\text{B}_{10}\text{H}_{10})_2\}\text{Ni}(\text{C}_{12}\text{H}_9\text{CH}=\text{CHCN})$ was also isolated as a minor product from the TLC plate. Biphenyl-4-acrylamide ($\text{C}_{12}\text{H}_9\text{CH}=\text{CH}-\text{CONH}_2$) (2 mg, 0.009 mmol, 4% yield) was formed by ligand dissociation during further purification of $\{(\text{C}_5\text{H}_3\text{N})(\text{C}_2\text{B}_{10}\text{H}_{10})_2\}\text{Ni}(\text{C}_{12}\text{H}_9\text{CH}=\text{CHCN})$ by preparative TLC.

$\text{K}[\{(\text{C}_5\text{H}_3\text{N})(\text{C}_2\text{B}_{10}\text{H}_{10})_2\}\text{Ni}(\text{OH})]$: ^1H NMR (CD_2Cl_2): δ 7.68 (t, 1H, $\text{C}_5\text{H}_3\text{N}$), 7.10 (d, 2H, $\text{C}_5\text{H}_3\text{N}$), 3.20–1.30 (overlapping, 20H, B–H, $\text{C}_2\text{B}_{10}\text{H}_{10}$), –3.31 (s, 1H, OH). $^{11}\text{B}\{^1\text{H}\}$ NMR (CD_2Cl_2): δ –4.02, –6.66, –11.32. ^{13}C NMR (CD_2Cl_2): δ 159.73 ($\text{C}_5\text{H}_3\text{N}$), 139.09 ($\text{C}_5\text{H}_3\text{N}$), 121.16 ($\text{C}_5\text{H}_3\text{N}$), 80.48 ($\text{C}_2\text{H}_{10}\text{B}_{10}$), 75.62 ($\text{C}_2\text{H}_{10}\text{B}_{10}$).

$\text{K}\{(\text{C}_5\text{H}_3\text{N})(\text{C}_2\text{B}_{10}\text{H}_{10})_2\}\text{Ni}(\text{C}_{15}\text{H}_{12}\text{NO})$: ^1H NMR (CD_2Cl_2): δ 7.81 (t, 1H, $\text{C}_5\text{H}_3\text{N}$), 7.75–7.40 (m, 9H, C_6H_5 – C_6H_4 –; broad, 1H, –CO–NH–; 1H, –CH=CH–CO–) 7.23 (d, 2H, $\text{C}_5\text{H}_3\text{N}$), 6.11 (d, 1H, –CH=CH–CO–), 3.30–1.60 (overlapping, 20H, B–H, $\text{C}_2\text{B}_{10}\text{H}_{10}$). $^{11}\text{B}\{^1\text{H}\}$ NMR (CD_2Cl_2): δ –3.57, –6.76, –10.86. ^{13}C NMR (CD_2Cl_2): δ 161.33 ($\text{C}_5\text{H}_3\text{N}$), 155.92 (–CH=CH–CO–), 145.81 (– C_6H_4 –), 141.40 (C_6H_5 –), 139.80

(C₅H₃N), 131.98 (-C₆H₄-CH=CH-), 129.42 (-C₆H₄-), 129.24 (-C₆H₄-), 128.85 (-C₆H₄-), 128.70 (C₆H₅-), 128.23 (C₆H₅-), 127.48 (C₆H₅-), 121.70 (C₅H₃N), 93.05 (-CH=CH-CO-), 80.03 (C₂H₁₀B₁₀), 73.53 (C₂H₁₀B₁₀).

C₆H₅-C₆H₄-CH=CH-CO-NH₂ (Biphenyl-4-acrylamide): ¹H NMR (CDCl₃): δ 7.68 (d, 1H, -C₆H₄-CH=CH-), 7.65–7.37 (m, 9H, C₆H₅-C₆H₄-), 6.48 (d, 1H, -CH=CH-CO-), 5.49 (b, 2H, -CO-NH₂). ¹³C NMR (CDCl₃): δ 167.70 (-CO-NH₂), 142.96 (-C₆H₄-), 142.36 (-C₆H₄-CH=CH-), 140.35 (C₆H₅-), 133.59 (-C₆H₄-), 129.05 (-C₆H₄-), 128.59 (C₆H₅-), 127.96 (C₆H₅-), 127.69 (C₆H₄-), 127.19 (C₆H₅-), 119.32 (-CH=CH-CO-). **HRMS** (EI, m/z): calculated for [C₁₅H₁₃NO]⁺ 223.0997, found 223.0994.

C₆H₅-C₆H₄-CH=CH-CN (Cis-biphenyl-4-acrylonitrile): ¹H NMR (CD₂Cl₂): δ 7.89 (δ, 2H, -C₆H₄-), 7.70 (d, 2H, -C₆H₄-), 7.65 (d, 2H, C₆H₅-), 7.48 (t, 2H, C₆H₅-), 7.39 (t, 1H, C₆H₅-), 7.18 (d, 1H, -C₆H₄-CH=CH-), 5.48 (d, 1H, -CH=CH-CN). ¹³C NMR (CD₂Cl₂): δ 148.42 (-C₆H₄-CH=CH-), 129.92 (-C₆H₄-), 129.34 (C₆H₅-), 128.46 (C₆H₅-), 127.80 (-C₆H₄-), 127.47 (C₆H₅-), 122.71 (-CN), 95.29 (-CH=CH-CN).

C₆H₅-C₆H₄-CH=CH-CN (Trans-biphenyl-4-acrylonitrile): ¹H NMR (CD₂Cl₂): δ 7.64 (m, 4H, -C₆H₄-), 7.55 (d, 2H, C₆H₅-), 7.48 (m, 2H, C₆H₅-; 1H, -C₆H₄-CH=CH-), 7.39 (t, 1H, C₆H₅-), 5.97 (d, 1H, -CH=CH-CN).

4.4.2 Reaction of K[{(C₅H₃N)(C₂B₁₀H₁₀)₂Ni(CH₂NC)] (**2**),

biphenyl-4-carboxaldehyde and acetonitrile

Biphenyl-4-carboxaldehyde (5 mg, 0.027 mmol) and acetonitrile (20 μL) were added to a solution of **2** (5 mg, 0.01 mmol) in C₆D₆ in a vial under nitrogen atmosphere. A

portion of the solution was transferred to a high-pressure J–Young NMR tube, and heated at 105 °C in a pre-heated oil bath for 4 days. The products were isolated by employing preparative TLC, and characterized by ¹H NMR spectroscopy.

4.4.3 Reaction of K[$\{(C_5H_3N)(C_2B_{10}H_{10})_2\}Ni(CH_2NC)$] (2**),**

biphenyl–4–carboxaldehyde and acetonitrile–*d*₃

Biphenyl–4–carboxaldehyde (5 mg, 0.027 mmol), acetonitrile–*d*₃ (5 μL) were added to a solution of **2** (5 mg, 0.01 mmol) in C₆D₆ in a vial under nitrogen atmosphere. A portion of the solution was transferred to a high-pressure J–Young NMR tube, and heated at 105 °C in a pre-heated oil bath for 4 days. The products were isolated by employing preparative TLC, and characterized by ¹H NMR spectroscopy.

4.4.4 H–D exchange reaction of K[$\{(C_5H_3N)(C_2B_{10}H_{10})_2\}Ni(CH_2NC)$] (2**) and**

acetonitrile–*d*₃

Acetonitrile–*d*₃ (5 μL) was added to a solution of **2** (5 mg, 0.01 mmol) in C₆D₆ under nitrogen atmosphere. A small portion of the solution was transferred in a high-pressure J–Young NMR tube, and heated at 105 °C in a pre-heated oil bath for 6 days. The progress of H–D exchange was monitored by the ¹H NMR spectroscopy.

4.4.5 CRYSTAL STRUCTURE DETERMINATION DETAILS

X-ray intensity data were collected at 100(2) K using a Bruker D8 QUEST diffractometer equipped with a PHOTON-100 CMOS area detector and an Incoatec microfocus source (Mo K α radiation, $\lambda = 0.71073$ Å). The raw area detector data frames were reduced, scaled and corrected for absorption effects using the Bruker APEX3, SAINT+ and SADABS programs.¹³⁻¹⁴ Final unit cell parameters were determined by least-squares refinement of 9990 reflections taken from the data set. The structure was

solved with SHELXT.¹⁵ Subsequent difference Fourier calculations and full-matrix least-squares refinement against F^2 were performed with SHELXL-2018¹⁵ using OLEX2.¹⁶

4.4.5.1 X-Ray Structure Determination of Ni(N≡CCH=CHC₁₂H₉)(C₉H₂₃B₂₀N) (4)

The compound crystallizes in the monoclinic system. The pattern of systematic absences in the intensity data was consistent with the space group $P2_1/c$, which was confirmed by structure solution. The asymmetric unit consists of one molecule. All non-hydrogen atoms were refined with anisotropic displacement parameters. Hydrogen atoms bonded to carbon were located in difference Fourier maps before being placed in geometrically idealized positions and included as riding atoms with $d(\text{C-H}) = 0.95 \text{ \AA}$ and $U_{\text{iso}}(\text{H}) = 1.2U_{\text{eq}}(\text{C})$. Hydrogen atoms bonded to boron atoms of the carborane cages were located in difference maps and refined freely. The largest residual electron density peak in the final difference map is $0.27 \text{ e}^-/\text{\AA}^3$, located 0.43 \AA from H20.

Crystal Data for C₂₄H₃₄B₂₀N₂Ni ($M = 625.44 \text{ g/mol}$): monoclinic, space group $P2_1/c$ (no. 14), $a = 21.9177(17) \text{ \AA}$, $b = 7.1427(5) \text{ \AA}$, $c = 21.5746(17) \text{ \AA}$, $\beta = 106.614(2)^\circ$, $V = 3236.5(4) \text{ \AA}^3$, $Z = 4$, $T = 100(2) \text{ K}$, $\mu(\text{MoK}\alpha) = 0.623 \text{ mm}^{-1}$, $D_{\text{calc}} = 1.284 \text{ g/cm}^3$, 36330 reflections measured ($4.672^\circ \leq 2\theta \leq 50.378^\circ$), 5804 unique ($R_{\text{int}} = 0.0721$, $R_{\text{sigma}} = 0.0409$) which were used in all calculations. The final R_1 was 0.0392 ($I > 2\sigma(I)$) and wR_2 was 0.0946 (all data).

4.4.5.2 X-Ray Structure Determination of K₂(CH₂Cl₂)₄[Ni(OH)(C₉H₂₃B₂₀N)]₂·CH₂Cl₂ (5)

The compound crystallizes in the triclinic system. The space group $P-1$ was confirmed by structure solution. The asymmetric unit consists of half of one K₂(CH₂Cl₂)₄[Ni(OH)(C₉H₂₃B₂₀N)]₂ complex located on a crystallographic inversion

center and half of a non-coordinated dichloromethane molecule, also situated about an inversion center. The non-coordinated dichloromethane is disordered within the asymmetric unit over three sites. The occupancy sum of the three components was constrained to sum to 0.5, and $d(\text{C-Cl}) = 1.75 \text{ \AA}$ and $d(\text{Cl-Cl}) = 2.89 \text{ \AA}$ distance restraints were applied. All non-hydrogen atoms were refined with anisotropic displacement parameters except for disordered atoms (isotropic). Hydrogen atoms bonded to carbon were placed in geometrically idealized positions and included as riding atoms with $d(\text{C-H}) = 0.95 \text{ \AA}$ and $U_{\text{iso}}(\text{H}) = 1.2U_{\text{eq}}(\text{C})$ for aromatic hydrogen atoms and $d(\text{C-H}) = 0.99 \text{ \AA}$ and $U_{\text{iso}}(\text{H}) = 1.2U_{\text{eq}}(\text{C})$ for methylene hydrogen atoms. Hydrogen atoms bonded to boron atoms of the carborane cage were located in difference Fourier maps and refined freely. The largest residual electron density peak in the final difference map is $1.68 \text{ e}^-/\text{\AA}^3$, located 0.98 \AA from Cl4.

Crystal Data for $\text{C}_{23}\text{H}_{58}\text{B}_{40}\text{Cl}_{10}\text{K}_2\text{N}_2\text{Ni}_2\text{O}_2$ ($M = 1377.23 \text{ g/mol}$): triclinic, space group $P-1$ (no. 2), $a = 10.4109(4) \text{ \AA}$, $b = 11.2533(4) \text{ \AA}$, $c = 14.1066(5) \text{ \AA}$, $\alpha = 93.9110(15)^\circ$, $\beta = 102.0035(15)^\circ$, $\gamma = 103.4383(14)^\circ$, $V = 1560.45(10) \text{ \AA}^3$, $Z = 1$, $T = 100(2) \text{ K}$, $\mu(\text{MoK}\alpha) = 1.198 \text{ mm}^{-1}$, $D_{\text{calc}} = 1.466 \text{ g/cm}^3$, 57200 reflections measured ($4.492^\circ \leq 2\Theta \leq 55.468^\circ$), 7333 unique ($R_{\text{int}} = 0.0538$, $R_{\text{sigma}} = 0.0405$) which were used in all calculations. The final R_1 was 0.0448 ($I > 2\sigma(I)$) and wR_2 was 0.1076 (all data).

4.4.5.3 X-Ray Structure Determination of

$[\text{K}(\text{C}_4\text{H}_8\text{O})_3\text{Ni}(\text{C}_{15}\text{H}_{12}\text{NO})(\text{C}_9\text{H}_{23}\text{B}_{20}\text{N})]_2 \cdot 4(\text{C}_4\text{H}_8\text{O})$ (6)

The compound crystallizes in the space group $P-1$ of the triclinic system. The asymmetric unit consists of half of one $[\text{K}(\text{C}_4\text{H}_8\text{O})_3\text{Ni}(\text{C}_{15}\text{H}_{12}\text{NO})(\text{C}_9\text{H}_{23}\text{B}_{20}\text{N})]_2$ complex, which is located on a crystallographic inversion center, and two non-

coordinated THF molecules. One coordinated THF (O5, C51-C54) and both non-coordinated THF molecules (O6, C61-C64 and O7, C71-C74) are disordered. The disorder of O5/C51-C54 is minor and was modeled with one split carbon atom (C54A/C54B), whose occupancies were fixed at 0.5 each. The non-coordinated THF molecules were each modeled with three disorder components. Total site occupancies for each were constrained to sum to one. The geometry of each component was restrained to be similar to that of an ordered THF (O3/C31-C34) using SHELX SAME instructions. All non-hydrogen atoms were refined with anisotropic displacement parameters except for the non-coordinated THF molecules (isotropic). Hydrogen atoms bonded to carbon were placed in geometrically idealized positions and included as riding atoms with $d(\text{C-H}) = 0.95 \text{ \AA}$ and $U_{\text{iso}}(\text{H}) = 1.2U_{\text{eq}}(\text{C})$ for aromatic hydrogen atoms and $d(\text{C-H}) = 0.99 \text{ \AA}$ and $U_{\text{iso}}(\text{H}) = 1.2U_{\text{eq}}(\text{C})$ for methylene hydrogen atoms. Hydrogen atoms bonded to boron were located in difference Fourier maps and refined freely. The hydrogen atom bonded to nitrogen N2 was located and refined isotropically subject to a $d(\text{N-H}) = 0.86(2) \text{ \AA}$ distance restraint. The largest residual electron density peak in the final difference map is 0.46 e-/\AA^3 , located 0.62 \AA from C72B.

Crystal Data for $\text{C}_{88}\text{H}_{150}\text{B}_{40}\text{K}_2\text{N}_4\text{Ni}_2\text{O}_{12}$ ($M = 2084.13 \text{ g/mol}$): triclinic, space group $P-1$ (no. 2), $a = 11.0032(4) \text{ \AA}$, $b = 13.0481(5) \text{ \AA}$, $c = 21.2374(8) \text{ \AA}$, $\alpha = 72.806(2)^\circ$, $\beta = 79.465(2)^\circ$, $\gamma = 82.739(2)^\circ$, $V = 2855.20(19) \text{ \AA}^3$, $Z = 1$, $T = 190(2) \text{ K}$, $\mu(\text{MoK}\alpha) = 0.458 \text{ mm}^{-1}$, $D_{\text{calc}} = 1.212 \text{ g/cm}^3$, 74063 reflections measured ($4.312^\circ \leq 2\theta \leq 50.168^\circ$), 10134 unique ($R_{\text{int}} = 0.0622$, $R_{\text{sigma}} = 0.0445$) which were used in all calculations. The final R_1 was 0.0561 ($I > 2\sigma(I)$) and wR_2 was 0.1356 (all data).

REFERENCES

1. Chakraborty, S.; Patel, Y. J.; Krause, J. A.; Guan, H. *Angew. Chem. Int. Ed.* **2013**, *52*, 7523.
2. Ariafard, A.; Ghari, H.; Khaledi, Y.; Bagi, A. H.; Wierenga, T. S.; Gardiner, M. G.; Canty, A. J. *ACS Catal.* **2016**, *6*, 60.
3. a) Kaiser, E. M.; Hauser, C. R. *J. Am. Chem. Soc.* **1967**, *89*, 4566. b) Lin, Y.; Zhu, X.; Xiang, M. *J. Organomet. Chem.* **1993**, *448*, 215. c) Murahashi, S. I.; Naota, T.; Taki, H.; Mizuno, M.; Takaya, H.; Komiya, S.; Mizuho, Y.; Oyasato, N.; Hiraoka, M.; Hirano, M.; Fukuoka, A. *J. Am. Chem. Soc.* **1995**, *117*, 12436. d) Motokura, K.; Nishimura, D.; Mori, K.; Mizugaki, T.; Ebitani, K.; Kaneda, K. *J. Am. Chem. Soc.* **2004**, *126*, 5662. e) Cheung, H. W.; Li, J.; Zheng, W.; Zhou, Z.; Chiu, Y. H.; Lin, Z.; Lau, C. P. *Dalton Trans.* **2010**, *39*, 265. f) Yazaki, R.; Kumagai, N.; Shibasaki, M. *J. Am. Chem. Soc.* **2010**, *132*, 5522.
4. a) Kaiser, E. M.; Hauser, C. R. *J. Org. Chem.* **1968**, *33*, 3402. b) Li, N. -S.; Yu, S.; Kabalka, G. W. *J. Org. Chem.* **1995**, *60*, 5973. c) Kisanga, P.; McLeod, D.; DSa, B.; Verkade, J. *J. Org. Chem.* **1999**, *64*, 3090. d) Rodriguez, A. L.; Bunlaksananusorn, T.; Knochel, P. *Org. Lett.* **2000**, *2*, 3285. e) Bunlaksananusorn, T.; Rodriguez, A. L.; Knochel, P. *Chem. Commun.* **2001**, 745. f) Sott, R.; Granander, J.; Hilmersson, G. *J. Am. Chem. Soc.* **2004**, *126*, 6798. g) Fleming, F. F.; Vu, V. A.; Shook, B. C.; Rahman, M.; Steward, O. W. *J. Org. Chem.* **2007**, *72*, 1431. h) Fleming, F. F.; Liu, W.; Ghosh, S.; Steward, O. W. *J. Org. Chem.* **2008**, *73*, 2803.
5. Anslyn, E. V.; Dougherty, D. A. *Modern Physical Organic Chemistry*; University Science Books: Sausalito, CA, **2006**.
6. Smith, J. B.; Miller, A. J. M. *Organometallics* **2015**, *34*, 4669.

7. Fan, L.; Ozerov, O. V. *Chem. Commun.* **2005**, 4450.
8. Kumagai, N.; Matsunaga, S.; Shibasaki, M. *J. Am. Chem. Soc.* **2004**, *126*, 13632.
9. Lapointe, D.; Fagnou, K. *Chem. Lett.* **2010**, *39*, 1118.
10. Islam, M. J.; Smith, M. D.; Peryshkov, D. V. *J. Organomet. Chem.* **2018**, *867*, 208.
11. Garcia, J. B.; Gutsulyak, D. V.; Burford, R. J.; Piers, W. E. *Dalton Trans.*, **2015**, *44*, 12082.
12. Shriver, D. F.; Drezdson, M. A. *The Manipulation of Air-sensitive Compounds*, second ed., Wiley-Interscience, New York, **1986**, 2 edition.
13. APEX3 Version 2016.5-0 and SAINT+ Version 8.37A. Bruker AXS, Inc., Madison, Wisconsin, USA, **2016**.
14. Krause, L.; Herbst-Irmer, R.; Sheldrick G. M.; Stalke D. *J. Appl. Cryst.* **2015**, *48*, 3.
15. (a) Sheldrick, G. M. *Acta Cryst.* **2015**, *A71*, 3. (b) Sheldrick, G. M. *Acta Cryst.* **2015**, *C71*, 3.
16. Dolomanov, O. V., Bourhis, L. J., Gildea, R. J., Howard J. A. K.; Puschmann, H. *J. Appl. Cryst.* **2009**, *42*, 339.
17. Anderson, N. H.; Boncella, J. M.; Tondreau, A. M. *Organometallics* **2018**, *37*, 4675.

Chapter 5

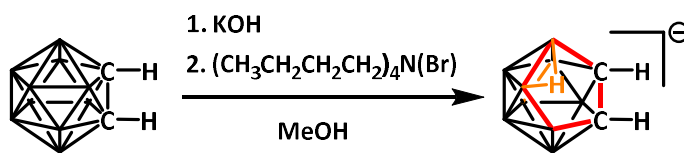
Synthesis and Characterization of Doubly Deboronated

2,6-bis{*nido*-(*ortho*-carborane)}pyridine Ligand and its Ruthenacarborane

Clusters

5.1 INTRODUCTION

In the last five decades, metallocarborane chemistry has advanced in various directions, and has become a major subdiscipline of inorganic and organometallic chemistry.¹ The applications of metallocarboranes have spanned across numerous fields, including catalysis, medicine and pharmacology, environmental chemistry and material science, because of their unique structure, great tunability, unparalleled stability and reactivity.²⁻³ Among the metallocarboranes, the icosahedral (12 vertex) framework with a general formula of $C_2B_9H_{11}M$ (M = metal) is one of the most common types reported in literature.³ The *nido*-carborane anion $7,8-C_2B_9H_{12}$ is a precursor for a large number of metallocarboranes which can be obtained by the removal of the most electropositive boron atom B3 or B6 of *ortho*-carborane. The decapitation of the boron vertex to yield *nido*-carborane is typically accomplished by employing alcoholic potassium hydroxide as a strong nucleophile, followed by cation exchange upon addition of tetrabutylammonium bromide (**Scheme 5.1**).⁴ Unlike an *exo*-metal complex of carborane, in a metallocarborane the metal is incorporated into the cluster framework upon removal of the bridging proton (B-H-B).⁴ The metal center of a metallocarborane cluster can be bonded simultaneously with other ligands, such as arenes.⁵⁻⁷



Scheme 5.1: Removal of B3/B6 atom by using methanolic KOH to yield *nido*-carborane anion $7,8-C_2B_9H_{12}$.

The *C*-functionalized metallocarboranes, specifically those derived from 1,1'-bis(*ortho*-carborane) have attracted significant attention in the last few years.⁸⁻¹⁰

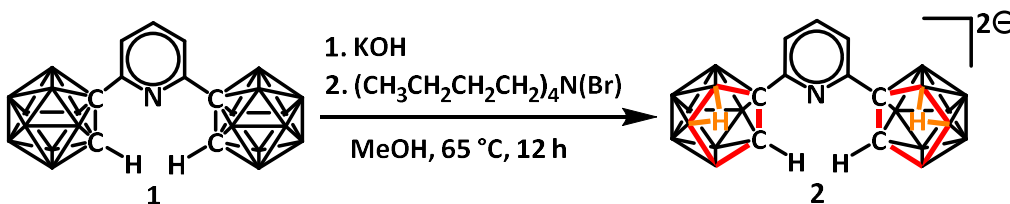
The compound 1,1'-bis(*ortho*-carborane) consists of two *ortho*-carborane clusters coupled with a C-C single bond.¹¹⁻¹³ The recent advancement of 1,1'-bis(*ortho*-carborane) chemistry is attributed to the CuCl assisted facile synthetic procedure explored by Xie and co-workers in 2008.¹² Welch and co-workers are the pioneer for the exploration of 1,1'-bis(*ortho*-carborane) based metallocarboranes. In 2010, they reported the C-C bond activation of an arene by a ruthenium based metallocarborane in which only one cage of 1,1'-bis(*ortho*-carborane) was metallated.⁵ The same group explored internally crowded cobalt containing first supracosahedral bis(heteroborane) as a mixture of racemic and meso diastereoisomers.⁸ Their other remarkable works include the synthesis of single deboronation and metalation,⁹ and double deboronation and metalation¹⁰ of 1,1'-bis(*ortho*-carborane) ligand.

Recently, we have reported the synthesis of the novel 2,6-bis(*ortho*-carborane)pyridine $\{(C_5H_3N)(C_2B_{10}H_{11})_2\}$ ligand in which two *ortho*-carborane clusters are connected to the pyridine backbone of a pincer-type framework.¹⁴ To the best of our knowledge, metallocarboranes based on bis(carborane) isolated by a linker has not been reported yet. Herein, we report the synthesis of Ru-metallocarboranes as a mixture of racemic and meso isomers derived from a doubly deboronated 2,6-bis(*ortho*-carborane)pyridine ligand. The isomers were isolated by performing preparative TLC, and were characterized by an array of multinuclear NMR spectroscopic techniques and single crystal X-ray crystallography.

5.2 RESULTS AND DISCUSSION

5.2.1 Double Deboronation of 2,6-bis(*ortho*-carborane)pyridine (**1**)

The ligand **1** was synthesized by following a procedure reported by our group recently.¹⁴ Double deboronation was accomplished by adding five equivalents of KOH to a solution of **1** in methanol, and heating the resulting mixture at 65°C for 12 hours. After removing methanol, the solid was dissolved in water, and five equivalents of tetrabutylammonium bromide ((Bu₄NBr)) was added to separate the double deboronated ligand as a water insoluble salt [2,6-bis{nido-(*ortho*-carborane)}pyridine](NBu₄)₂ (**2**) (Scheme 5.2).



Scheme 5.2: Synthesis of [2,6-bis{nido-(*ortho*-carborane)}pyridine](NBu₄)₂ (**2**).

The compound, **2**, was characterized by an array of ¹H, ¹¹B{¹H}, ¹¹B and ¹³C NMR spectroscopy, and single crystal X-ray crystallography. In ¹H NMR, a characteristic signal was observed at 2.18 ppm for the two C–H protons of the two *nido*-clusters, and the two bridging (B–H–B) protons exhibited a broad signal at –2.44 ppm. Hawthorne and co-workers hypothesized that in the case of double deboronation of 1,1'-bis(*ortho*-carborane), the meso form is more likely to form because of its higher stability.¹⁵ Recently, Welch and co-workers demonstrated the formation of a mixture of both racemic and meso diastereoisomers upon double deboronation of 1,1'-bis(*ortho*-carborane). Based on ¹¹B{¹H} spectra, they described two sets of resonances which indicated the sample being a mixture of diastereoisomers.¹⁰ In our case,

we observed only one set of resonance in $^{11}\text{B}\{^1\text{H}\}$ NMR of **2** which supports the presence of only the racemic isomeric form.

The complete structural elucidation by single crystal X-ray crystallography was problematic because of extensive disorder, however, the basic structure was established. Frustratingly, hydrogen atoms distribution on the clusters was not possible to assign, and the position of the two bridged protons could not be resolved due to disorder. The rotation of both of the *nido*-clusters about C2–C3 and C7–C9 bonds afforded two orientations that were superimposed to each other. Therefore, a combination of data from NMR spectroscopy and single crystal X-ray crystallography support the formation of the racemic isomer upon double deboronation of 2,6-bis(*ortho*-carborane)pyridine ligand (Figure 5.1).

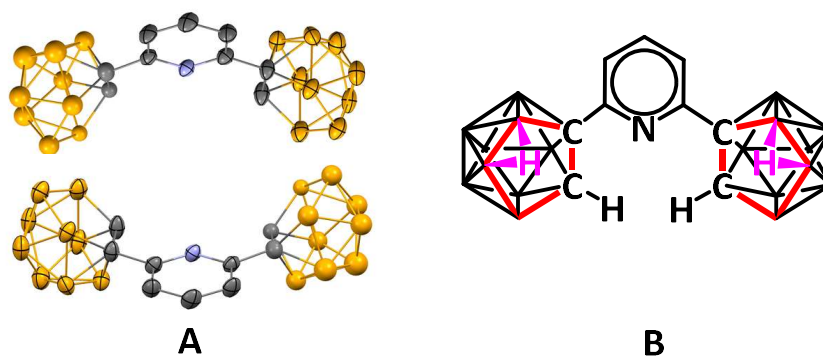


Figure 5.1: (A) Two orientations of **2** which are superimposed to each other. The hydrogen atoms are omitted for clarity. (B) Depiction of **2** showing the bridged protons based on the NMR spectroscopy and the single crystal X-ray crystallography.

5.2.2 Synthesis of Ruthenacarboranes

The removal of the two bridging hydrogen atoms (B–H–B) from the two open faces of the *nido*-clusters of [2,6-bis(*nido*-(*ortho*-carborane))pyridine](NBu₄)₂ by [(CH₃)₃Si]₂NK, followed by the addition of [RuCl₂(*p*-cymene)]₂ afforded a mixture of

two isomeric ruthenacarboranes. The isomers were isolated by employing preparative TLC and fully characterized by an array of multinuclear NMR spectroscopic techniques and single crystal X-ray crystallography.

In the ^1H NMR spectrum of the racemic isomeric form of ruthenacarborane (**3**), the characteristic resonance for two carborane cluster C–H protons was observed as a singlet at 4.66 ppm, suggesting a highly symmetric complex. The high symmetry of **3** was also supported by the presence of four aromatic proton resonances of each of the two *p*-cymene moieties that were observed as a set of four doublets in the region from 5.77 ppm to 4.74 ppm. The ^{11}B and $^{11}\text{B}\{^1\text{H}\}$ NMR spectra of **3** exhibited a set of partially overlapping signals in the range from 0.93 ppm to -20.76 ppm.

Single crystals of **3** were obtained by slow diffusion of hexanes into a saturated solution in methylene chloride (**Figure 5.2 (a)**). The compound crystallizes in the orthorhombic system. The asymmetric unit consists of one $(\text{Ru}(\text{C}_{10}\text{H}_{14}))_2(\text{C}_9\text{B}_{18}\text{H}_{23}\text{N})$ molecule and one dichloromethane molecule. The dichloromethane is disordered, with chlorine atom Cl2 occupying two closely separated positions. The idealized molecular structure possesses a two-fold axis of rotation which passes through the C5, N1 atoms of the pyridine ring. Interestingly, the molecular structure of **3** in the solid state also revealed that both of the C–H bonds of the two clusters point towards the nitrogen atom of the pyridine backbone. The Ru atoms are located on opposite sides of the pyridine ring plane to minimize the steric hindrance of the η^6 -bound *p*-cymene groups. The isopropyl groups of both of the *p*-cymene ligands are on the 'same side' of the molecule as the pyridyl N atom and both of the methyl groups point away from the pyridine moiety. The C1–C2 and C8–C9 bond distances are 1.626(3) Å and 1.629(3) Å, respectively. The

C2–C3, B1–Ru1 and C1–Ru1 bond distances are 1.507(3) Å, 2.201(2) Å and 2.1804(19) Å, respectively. In addition, the C7–C8, B13–Ru2, and C9–Ru2 bond distances are 1.507(3) Å, 2.188(2) Å and 2.177(2) Å, respectively. The C1–C2–C3 and C7–C8–C9 bond angles are 118.32(16)° and 119.64(16)°, respectively (**Figure 5.2 (b)**).

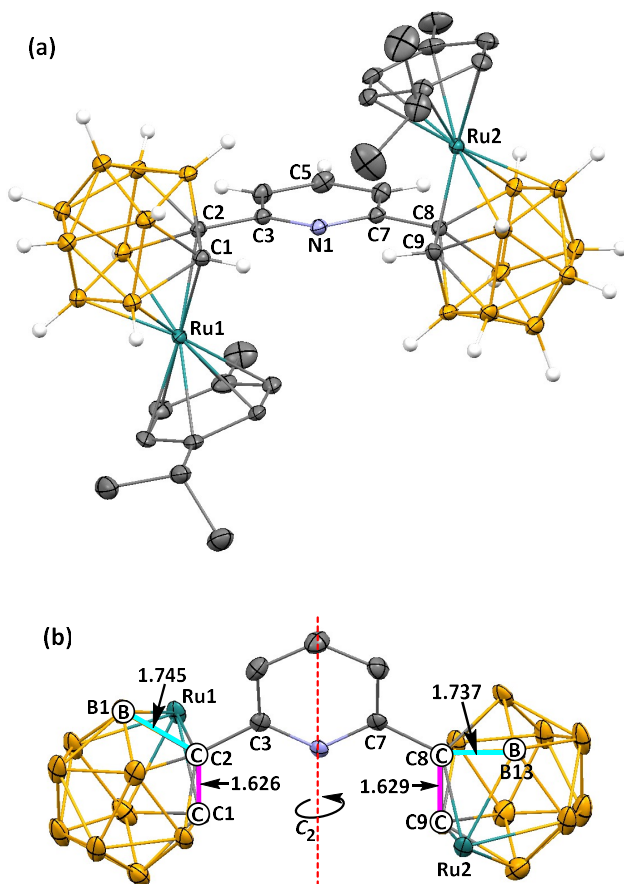


Figure 5.2: (a) The 40 % probability displacement ellipsoid plot of **3**. (b) The comparison of the relevant bond distances of the two ruthenacarborane clusters. The complex is located on an idealized C_2 rotational axis. The two *p*-cymene ligands and the cluster hydrogen atoms are omitted for clarity.

Isomerization of the racemic deboronated ligand upon metalation afforded the meso form of ruthenacarborane (**4**), in which the asymmetric environment was revealed by two sets of resonances in the ^1H NMR spectra for two structurally distinct

ruthenacarborane clusters. Unlike complex **3**, the two cluster C–H protons of **4** exhibited two broad resonances at 4.93 ppm and 4.15 ppm. In addition, two sets of signals were observed for the two Ru–bound *p*-cymene groups. The ^{11}B and $^{11}\text{B}\{^1\text{H}\}$ NMR spectra of **4** contained a set of partially overlapping signals in the range from 1.33 ppm to -20.13 ppm.

The single crystals of $4 \cdot 2\text{C}_6\text{H}_6$ were grown by slow evaporation of benzene in air (**Figure 5.3**). The compound crystallizes in the monoclinic system. The space group $C2/c$ was confirmed by structure solution and refinement. The asymmetric unit consists of half of one complex, which is located on a crystallographic two-fold axis of rotation. Within the carborane cage there is B/C site disorder affecting the carbon atom which is not bonded to the pyridyl ring (C9). Carbon C9 is scrambled with a boron atom over two sites adjacent to C8. The unique isopropyl group is also disordered over two conformations A/B.

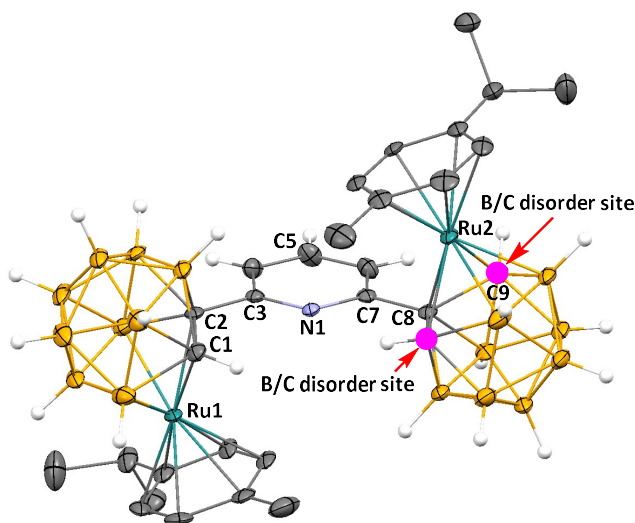


Figure 5.3: The 30 % probability displacement ellipsoid plot of **4** where the C1/B1(A/B) sites are scrambled (shown in pink color). The hydrogen atoms of *p*-cymene moieties are omitted for clarity. The C3–C2, B1–Ru1 and C1–Ru1 bond distances are 1.597(5) Å, 2.180(4) Å and 2.182(4) Å, respectively. The C2–C1 and C2–B1 bond distances are 1.665(6) Å and 1.691(6) Å, respectively.

In addition, the single crystal X-ray data confirmed the formation of the meso form, in which the two cluster incorporated Ru centers are located on the opposite sides of the pyridine backbone to minimize steric hindrance of *p*-cymene groups. The only molecular structural difference between **3** and **4** is in the orientation of the cymene groups. In contrast to **3**, both of the isopropyl groups of two *p*-cymene ligands in **4** are pointed away from the N atom of the pyridine moiety. Despite the B/C site disorder, a detailed analysis of the ¹H and ¹³C NMR data of **4** clearly suggests an asymmetric environment on two sides of the pyridine ring, presumably, due to the dissimilar location of the C9 carbon atom compared to the C1 atom of the unaffected cluster.

5.4 CONCLUSION

In conclusion, the ligand [2,6-bis(*nido*-(*ortho*-carborane))pyridine]](NBu₄)₂ (**2**) was synthesized from 2,6-bis(*ortho*-carborane)pyridine by employing an alcoholic potassium hydroxide solution. The homometalation of the doubly deboronated ligand **2** by [Ru(*p*-cymene)Cl₂]₂ afforded a mixture of racemic and meso ruthenacarboranes. In racemic ruthenacarborane **3**, both of the C-H moieties of both of the clusters are pointing towards the N atom of the pyridine backbone, resulted in the formation of a symmetric molecular structure. Despite disorder of the non-linking cage C atoms in the crystal structure of the meso isomer **4**, detailed analysis of the ¹H NMR data suggests an asymmetric structure in which the cage C-H fragment of one of the clusters is not close to the N atom of the pyridine ring.

5.4 EXPERIMENTAL SECTION

All synthetic manipulations, unless stated otherwise, were carried out either in a nitrogen-filled VAC drybox or on a dual manifold Schlenk-style vacuum line. The

solvents were sparged with nitrogen, passed through activated alumina, and stored over activated 4 Å Linde-type molecular sieves. CD₂Cl₂ was degassed and stored over activated 4 Å Linde-type molecular sieves. NMR spectra were recorded using Varian spectrometers at 400 (¹H), 100 (¹³C), 128 (¹¹B) MHz, reported in δ (parts per million) and referenced to the residual ¹H/¹³C signals of the deuterated solvent or an external BF₃(Et₂O) (¹¹B(δ): 0.0 ppm) standard.

5.4.1 Synthesis of [2,6-bis{nido-(ortho-carborane)}pyridine](NBu₄)₂ (2)

Potassium hydroxide (150 mg, 2.67 mmol) was added to a solution of 2,6-bis(ortho-carboranyl)pyridine (200 mg, 0.55 mmol) in methanol (20 mL) in a storage flask. The reaction mixture was heated at 65 °C temperature for 12 hours, then volatiles were removed under vacuum. The potassium salt of double deboronated ligand was dissolved in water (20 ml), and tetrabutylammonium bromide (600 mg, 1.86 mmol) was added and the resulting mixture was stirred for 15 minutes. {(C₅H₃N)(C₂B₉H₉)₂} {N(C₄H₉)₄}₂ was formed as a white precipitate which was filtered and washed with deionized water (2 × 5 ml). The air stable solid was then washed with dry hexane (3 × 3 mL) and dried under vacuum (380 mg, 83.8 % yield).

¹H NMR (CD₂Cl₂): δ 7.58 (t, 1H, C₅H₃N), 6.95 (d, 2H, C₅H₃N), 5.75 (d, overlapping, 4H, C₆H₄), 5.45 (δ, 2H, C₆H₄), 4.74 (δ, 2H, C₆H₄), 4.66 (s, 2H, (C-H, RuC₂B₉H₁₀), 2.79 (sept, 2H, CH(CH₃)₂), 2.09 (s, 6H, C₆H₄-CH₃), 1.28 (d, 6H, CH(CH₃)₂), 1.25 (d, 6H, CH(CH₃)₂). ¹¹B{¹H} NMR (CD₂Cl₂): δ 0.93, -5.43, -7.51, -9.19, -16.57, -19.76. ¹³C NMR (CD₂Cl₂): δ 161.18 (C₅H₃N), 138.00 (C₅H₃N), 118.21 (C₅H₃N), 113.73 (C₅H₃N), 104.38 (C₅H₃N), 92.76 (C₆H₄), 90.39 (C₆H₄), 88.79 (C₆H₄), 87.53 (C₆H₄), 72.31

(C₂B₉H₁₀), 48.24 (C₂B₉H₁₀), 31.70 (CH(CH₃)₂), 24.03 (CH(CH₃)₂), 21.29 (CH₃-C₆H₄), 18.50 (CH(CH₃)₂) ppm.

5.4.2 Synthesis of (Ru(C₁₀H₁₄))₂(C₉B₁₈H₂₃N) (racemic form 3, and meso form 4)

Potassium bis(trimethylsilyl)amide (0.7 M, 0.50 mL, 0.35 mmol) was added to a solution of [2,6-bis{nido-(ortho-carborane)}pyridine](NBu₄)₂ (100 mg, 0.12 mmol) in THF in a storage flask under nitrogen atmosphere. The mixture was stirred at room temperature for 12 hours, after which time the solvent was removed in vacuo. The white solid was washed with hexane (3 × 3 mL) to remove excess unreacted base. The solid was dissolved in THF (20 mL), and [Ru(*p*-cymene)Cl₂]₂ (75 mg, 0.12 mmol) was added into the solution. After stirring the solution at room temperature for 12 hours, the volatiles were removed in vacuo. The two isomers of ruthenacarboranes 3 (80 mg, 41 % yield) and 4 (70 mg, 36 % yield) were isolated as a light yellow solid by employing preparative TLC.

5.4.3 CRYSTAL STRUCTURE DETERMINATION DETAILS

X-ray intensity data from a colorless plate were collected at 100(2) K using a Bruker D8 QUEST diffractometer equipped with a PHOTON-100 CMOS area detector and an Incoatec microfocus source (Mo K α radiation, $\lambda = 0.71073$ Å). The raw area detector data frames were reduced and corrected for absorption effects using the Bruker APEX3, SAINT+ and SADABS programs.^{16,17} The structure was solved with SHELXT.¹⁸ Subsequent difference Fourier calculations and full-matrix least-squares refinement against *F*² were performed with SHELXL-2018¹⁸ using OLEX2.¹⁹

5.4.3.1 X-Ray Structure Determination of (Ru(C₁₀H₁₄))₂(C₉B₁₈H₂₃N) (3)

The compound crystallizes in the monoclinic system. The space group *C2/c* was confirmed by structure solution and refinement. The asymmetric unit consists of half of one complex, which is located on a crystallographic two-fold axis of rotation. Within the carborane cage there is B/C site disorder affecting the carbon atom which is not bonded to the pyridyl ring (C1). Carbon C1 is scrambled with a boron atom over two sites adjacent to C2. This was established by observation of the displacement parameter behavior upon assignment of the two affected sites as either B or C. Refining either site as 100% carbon gave an abnormally large U_{eq} value; conversely refining these two sites as 100% boron gave abnormally small U_{eq} values. Trial free refinements of occupancies of the mixed C/B sites (C1/B1 A/B) initially refined to near, and were subsequently fixed at, 0.5 C/B for the remaining cycles. The unique isopropyl group is also disordered over two conformations A/B. The major component population refined to C18A-C20A = 0.728(9). The isopropyl disorder was refined with the aid of 1,2- and 1,3- C-C same-distance restraints. The methine carbons C18A/B were kept in the same plane as the tolyl part of the cymene ligand with a FLAT instruction. All non-hydrogen atoms were refined with anisotropic displacement parameters. Hydrogen atoms bonded to carbon were placed in geometrically idealized positions and included as riding atoms with $d(\text{C-H}) = 1.00 \text{ \AA}$ and $U_{iso}(\text{H}) = 1.2U_{eq}(\text{C})$ for methine hydrogen atoms, $d(\text{C-H}) = 0.95 \text{ \AA}$ and $U_{iso}(\text{H}) = 1.2U_{eq}(\text{C})$ for arene hydrogen atoms and $d(\text{C-H}) = 0.98 \text{ \AA}$ and $U_{iso}(\text{H}) = 1.5U_{eq}(\text{C})$ for methyl hydrogens. The methyl hydrogens were allowed to rotate as a rigid group to the orientation of maximum observed electron density. Hydrogen atoms of carborane cage could be located in difference Fourier maps but were placed in

geometrically idealized positions with $d(\text{B-H}) = 1.120 \text{ \AA}$ and $U_{\text{iso}}(\text{H}) = 1.2U_{\text{eq}}(\text{B})$ and $d(\text{C-H}) = 0.97 \text{ \AA}$ and $U_{\text{iso}}(\text{H}) = 1.2U_{\text{eq}}(\text{C})$. The largest residual electron density peak in the final difference map is 0.67 e-/\AA^3 , located 0.98 \AA from Ru1.

Crystal Data for $\text{C}_{29}\text{H}_{51}\text{B}_{18}\text{NRu}_2$ ($M=810.42 \text{ g/mol}$): monoclinic, space group $C2/c$ (no. 15), $a = 28.287(4) \text{ \AA}$, $b = 7.9881(11) \text{ \AA}$, $c = 17.630(2) \text{ \AA}$, $\beta = 112.726(2)^\circ$, $V = 3674.3(9) \text{ \AA}^3$, $Z = 4$, $T = 100(2) \text{ K}$, $\mu(\text{MoK}\alpha) = 0.847 \text{ mm}^{-1}$, $D_{\text{calc}} = 1.465 \text{ g/cm}^3$, 19384 reflections measured ($3.122^\circ \leq 2\Theta \leq 52.868^\circ$), 3775 unique ($R_{\text{int}} = 0.0693$, $R_{\text{sigma}} = 0.0485$) which were used in all calculations. The final R_1 was 0.0383 ($I > 2\sigma(I)$) and wR_2 was 0.0913 (all data).

5.4.3.2 X-Ray Structure Determination of $(\text{Ru}(\text{C}_{10}\text{H}_{14}))_2(\text{C}_9\text{B}_{18}\text{H}_{23}\text{N}) \cdot 2\text{C}_6\text{H}_6$ (4)

The compound crystallizes in the triclinic system. The space group $P-1$ (No. 2) was confirmed by structure solution. The asymmetric unit consists of one $(\text{Ru}(\text{C}_{10}\text{H}_{14}))_2(\text{C}_9\text{B}_{20}\text{H}_{23}\text{N})$ complex and two independent benzene molecules. One of the carborane cage substituents (C8/C9/B11-B19) is mildly disordered, affecting only the position of the carbon atom C9. Carbon atom C9 is scrambled over two sites neighboring C8. The disorder was identified by observation and refinement of the displacement parameters of these two sites, both of which became abnormally small if refined as 100% B, or large if refined as 100% C. Likewise the site occupation factor refined to greater than 100% B or lesser than 100% C. Trial free refinements of occupancies of the mixed C/B sites (C9/B13 A/B) initially refined to near, and were subsequently fixed at, 0.5 C/B for the remaining cycles. All non-hydrogen atoms were refined with anisotropic displacement parameters. Hydrogen atoms bonded to carbon were placed in geometrically idealized positions and included as riding atoms with $d(\text{C-H}) = 1.00 \text{ \AA}$ and

$U_{\text{iso}}(\text{H}) = 1.2U_{\text{eq}}(\text{C})$ for methine hydrogen atoms, $d(\text{C-H}) = 0.95 \text{ \AA}$ and $U_{\text{iso}}(\text{H}) = 1.2U_{\text{eq}}(\text{C})$ for arene hydrogen atoms and $d(\text{C-H}) = 0.98 \text{ \AA}$ and $U_{\text{iso}}(\text{H}) = 1.5U_{\text{eq}}(\text{C})$ for methyl hydrogens. The methyl hydrogens were allowed to rotate as a rigid group to the orientation of maximum observed electron density. Hydrogen atoms of carborane cage C1/C2/B1-B9 were located in difference maps and refined freely; those of the disordered cage were placed in geometrically idealized positions with $d(\text{B-H}) = 1.120 \text{ \AA}$ and $U_{\text{iso}}(\text{H}) = 1.2U_{\text{eq}}(\text{B})$ and $d(\text{C-H}) = 0.97 \text{ \AA}$ and $U_{\text{iso}}(\text{H}) = 1.2U_{\text{eq}}(\text{C})$. The largest residual electron density peak in the final difference map is 1.18 e-/\AA^3 , located 0.29 \AA from H1A. This peak may represent a minor substituent impurity at this site (near B1) but could not be successfully identified and refined.

Crystal Data for $\text{C}_{41}\text{H}_{63}\text{B}_{18}\text{NRu}_2$ ($M = 966.64 \text{ g/mol}$): triclinic, space group $P-1$ (no. 2), $a = 12.8896(10) \text{ \AA}$, $b = 13.6620(10) \text{ \AA}$, $c = 15.7193(12) \text{ \AA}$, $\alpha = 82.160(4)^\circ$, $\beta = 71.909(4)^\circ$, $\gamma = 63.561(3)^\circ$, $V = 2356.1(3) \text{ \AA}^3$, $Z = 2$, $T = 100(2) \text{ K}$, $\mu(\text{MoK}\alpha) = 0.673 \text{ mm}^{-1}$, $D_{\text{calc}} = 1.363 \text{ g/cm}^3$, 39638 reflections measured ($3.678^\circ \leq 2\Theta \leq 55.264^\circ$), 10908 unique ($R_{\text{int}} = 0.0435$, $R_{\text{sigma}} = 0.0378$) which were used in all calculations. The final R_1 was 0.0303 ($I > 2\sigma(I)$) and wR_2 was 0.0721 (all data).

REFERENCES

1. General reviews: (a) R.N. Grimes, in: E. Abel, F.G.A. Stone, G. Wilkinson (Eds.), *Comprehensive Organometallic Chemistry II*, Vol. 1, Chap. 9, Pergamon Press, Oxford, England, 1995, pp. 373–430. (b) R.N. Grimes, in: E. Abel, F.G.A. Stone, G. Wilkinson (Eds.), *Comprehensive Organometallic Chemistry*, Pergamon Press, Oxford, England, 1982, Chapter 5.5. (c) Grimes, R. N. *J. Organomet. Chem.* **1999**, *581*, 1. (d) Hosmane, N. S. *J. Organomet. Chem.* **1999**, *581*, 13. (e) N.S. Hosmane, in: W. Siebert (Ed.), *Advances in Boron Chemistry*, Royal Society of Chemistry: Cambridge, U.K., 349–357 (1997). (f) Grimes, R. N. *Appl. Organomet. Chem.* **1996**, *10*, 209.
2. Plesek, J. *Chem. Rev.* **1992**, *92*, 269.
3. Grimes, R. N. *Coord. Chem. Rev.* **2002**, *200-202*, 773.
4. Fox M. A.; Wade, K. *J. Organomet. Chem.* **1999**, *573*, 279.
5. Ellis, D.; McKay, D.; Macgregor, S. A.; Rosair, G. M.; Welch, A. J. *Angew. Chem. Int. Ed.* **2010**, *49*, 4943.
6. Ellis, D.; Rosair, G. M.; Welch, A. J. *J. Chem. Commun.* **2010**, *46*, 7394.
7. Zhang, J.; Deng, L.; Chan, H. -S.; Xie, Z. *J. Am. Chem. Soc.* **2007**, *129*, 18.
8. Ellis, D.; Rosair, G. M.; Welch, A. J. *J. Chem. Commun.* **2010**, *46*, 7394.
9. Thiripuranathar, G.; Man, W. Y.; Palmero, C.; Chan, A. P. Y.; Leube, B. T.; Ellis, D.; McKay, D.; Macgregor, S. A.; Jourdan, L.; Rosair, G. M.; Welch A. J. *Dalton Trans.* **2015**, *44*, 5628.
10. Thiripuranathar, G.; Chan, A. P. Y.; Mandal, D.; Man, W. Y.; Argentari, M.; Rosair, G. M.; Welch, A. J. *Dalton Trans.* **2017**, *46*, 1811.
11. Dupont, J. A.; Hawthorne, M. F. *J. Am. Chem. Soc.* **1964**, *86*, 1643.

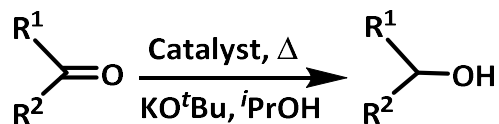
12. Ren S.; Xie, Z. *Organometallics* **2008**, *27*, 5167.
13. Man, W. Y.; Rosair G. M.; Welch, A. J. *Acta Crystallogr., Sect. E: Struct. Rep. Online* **2014**, *70*, 462.
14. Islam, M. J.; Smith, M. D.; Peryshkov, D. V. *J. Organomet. Chem.* **2018**, *867*, 208.
15. Hawthorne, M. F.; Owen, D. A.; Wiggins, J. W. *Inorg. Chem.* **1971**, *10*, 1034.
16. APEX3 Version 2016.5-0 and SAINT+ Version 8.37A. Bruker AXS, Inc., Madison, Wisconsin, USA, **2016**.
17. Krause, L.; Herbst-Irmer, R.; Sheldrick G. M.; Stalke D. *J. Appl. Cryst.* **2015**, *48*, 3.
18. (a) Sheldrick, G. M. *Acta Cryst.* **2015**, *A71*, 3. (b) Sheldrick, G. M. *Acta Cryst.* **2015**, *C71*, 3.
19. Dolomanov, O. V., Bourhis, L. J., Gildea, R. J., Howard J. A. K.; Puschmann, H. *J. Appl. Cryst.* **2009**, *42*, 339.

Chapter 6

Synthesis and Characterization of Ru(II) Complexes of (*ortho*-Carboranyl)pyridine and their Role on Transfer Hydrogenation of Ketones

6.1 INTRODUCTION

Transfer hydrogenation of ketones under basic conditions employing a non-H₂ hydrogen source is one of the most fundamental transformations in organic synthesis. The applications of transfer hydrogenation span from fine chemicals to pharmaceuticals synthesis because of its excellent selectivity, operational simplicity, and wide substrate scope.¹⁻⁴ Transfer hydrogenation of ketones for the synthesis of secondary alcohols using *i*PrOH or other H₂-donor solvents is a convenient, powerful, inexpensive, and less hazardous process compared to direct hydrogenation (**Scheme 6.1**).⁵



Scheme 6.1: Transfer hydrogenation of ketone to yield secondary alcohol.

In the past few years, plenty of ligands, bases, hydrogen sources, supports and reaction media have been developed for the reduction of ketones to secondary alcohols. Transition metal based transfer hydrogenation catalysts with desired properties and reactivity can be designed by incorporating electronic and steric tunable ligands with the metal center.¹²⁻¹³ *N*-heterocyclic carbenes, NHCs, have drawn significant attention as an alternative to organophosphine ligands because of their strong σ -donor coordination property, steric and electronic tunability, and topological adjustability.⁶⁻¹¹ The NHC based ruthenium complexes exhibited promising catalytic efficiency for transformation of ketones.¹⁴⁻²² Specifically, pyridine, pyrimidine, phosphine, and carboxylate donor group functionalized NHCs have been studied extensively due to the hemilabile property of the donor moieties that enables robust transfer hydrogenation by reversible dissociation of the donor groups from the metal center.⁵ Although NHCs and organophosphine ligand

based ruthenium complexes have been successfully explored for transfer hydrogenation of ketones, to the best of our knowledge carborane based ruthenium complexes have not been reported as transfer hydrogenation catalyst yet.

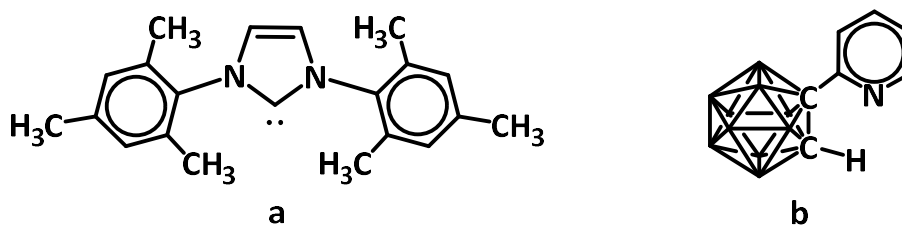


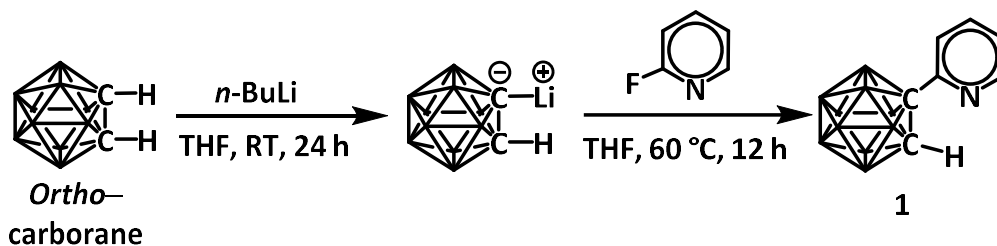
Figure 6.1: (a) 1,3-Bis(2,4,6-trimethylphenyl)imidazol-2-ylidene, a general example of *N*-heterocyclic carbene. (b) (*ortho*-carboranyl)pyridine ligand, used in this work.

Catalysts for specific applications can be designed by tailoring steric properties and functional versatility of carborane cage. Icosahedral *closo*-dicarbadodecaboranes are remarkably robust electron deficient three-dimensional boron-carbon clusters with two slightly acidic C–H bonds. Coordinatively unsaturated transition metal complexes containing C-functionalized *ortho*-carborane are considered as potential catalysts for activation of polar chemical bonds like C=O.²³⁻²⁵ Recently, we reported the synthesis of a pyridine-backbone pincer complex $\{(C_5H_3N)(C_2B_{10}H_{10})_2\}Ni(CH_3CN)$ in which two *ortho*-carborane clusters act as the donor arms of the pincer framework. The pincer complex is a competent catalyst for nucleophilic addition of piperidine to acetonitrile.²⁶ Herein, we report the synthesis and characterization of ruthenium(II) complexes with a bidentate (*ortho*-carboranyl)pyridine ligand and their remarkable catalytic efficiency for transfer hydrogenation of a wide variety of aliphatic and aromatic ketones to corresponding secondary alcohols.

6.2 RESULTS AND DISCUSSION

6.2.1 Synthesis of (*ortho*-carboranyl)pyridine (**1**)

The ligand (*ortho*-carboranyl)pyridine was synthesized by the S_NAr reaction of 2-fluoropyridine with one equivalent of lithiated carborane in THF at 60 °C overnight under nitrogen atmosphere (**Scheme 6.2**). After aqueous workup and extraction to dichloromethane, unreacted *ortho*-carborane was removed by sublimation under vacuum at 60 °C. The ligand was obtained as sublimed white solid under vacuum at 90 °C (yield 60 %). The NMR data are in good agreement with those of the original report.²⁷



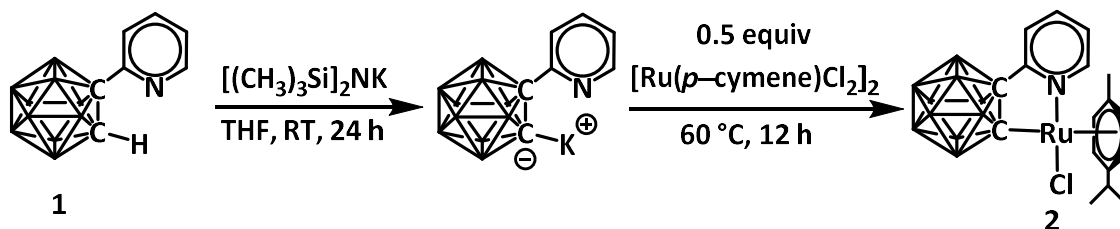
Scheme 6.2: Synthesis of (*ortho*-carboranyl)pyridine (C₅H₃N)(C₂B₁₀H₁₁) (**1**).

6.2.2 Synthesis of RuCl(C₁₀H₁₄)(C₇H₁₄B₁₀N) (Ru-C) (**2**)

Deprotonation of the slightly acidic C-H bond of the carborane cage of (*ortho*-carboranyl)pyridine using 1 equivalent of potassium bis-(trimethylsilyl)amide in THF afforded C₇H₁₄B₁₀NK, in which 0.5 equivalent of [Ru(*p*-cymene)Cl₂]₂ was added. The resulting mixture was stirred at 60 °C overnight, and the target yellow product RuCl(C₁₀H₁₄)(C₇H₁₄B₁₀N) (**2**) was isolated by performing preparative TLC (**Scheme 6.3**).

The complex **2** was characterized by ¹H, ¹¹B, and ¹³C NMR spectroscopy and single crystal X-ray crystallography. The ¹H spectrum of complex **2** exhibited the disappearance of the characteristic C-H signal of the carborane cage at δ = 4.99 ppm,

confirming the formation of a Ru–C bond. All the ^1H signals of the pyridine ring were shifted downfield due to coordination of the ring through the nitrogen atom to the ruthenium center. The four asymmetric protons of the η^6 -coordinated *p*-cymene moiety showed four doublets in the range from 5.57 ppm to 5.03 ppm. The ^{11}B and $^{11}\text{B}\{^1\text{H}\}$ NMR spectra of compound **2** exhibited a set of partially overlapping signals in the range from -2.60 ppm to -8.43 ppm.



Scheme 6.3: Synthesis of $\text{RuCl}(\text{C}_{10}\text{H}_{14})(\text{C}_7\text{H}_{14}\text{B}_{10}\text{N})$ (Ru–C) (**2**).

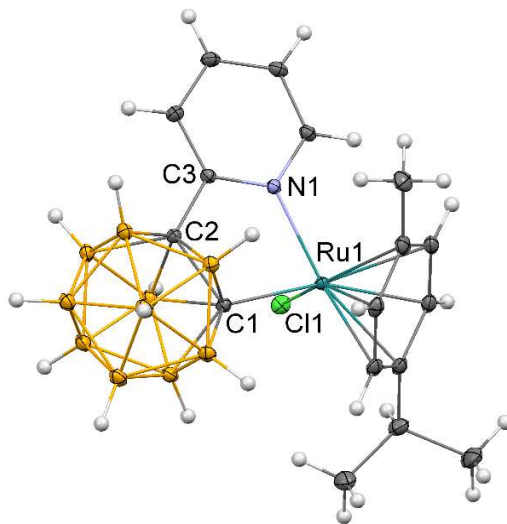


Figure 6.2: Displacement ellipsoid plot (50 % probability) of the $\text{RuCl}(\text{C}_{10}\text{H}_{14})(\text{C}_7\text{H}_{14}\text{B}_{10}\text{N})$ complex (**2**).

The single crystals of $2 \cdot \text{C}_6\text{H}_6$ were obtained by slow evaporation of benzene solution in air (**Figure 6.2**). The Ru1–C1 bond length in complex **2** is $2.113(10)$ Å and the Ru1–N1 bond length is $2.116(9)$ Å. The C2–C3 bond length is shortened ($1.488(14)$

Å) in the complex compared to the C2–C3 bond length (1.512 Å) of the uncoordinated ligand. The C1–C2 bond length of the coordinated ligand is 1.669(14) Å, which is longer than the C1–C2 bond length of 1.632 Å of the free (*ortho*-carboranyl)pyridine.

6.2.3 Synthesis of [Ru(CH₃CN)(C₁₀H₁₄)(C₇H₁₄B₁₀N)](BF₄) (3)

The cationic complex **3** was synthesized by reacting complex **2** with AgBF₄ using acetonitrile as solvent and was purified as yellow air-stable solid in excellent yield of 79 %. The complex **3** was characterized by an array of multinuclear NMR spectroscopic techniques and single crystal X-ray crystallography. In the ¹H NMR spectrum, a singlet was observed for three protons of Ru-bound acetonitrile at 2.40 ppm. The four aromatic protons of the *p*-cymene moiety were observed as four doublets in the region from 6.18 ppm to 5.30 ppm due to loss of symmetry of the complex. The presence of BF₄[−] counter-anion in complex **3** was also confirmed by ¹⁹F and ¹¹B NMR spectroscopy.

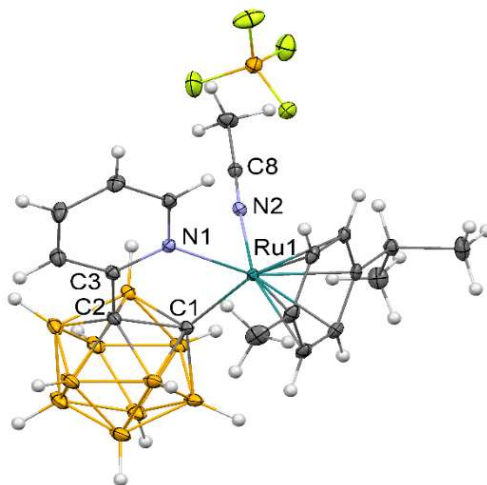


Figure 6.3: Displacement ellipsoid plot (50 % probability) of the [Ru(CH₃CN)(C₁₀H₁₄)(C₇H₁₄B₁₀N)](BF₄) complex (**3**).

The complex **3** was crystallized by slow evaporation of benzene solution in air (**Figure 6.3**). Coordination of the C_{carborane} and N_{pyridine} atoms to the ruthenium center

resulted in a five membered chelate ring. The intraligand angle C3–C2–C1 of the free ligand is 116.08(15)°. Incorporation of the ruthenium with the ligand applied increased strain at the complex indicated by the decreased of the intraligand angle C3–C2–C1 to 112.05(15)°. The C≡N bond shortens from 1.153 Å in acetonitrile²⁸ to 1.136(2) Å (N2≡C8) in **3**, indicating strong interaction of coordinated acetonitrile with the ruthenium center.

6.2.4 Synthesis of RuCl(C₁₀H₁₄)(C₇H₁₄B₁₀N) (Ru–B) (**4**)

The complex **4** was isolated as a minor product from the reaction mixture of **2** synthesis by employing preparative TLC. Full characterization of complex **4** was performed by ¹H, ¹¹B, and ¹³C NMR spectroscopy, as well as single crystal X-ray diffraction studies. The ¹H NMR resonance of the C–H of the carborane cage in CD₂Cl₂ was observed at 4.53 ppm, which is shifted upfield compared to (*ortho*-carboranyl)pyridine compound of 4.99 ppm. The formation of Ru–B bond was confirmed by the presence of a resonance at 9.3 ppm in ¹¹B and ¹¹B{¹H} NMR spectra.

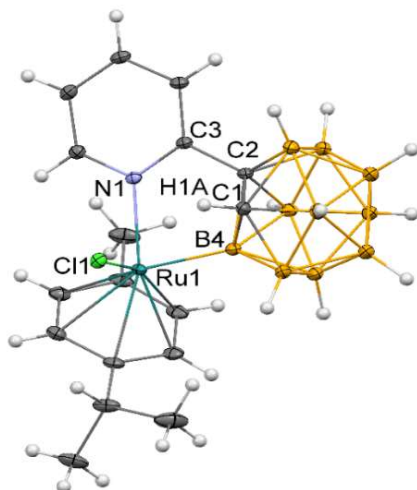


Figure 6.4: Displacement ellipsoid plot (50 % probability) of the RuCl(C₁₀H₁₄)(C₇H₁₄B₁₀N) (Ru–B) complex (**4**).

Single crystals of complex **4** were obtained by slow diffusion of hexane into a saturated solution of **4** in dichloromethane (**Figure 6.4**). The Ru1–B4 bond distance is 2.080(13) Å, the Ru1–N1 bond distance is 2.116(9) Å. The C1–C2 bond distance (1.629(16) Å) is similar to that of the carborane cluster of uncoordinated carboranyl ligand. The carborane cage is rotated by 62.78° along the C2–C3 bond due to the coordination to the ruthenium center through the B4 atom of the cage.

6.2.5 Synthesis of Ru(C₂₀H₂₅)(C₇H₁₄B₁₀N) (**5**)

The compound **5** was obtained as a minor product during the synthesis of compound **2** and was purified by preparative TLC. The ¹H, ¹¹B, and ¹³C NMR spectroscopy and single crystal X-ray crystallography were employed to fully characterize compound **5**. The diastereotopic nature of the Ru–bound bridging –CH₂– protons is revealed by the appearance of two doublets at 3.86 and 3.45 ppm in the ¹H NMR spectrum. The presence of the bridging –CH₂– group in between two *p*-cymene rings is manifested by the diastereotopic nature of the two –CH₂– protons (split into AB doublets at 2.70 and 1.60 ppm). Loss of symmetry of complex **5** was exhibited by the presence of four doublets of η⁶-coordinated *p*-cymene moiety representing four aromatic protons in the range of 5.43 to 3.82 ppm. The –CH₂– tethered *p*-cymene moiety showed one characteristic singlet at 7.11 ppm (one aromatic proton) and two doublets at 6.87 and 6.70 ppm (two aromatic protons).

Single crystals of complex **5** were grown by slow diffusion of hexane into a saturated solution of **5** in dichloromethane (**Figure 6.5**). The η⁶-coordinated *p*-cymene ligand is bridged through a –CH₂– group with the other *p*-cymene. The coordination of one *p*-cymene through –CH₂– bridging and another *p*-cymene in η⁶-fashion to the

Ru(II) center resulted in formation of a six membered ring. The rigidity of this ring makes the protons attached to the two bridging carbon atoms (C11 and C21) diastereotopic, which was also hypothesized by ^1H NMR spectroscopy of the complex.

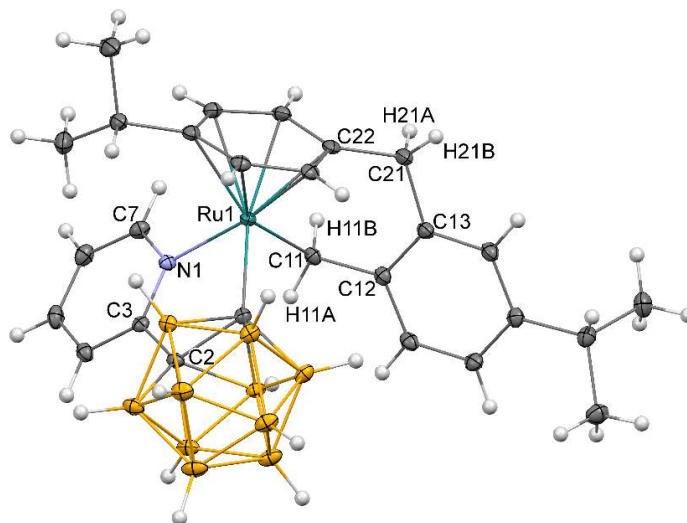
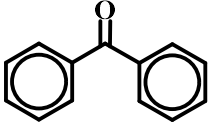
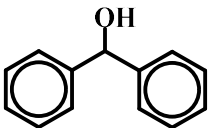
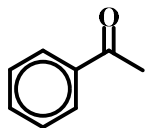
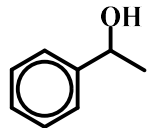
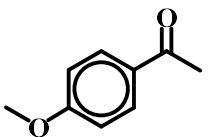
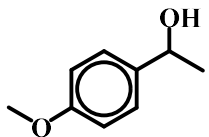
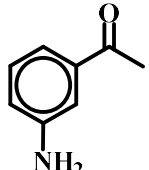
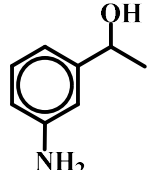
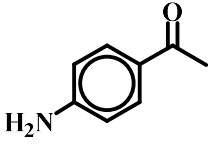
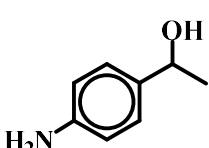
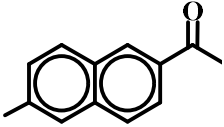
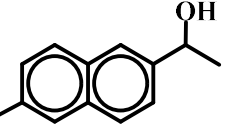
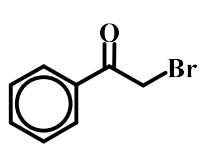
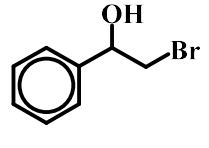
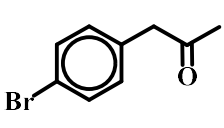
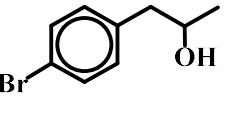
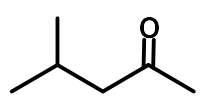
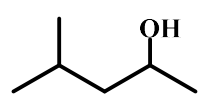


Figure 6.5: Displacement ellipsoid plot (50 % probability) of the $\text{Ru}(\text{C}_{20}\text{H}_{25})(\text{C}_7\text{H}_{14}\text{B}_{10}\text{N})$ complex (**5**).

6.2.6 Transfer Hydrogenation of Carbonyl Compounds

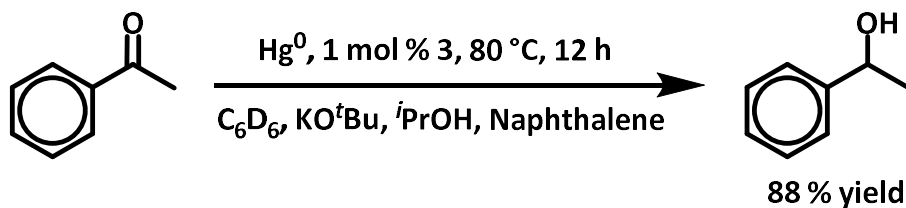
We found that the complexes **2** and **3** are competent catalysts for transfer hydrogenation of a wide variety of ketones in moisture-free conditions. All transfer hydrogenation studies were carried out employing 1 mol % of either complex **2** or **3**, excess 2-propanol as a non- H_2 hydrogen source, 5 mol % KO^tBu as an activator/base, naphthalene as an internal standard and C_6D_6 as reaction medium. The reactants were mixed in a vial for each entry and transferred to a J-Young tube afterwards to monitor the progress of the substrate conversion by ^1H NMR spectroscopy (**Table 1**).

Table 6.1: Transfer Hydrogenation of Ketones Catalyzed by Complexes 2 and 3.

Entry	Substrate	Secondary Alcohol	Conversion, %					
			Complex 2			Complex 3		
			6 h	12 h	24 h	6 h	12 h	24 h
1.			48	62	94	49	63	93
2.			89	96	99	57	72	99
3.			48	50	61	11	20	31
4.			67	71	81	35	45	61
5.			20	20	22	4	7	12
6.			63	78	85	48	59	75
7.			15	16	29	0	4	16
8.			86	97	100	12	19	27
9.			52	66	75	18	29	55

The performance of the transfer hydrogenation catalysts **2** and **3** is temperature and base dependent. All the catalytic reactions were carried out at 80 °C temperature, since very low conversions were recorded for all the substrates at room temperature. In the absence of base KO^tBu, no conversion was observed, even at elevated temperature (80 °C). We found the superior catalytic efficiency of complex **2** compared to complex **3** is likely due to the lower stability of complex **3** at higher temperatures under basic conditions, indicated by the formation of black precipitate (presumably ruthenium metal) in the J–Young tube. We also hypothesized that the active ruthenium site is hindered in complex **3** for the incoming substrates by the coordinated acetonitrile ligand that is not efficiently removed by the base.

The determination of the nature of active catalytic centers to elucidate the mechanism of transition-metal catalyzed reactions in solutions is often challenging.²⁹⁻⁴³ To explore this issue, the mercury poisoning experiment is widely used among other diagnostic tools for its rapid and easy procedures to distinguish truly homogeneous molecular catalysis from nanoparticle metal catalysis.⁴⁴⁻⁴⁵ We proceeded with catalyst **2** to assess the nature of the active catalytic ruthenium center by applying it for the transfer hydrogenation of acetophenone in the presence of one drop of mercury (excess) (**Scheme 6.4**). The progress of acetophenone conversion was not hindered after the addition of Hg⁰, implying homogeneous molecular catalysis by the ruthenium center.



Scheme 6.4: Mercury test: transfer hydrogenation of acetophenone by complex **3** in the presence of excess Hg⁰.

6.3 CONCLUSION

In conclusion, a series of Ru(II) complexes of bidentate ligand 2-(*ortho*-carboranyl)pyridine were synthesized and characterized fully by the array of multinuclear NMR spectroscopic techniques and single crystal X-ray diffraction. The complexes **2** and **3** are competent catalyst for transfer hydrogenation of a wide variety of ketones.

6.4 EXPERIMENTAL SECTION

All synthetic manipulations, unless stated otherwise, were carried out either in a nitrogen-filled VAC drybox or on a dual manifold Schlenk-style vacuum line.⁴⁶ The solvents were sparged with nitrogen, passed through activated alumina, and stored over activated 4 Å Linde-type molecular sieves. CD₂Cl₂ was degassed and stored over activated 4 Å Linde-type molecular sieves. NMR spectra were recorded using Varian spectrometers at 400 (¹H), 100 (¹³C), 128 (¹¹B) MHz, reported in δ (parts per million) and referenced to the residual ¹H/¹³C signals of the deuterated solvent or an external BF₃(Et₂O) (¹¹B(δ): 0.0 ppm) standard.

6.4.1 Synthesis of RuCl(C₁₀H₁₄)(C₇H₁₄B₁₀N) (Ru-C) (**2**)

Potassium bis(trimethylsilyl)amide (0.65 mL, 0.45 mmol) was transferred to a solution of (*ortho*-carboranyl)pyridine (100 mg, 0.45 mmol) in toluene (10 mL) under nitrogen atmosphere in a glove box. The mixture was stirred at room temperature for 24 h, leading to the formation of a white C₇H₁₅B₁₀NNa salt. Dichloro(*p*-cymene)ruthenium(II) dimer (140 mg, 0.23 mmol) was added, and the resulting solution was stirred at 60 °C for 12 h, after which time volatiles were removed under vacuum. The black solid was washed with ether, and the filtrate was collected and

dried in vacuum. Preparative TLC was performed to purify RuCl(C₁₀H₁₄)(C₇H₁₄B₁₀N) as a yellow solid (30 mg, 0.06 mmol, 14% yield).

¹H NMR (CD₂Cl₂): δ 9.20 (d, 1H, C₅H₄N), 7.80 (t, 1H, C₅H₄N), 7.41 (d, 1H, C₅H₄N), 7.37 (t, 1H, C₅H₄N), 5.56 (dd, 2H, C₆H₄), 5.48 (d, 1H, C₆H₄), 5.03 (d, 1H, C₆H₄), 2.81 (*sept*, 1H, CH(CH₃)₂), 1.69 (s, 3H, CH₃C₆H₄), 1.21 (d, 3H, CH(CH₃)₂), 1.17 (d, 3H, CH(CH₃)₂). ¹¹B{¹H} NMR (CD₂Cl₂): δ -2.60, -5.16, -7.21, -8.43. ¹³C NMR (CD₂Cl₂): δ 160.48 (C₅H₄N), 156.71 (C₅H₄N), 139.27 (C₅H₄N), 125.56 (C₅H₄N), 123.14 (CH₃CN), 104.69 (C₆H₄), 96.09 (C₆H₄), 92.68 (C₆H₄), 92.18 (C₆H₄), 90.54 (C₆H₄), 84.02 (C₆H₄), 81.85 (C₂H₁₀B₁₀), 77.97 (C₂H₁₀B₁₀), 30.94 (CH(CH₃)₂), 24.60 (CH(CH₃)₂), 19.44 (CH₃C₆H₄), 17.49 (CH(CH₃)₂) ppm.

6.4.2 Synthesis of [Ru(CH₃CN)(C₁₀H₁₄)(C₇H₁₄B₁₀N)](BF₄) (3)

Silver tetrafluoroborate (14 mg, 0.07 mmol) was transferred to a solution of RuCl(C₁₀H₁₄)(C₇H₁₄B₁₀N) (30 mg, 0.06 mmol) in acetonitrile (5 mL) under nitrogen atmosphere in a glove box. The mixture was stirred at room temperature for 12 h, after which time volatiles were removed under vacuum. The greyish yellow solid was washed with benzene, and the filtrate was collected and dried in vacuum to obtain [Ru(CH₃CN)(C₁₀H₁₄)(C₇H₁₄B₁₀N)](BF₄) (28 mg, 0.05 mmol, 79 % yield) as a yellow solid.

¹H NMR (CD₂Cl₂): δ 9.51 (d, 1H, C₅H₄N), 7.91 (t, 1H, C₅H₄N), 7.59 (t, 1H, C₅H₄N), 7.49 (d, 1H, C₅H₄N), 6.17 (d, 2H, CH₃-C₆H₄-CH(CH₃)₂), 6.10 (d, 2H, CH₃-C₆H₄-CH(CH₃)₂), 5.72 (d, 2H, CH₃-C₆H₄-CH(CH₃)₂), 5.30 (d, 2H, CH₃-C₆H₄-CH(CH₃)₂), 2.61 (*sept*, 1H, CH₃-C₆H₄-CH(CH₃)₂), 2.40 (s, 3H, CH₃CN), 1.71 (s, 3H, CH₃-C₆H₄), 1.21 (dd, 6H, CH(CH₃)₂). ¹¹B{¹H} NMR (CD₂Cl₂): δ -0.92, -2.17, -4.70, -7.47, -8.90.

^{13}C NMR (CD_2Cl_2): δ 160.26 ($\text{C}_5\text{H}_4\text{N}$), 158.49 ($\text{C}_5\text{H}_4\text{N}$), 140.55 ($\text{C}_5\text{H}_4\text{N}$), 127.03 ($\text{C}_5\text{H}_4\text{N}$), 126.03 (CH_3CN), 123.61 ($\text{C}_5\text{H}_4\text{N}$), 107.87 ($\text{CH}_3\text{C}_6\text{H}_4\text{CH}(\text{CH}_3)_2$), 98.23 ($\text{CH}_3\text{C}_6\text{H}_4\text{CH}(\text{CH}_3)_2$), 95.77 ($\text{CH}_3\text{C}_6\text{H}_4\text{CH}(\text{CH}_3)_2$), 95.63 ($\text{CH}_3\text{C}_6\text{H}_4\text{CH}(\text{CH}_3)_2$), 92.83 ($\text{CH}_3\text{C}_6\text{H}_4\text{CH}(\text{CH}_3)_2$), 86.10 ($\text{CH}_3\text{C}_6\text{H}_4\text{CH}(\text{CH}_3)_2$), 82.13 ($\text{C}_2\text{H}_{10}\text{B}_{10}$), 74.66 ($\text{C}_2\text{H}_{10}\text{B}_{10}$), 31.76 ($\text{CH}(\text{CH}_3)_2$), 24.55 ($\text{CH}(\text{CH}_3)_2$), 19.85 ($\text{CH}_3\text{C}_6\text{H}_4$), 17.68 ($\text{CH}(\text{CH}_3)_2$), 4.39 (CH_3CN). ^{19}F NMR (CD_2Cl_2): δ -151.93 ppm.

6.4.3 Synthesis of $\text{RuCl}(\text{C}_{10}\text{H}_{14})(\text{C}_7\text{H}_{14}\text{B}_{10}\text{N})$ (**Ru-B**) (**4**)

Complex **4** was isolated during purification of complex **2** by preparative TLC.

^1H NMR (CD_2Cl_2): δ 9.54 (d, 1H, $\text{C}_5\text{H}_4\text{N}$), 7.76 (t, 1H, $\text{C}_5\text{H}_4\text{N}$), 7.49 (d, 1H, $\text{C}_5\text{H}_4\text{N}$), 7.33 (t, 1H, $\text{C}_5\text{H}_4\text{N}$), 5.94 (d, 1H, C_6H_4), 5.80 (d, 1H, C_6H_4), 5.72 (d, 1H, C_6H_4), 5.07 (d, 1H, C_6H_4), 4.53 (s, 1H, $\text{C}_1\text{H}_9\text{B}_{10}\text{C-H}$) 2.49 (*sept*, 1H, $\text{CH}(\text{CH}_3)_2$), 1.54 (s, 3H, $\text{CH}_3\text{C}_6\text{H}_4$), 1.15 (d, 3H, $\text{CH}(\text{CH}_3)_2$), 1.10 (d, 3H, $\text{CH}(\text{CH}_3)_2$). $^{11}\text{B}\{^1\text{H}\}$ NMR (CD_2Cl_2): δ 9.30, -2.40, -3.97, -7.44, -11.45, -13.14. ^{13}C NMR (CD_2Cl_2): δ 159.53 ($\text{C}_5\text{H}_4\text{N}$), 158.92 ($\text{C}_5\text{H}_4\text{N}$), 138.30 ($\text{C}_5\text{H}_4\text{N}$), 126.05 ($\text{C}_5\text{H}_4\text{N}$), 125.85 ($\text{C}_5\text{H}_4\text{N}$), 100.24 (C_6H_4), 99.55 (C_6H_4), 98.91 (C_6H_4), 88.57 (C_6H_4), 86.36 (C_6H_4), 83.20 (C_6H_4), 63.67 ($\text{C}_2\text{H}_{10}\text{B}_{10}$), 30.90 ($\text{CH}(\text{CH}_3)_2$), 24.14 ($\text{CH}(\text{CH}_3)_2$), 20.23 ($\text{CH}_3\text{C}_6\text{H}_4$), 17.79 ($\text{CH}(\text{CH}_3)_2$) ppm.

6.4.4 Synthesis of $\text{Ru}(\text{C}_{20}\text{H}_{25})(\text{C}_7\text{H}_{14}\text{B}_{10}\text{N})$ (**5**)

Complex **5** was obtained as a minor product during purification of the complex **2** by preparative TLC.

^1H NMR (CD_2Cl_2): δ 8.19 (d, 1H, $\text{C}_5\text{H}_4\text{N}$), 7.69 (t, 1H, $\text{C}_5\text{H}_4\text{N}$), 7.45 (d, 1H, $\text{C}_5\text{H}_4\text{N}$), 7.11 (s, 1H, C_6H_3), 7.05 (t, 1H, $\text{C}_5\text{H}_4\text{N}$), 6.85 (d, 1H, C_6H_3), 6.68 (d, 1H, C_6H_3), 5.42 (d, 1H, C_6H_4), 5.02 (d, 1H, C_6H_4), 4.32 (d, 1H, C_6H_4), 3.84 (d, 1H, C_6H_4), 3.82 (d, 1H, $\text{C}_6\text{H}_4\text{-CH}_2\text{-C}_6\text{H}_3$), 3.41 (d, 1H, $\text{C}_6\text{H}_4\text{-CH}_2\text{-C}_6\text{H}_3$), 2.86 (*sept*, 1H, $\text{CH}(\text{CH}_3)_2$), 2.67 (d,

1H, Ru-CH₂), 2.59 (sept, 1H, CH(CH₃)₂) 1.58 (d, 1H, Ru-CH₂), 1.26 (dd, 6H, CH(CH₃)₂) 1.09 (d, 3H, CH(CH₃)₂), 0.58 (d, 3H, CH(CH₃)₂). ¹¹B{¹H} NMR (CD₂Cl₂): δ -2.61, -5.76, -7.91, -13.73. ¹³C NMR (CD₂Cl₂): δ 160.25 (C₅H₄N), 155.50 (C₅H₄N), 150.45 (C₅H₄N), 144.12 (C₅H₄N), 140.14 (C₅H₄N), 137.32 (C₆H₃), 127.72 (C₆H₃), 126.92 (C₆H₃), 124.72 (C₆H₃), 124.30 (C₆H₃), 123.06 (C₆H₃), 116.15 (C₆H₄), 108.66 (C₆H₄), 100.02 (C₆H₄), 88.56 (C₆H₄), 83.94 (C₆H₄), 82.57 (C₂H₁₀B₁₀), 70.24 (C₂H₁₀B₁₀). 37.30 (Ru-CH₂), 34.00 (C₆H₄-CH₂-C₆H₃), 31.15 (CH(CH₃)₂), 30.33 (CH(CH₃)₂), 26.24, 24.40, 24.33, 19.32 ppm.

6.4.5 CRYSTAL STRUCTURE DETERMINATION DETAILS

X-ray intensity data were collected at 100(2) K using a Bruker D8 QUEST diffractometer equipped with a PHOTON-100 CMOS area detector and an Incoatec microfocus source (Mo K α radiation, $\lambda = 0.71073$ Å). The raw area detector data frames were reduced, scaled and corrected for absorption effects using the Bruker APEX3, SAINT+ and SADABS programs.⁴⁷⁻⁴⁸ Final unit cell parameters were determined by least-squares refinement of 9990 reflections taken from the data set. The structure was solved with SHELXT.⁴⁹ Subsequent difference Fourier calculations and full-matrix least-squares refinement against F^2 were performed with SHELXL-2018³ using OLEX2.⁵⁰

6.4.5.1 The X-Ray Structure Determination of RuCl(C₁₀H₁₄)(C₇H₁₄B₁₀N).C₆H₆

The compound crystallizes in the monoclinic system. The pattern of systematic absences in the intensity data was consistent with the space group $P2_1/n$, which was confirmed by structure solution. The asymmetric unit consists of one RuCl(C₁₀H₁₄)(C₇H₁₄B₁₀N) complex and half each of two benzene molecules. Both independent benzene molecules are located on crystallographic inversion centers. All

non-hydrogen atoms were refined with anisotropic displacement parameters. Hydrogen atoms bonded to carbon were located in difference Fourier maps before being placed in geometrically idealized positions and included as riding atoms with $d(\text{C-H}) = 1.00 \text{ \AA}$ and $U_{\text{iso}}(\text{H}) = 1.2U_{\text{eq}}(\text{C})$ for methine hydrogen atoms, $d(\text{C-H}) = 0.95 \text{ \AA}$ and $U_{\text{iso}}(\text{H}) = 1.2U_{\text{eq}}(\text{C})$ for arene hydrogen atoms and $d(\text{C-H}) = 0.98 \text{ \AA}$ and $U_{\text{iso}}(\text{H}) = 1.5U_{\text{eq}}(\text{C})$ for methyl hydrogens. The methyl hydrogens were allowed to rotate as a rigid group to the orientation of maximum observed electron density. Hydrogen atoms bonded to boron were located and refined freely. The largest residual electron density peak in the final difference map is $0.47 \text{ e}^{-}/\text{\AA}^3$, located 0.62 \AA from C7.

Crystal Data for $\text{C}_{23}\text{H}_{34}\text{B}_{10}\text{ClNRu}$ ($M = 569.13 \text{ g/mol}$): monoclinic, space group $P2_1/n$ (no. 14), $a = 11.3724(5) \text{ \AA}$, $b = 8.6874(4) \text{ \AA}$, $c = 27.7025(12) \text{ \AA}$, $\beta = 98.3280(16)^\circ$, $V = 2708.1(2) \text{ \AA}^3$, $Z = 4$, $T = 100(2) \text{ K}$, $\mu(\text{MoK}\alpha) = 0.693 \text{ mm}^{-1}$, $D_{\text{calc}} = 1.396 \text{ g/cm}^3$, 177642 reflections measured ($4.918^\circ \leq 2\theta \leq 61.996^\circ$), 8599 unique ($R_{\text{int}} = 0.0311$, $R_{\text{sigma}} = 0.0104$) which were used in all calculations. The final R_1 was 0.0201 ($I > 2\sigma(I)$) and wR_2 was 0.0494 (all data).

6.4.5.2 The X-Ray Structure Determination of

$[\text{Ru}(\text{CH}_3\text{CN})(\text{C}_{10}\text{H}_{14})(\text{C}_7\text{H}_{14}\text{B}_{10}\text{N})](\text{BF}_4)$

The compound crystallizes in the monoclinic system. The pattern of systematic absences in the intensity data was consistent with the space groups Pc and $P2/c$. The solution program XT found $P2/c$, which was confirmed by subsequent refinement. The asymmetric unit in $P2/c$ consists of one $[\text{Ru}(\text{CH}_3\text{CN})(\text{C}_{10}\text{H}_{14})(\text{C}_7\text{H}_{14}\text{B}_{10}\text{N})]^+$ complex, one tetrafluoroborate anion and half each of two independent benzene molecules. Both benzene molecules are disordered. Benzene C21-C26 is disordered about a C_2 axis, and

was refined with occupancies fixed at 0.5. Disorder of the other benzene molecule was modeled with two independent components per asymmetric unit (C27-C32 A/B), both also further disordered about a C_2 axis. The total occupancy of these components was constrained to sum to 0.5, and refined to $A/B = 0.31(2)/0.19(2)$. All benzene rings were refined as rigid hexagons with $d(\text{C-C}) = 1.39 \text{ \AA}$. All non-hydrogen atoms were refined with anisotropic displacement parameters, except for those of benzene molecule C32-C32, which were refined isotropically. Hydrogen atoms bonded to carbon were located in Fourier difference maps before being placed in geometrically idealized positions and included as riding atoms with $d(\text{C-H}) = 1.00 \text{ \AA}$ and $U_{\text{iso}}(\text{H}) = 1.2U_{\text{eq}}(\text{C})$ for methine hydrogen atoms, $d(\text{C-H}) = 0.95 \text{ \AA}$ and $U_{\text{iso}}(\text{H}) = 1.2U_{\text{eq}}(\text{C})$ for arene hydrogen atoms, and $d(\text{C-H}) = 0.98 \text{ \AA}$ and $U_{\text{iso}}(\text{H}) = 1.5U_{\text{eq}}(\text{C})$ for methyl hydrogens. The methyl hydrogens were allowed to rotate as a rigid group to the orientation of maximum observed electron density. Hydrogen atoms bonded to boron of the carborane cage were located and refined freely. The largest residual electron density peak in the final difference map is $0.68 \text{ e}^-/\text{\AA}^3$, located 1.06 \AA from N1.

Crystal Data for $\text{C}_{25}\text{H}_{37}\text{B}_{11}\text{F}_4\text{N}_2\text{Ru}$ ($M = 661.54 \text{ g/mol}$): monoclinic, space group $P2/c$ (no. 13), $a = 19.7365(8) \text{ \AA}$, $b = 10.3993(4) \text{ \AA}$, $c = 16.3644(6) \text{ \AA}$, $\beta = 112.132(2)^\circ$, $V = 3111.2(2) \text{ \AA}^3$, $Z = 4$, $T = 100(2) \text{ K}$, $\mu(\text{MoK}\alpha) = 0.549 \text{ mm}^{-1}$, $D_{\text{calc}} = 1.412 \text{ g/cm}^3$, 63931 reflections measured ($4.506^\circ \leq 2\Theta \leq 60.24^\circ$), 9156 unique ($R_{\text{int}} = 0.0952$, $R_{\text{sigma}} = 0.0525$) which were used in all calculations. The final R_1 was 0.0344 ($I > 2\sigma(I)$) and wR_2 was 0.0707 (all data).

6.4.5.3 The X-Ray Structure Determination of RuCl(C₁₀H₁₄)(C₇H₁₄B₁₀N) (Ru–B)

The compound crystallizes in the monoclinic system. The pattern of systematic absences in the intensity data was consistent with the space group $P2_1/n$, which was confirmed by structure solution. The asymmetric unit consists of one complex. All non-hydrogen atoms were refined with anisotropic displacement parameters. Hydrogen atoms were located in Fourier difference maps before being placed in geometrically idealized positions and included as riding atoms with $d(\text{C-H}) = 1.00 \text{ \AA}$ and $U_{\text{iso}}(\text{H}) = 1.2U_{\text{eq}}(\text{C})$ for methine hydrogen atoms, $d(\text{C-H}) = 0.95 \text{ \AA}$ and $U_{\text{iso}}(\text{H}) = 1.2U_{\text{eq}}(\text{C})$ for arene hydrogen atoms and $d(\text{C-H}) = 0.98 \text{ \AA}$ and $U_{\text{iso}}(\text{H}) = 1.5U_{\text{eq}}(\text{C})$ for methyl hydrogens. The methyl hydrogens were allowed to rotate as a rigid group to the orientation of maximum observed electron density. All hydrogen atoms of the carborane cage were located and refined freely. The largest residual electron density peak in the final difference map is $0.53 \text{ e}^-/\text{\AA}^3$, located 0.75 \AA from Ru1.

Crystal Data for C₁₇H₂₈B₁₀ClNRu ($M = 491.02 \text{ g/mol}$): monoclinic, space group $P2_1/n$ (no. 14), $a = 11.6247(4) \text{ \AA}$, $b = 13.7712(5) \text{ \AA}$, $c = 14.7650(5) \text{ \AA}$, $\beta = 108.6580(10)^\circ$, $V = 2239.45(14) \text{ \AA}^3$, $Z = 4$, $T = 100(2) \text{ K}$, $\mu(\text{MoK}\alpha) = 0.825 \text{ mm}^{-1}$, $D_{\text{calc}} = 1.456 \text{ g/cm}^3$, 56074 reflections measured ($4.15^\circ \leq 2\Theta \leq 65.712^\circ$), 8321 unique ($R_{\text{int}} = 0.0299$, $R_{\text{sigma}} = 0.0198$) which were used in all calculations. The final R_1 was 0.0211 ($I > 2\sigma(I)$) and wR_2 was 0.0490 (all data).

6.4.5.4 The X-Ray Structure Determination of Ru(C₂₀H₂₅)(C₇H₁₄B₁₀N)

The compound crystallizes in the triclinic system. The space group $P-1$ (No. 2) was confirmed by structure solution. The asymmetric unit consists of one molecule. All non-hydrogen atoms were refined with anisotropic displacement parameters. Hydrogen

atoms bonded to carbon were located in difference Fourier maps before being placed in geometrically idealized positions and included as riding atoms with $d(\text{C-H}) = 1.00 \text{ \AA}$ and $U_{\text{iso}}(\text{H}) = 1.2U_{\text{eq}}(\text{C})$ for methine hydrogen atoms, $d(\text{C-H}) = 0.95 \text{ \AA}$ and $U_{\text{iso}}(\text{H}) = 1.2U_{\text{eq}}(\text{C})$ for arene hydrogen atoms, $d(\text{C-H}) = 0.99 \text{ \AA}$ and $U_{\text{iso}}(\text{H}) = 1.2U_{\text{eq}}(\text{C})$ for methylene hydrogen atoms, and $d(\text{C-H}) = 0.98 \text{ \AA}$ and $U_{\text{iso}}(\text{H}) = 1.5U_{\text{eq}}(\text{C})$ for methyl hydrogens. The methyl hydrogens were allowed to rotate as a rigid group to the orientation of maximum observed electron density. Hydrogen atoms bonded to boron were located and refined freely. The largest residual electron density peak in the final difference map is $0.52 \text{ e}^{-}/\text{\AA}^3$, located 0.73 \AA from C2.

Crystal Data for $\text{C}_{27}\text{H}_{39}\text{B}_{10}\text{NRu}$ ($M = 586.76 \text{ g/mol}$): triclinic, space group $P-1$ (no. 2), $a = 9.4261(5) \text{ \AA}$, $b = 9.8840(5) \text{ \AA}$, $c = 16.5837(8) \text{ \AA}$, $\alpha = 104.382(2)^\circ$, $\beta = 98.293(2)^\circ$, $\gamma = 107.095(2)^\circ$, $V = 1390.58(12) \text{ \AA}^3$, $Z = 2$, $T = 100(2) \text{ K}$, $\mu(\text{MoK}\alpha) = 0.584 \text{ mm}^{-1}$, $D_{\text{calc}} = 1.401 \text{ g/cm}^3$, 49686 reflections measured ($2.608^\circ \leq 2\Theta \leq 60.118^\circ$), 8135 unique ($R_{\text{int}} = 0.0347$, $R_{\text{sigma}} = 0.0240$) which were used in all calculations. The final R_1 was 0.0251 ($I > 2\sigma(I)$) and wR_2 was 0.0621 (all data).

REFERENCES

1. a) Gladiali, S.; Alberico, E. *Chem. Soc. Rev.* **2006**, *35*, 226; b) Samec, J. S. M.; BGckvall, J.-E.; Andersson, P. G.; Brandt, P. *Chem. Soc. Rev.* **2006**, *35*, 237; c) Clapham, S. E.; Hadzovic, A.; Morris, R. H. *Coord. Chem. Rev.* **2004**, *248*, 2201.
2. Cerveny, L. Ed. *Catalytic Hydrogenation*; Elsevier: Amsterdam, **1986**.
3. de Vries, J. G., Elsevier, C. J. Eds. *The Handbook of Homogeneous Hydrogenation*; Wiley-VCH: Weinheim, **2007**.
4. Andersson, P. G., Munslow, I. J. Eds. *Modern Reduction Methods*; Wiley-VCH Verlag GmbH & Co. KGaA: Weinheim, **2008**.
5. Wang, D.; Astruc, D. *Chem. Rev.* **2015**, *115*, 6621 and references therein.
6. César, V.; Gade, L. H.; Bellemin-Lapponnaz, S. In *N-Heterocyclic Carbenes: From Laboratory Curiosities to Efficient Synthetic Tools*; Díez-González, S., Ed.; RSC Catalysis Series No. 6; Royal Society of Chemistry: Cambridge, **2011**.
7. Díez-González, S.; Marion, N.; Nolan, S. P. *Chem. Rev.* **2009**, *109*, 3612.
8. Dupont, J.; Consorti, C. S.; Spencer, J. *Chem. Rev.* **2005**, *105*, 2527.
9. van der Boom, M. E.; Milstein, D. *Chem. Rev.* **2003**, *103*, 1759.
10. Albrecht, M.; van Koten, G. *Angew. Chem., Int. Ed.* **2001**, *40*, 3750.
11. Peris, E.; Crabtree, R. H. *Coord. Chem. Rev.* **2004**, *248*, 2239.
12. Hindson, K.; de Bruin, B. *Eur. J. Inorg. Chem.* **2012**, 340.
13. Grützmacher, H. *Angew. Chem., Int. Ed.* **2008**, *47*, 1814.
14. Strassberger, Z.; Mooijman, M.; Ruijter, E.; Alberts, A. H.; de Graaff, C.; Orru, R. V. A.; Rothenberg, G. *Appl. Organometal. Chem.* **2010**, *24*, 142.
15. Monney, A.; Venkatachalam, G.; Albrecht, M. *Dalton Trans.* **2011**, *40*, 2716.

16. Akta, A.; Gök, Y. *Transition Met. Chem.* **2014**, *39*, 925.
17. Yasar, S.; Çekirdek, S.; Özdemir, I. *J. Coord. Chem.* **2014**, *67*, 1236.
18. DePasquale, J.; White, N. J.; Ennis, E. J.; Zeller, M.; Foley, J. P.; Papish, E. T. *Polyhedron* **2013**, *58*, 162.
19. Wdowik, T.; Samojłowicz, C.; Jawiczuk, M.; Malińska, M.; Woźniak, K.; Grela, K. *Chem. Commun.* **2013**, *49*, 674.
20. Yigit, B.; Yigit, M.; Özdemir, I.; Çetinkaya, E. *Transition Met. Chem.* **2012**, *37*, 297.
21. Witt, J.; Pöthig, A.; Kühn, F. E.; Baratta, W. *Organometallics* **2013**, *32*, 4042.
22. Aktas, A.; Gok, Y. *Catal. Lett.* **2015**, *145*, 631.
23. Wang, H.; Chan, H. S.; Okuda, J.; Xie, Z. *Organometallics* **2005**, *24*, 3118.
24. Zi, G.; Li, H. W.; Xie, Z. *Organometallics* **2002**, *21*, 3850.
25. Shen, H.; Xie, Z. *Chem. Commun.* **2009**, 2431.
26. Islam, M. J.; Smith, M. D.; Peryshkov, D. V. *J. Organomet. Chem.* **2018**, *867*, 208.
27. Axtell, J. C.; Kirlikovali, K.O.; Djurovich, P. I.; Jung, D.; Nguyen, V. T.; Munekiyo, B.; Royappa, A. T.; Rheingold, A. L.; Spokoyny, A. M. *J. Am. Chem. Soc.* **2016**, *138*, 15758.
28. Kratochwill, A.; Weidner, J. U.; Zimmermann, H. *Ber. Dtsch. Bunsen-Ges.* **1973**, *77*, 408.
29. Lewis, L. N. *Chem. Rev.* **1993**, *93*, 2693.
30. Lin, Y.; Finke, R. G. *Inorg. Chem.* **1994**, *33*, 4891.
31. Widegren, J. A.; Finke, R. G. *J. Mol. Catal. A: Chem.* **2003**, *198*, 317.
32. Phan, N. T. S.; Sluys, M. V. D.; Jones, C. W. *Adv. Synth. Catal.* **2006**, *348*, 609.
33. Crabtree, R. H. *Chem. Rev.* **2012**, *112*, 1536.

34. Barreiro, E. M.; Hao, Z.; Adrio, L. A.; van Ommen, J. R.; Hellgardt, K.; Hii, K. K. *Catal. Today* **2018**, *308*, 64.
35. Schmidt, A. F.; Kurokhtina, A. A. *Kinet. Catal.* **2012**, *53*, 714.
36. Artero, V.; Fontecave, M. *Chem. Soc. Rev.* **2013**, *42*, 2338.
37. Yan, N.; Yuan, Y.; Dyson, P. J. *Dalton Trans.* **2013**, *42*, 13294.
38. Fukuzumi, S.; Hong, D. *Eur. J. Inorg. Chem.* **2014**, *2014*, 645.
39. Sonnenberg, J. F.; Morris, R. H. *Catal. Sci. Technol.* **2014**, *4*, 3426.
40. Schmidt, A. F.; Kurokhtina, A. A.; Larina, E. V. *Catal. Sci. Technol.* **2014**, *4*, 3439.
41. Stracke, J. J.; Finke, R. G. *ACS Catal.* **2014**, *4*, 909.
42. Asraf, M. A.; Younus, H. A.; Yusubov, M.; Verpoort, F. *Catal. Sci. Technol.* **2015**, *5*, 4901.
43. Eremin, D. B.; Ananikov, V. P. *Coord. Chem. Rev.* **2017**, *346*, 2.
44. Gorunova, O. N.; Novitskiy, I. M.; Grishin, Y. K.; Gloriozov, I. P.; Roznyatovsky, V. A.; Khrustalev, V. N.; Kochetkov, K. A.; Dunina, V. V. *Organometallics* **2018**, *37*, 2842.
45. Chernyshev, V. M.; Astakhov, A. V.; Chikunov, I. E.; Tyurin, R. V.; Eremin, D. B.; Ranny, G. S.; Khrustalev, V. N.; Ananikov, V. P. *ACS Catal.* **2019**, *9*, 2984.
46. Shriver, D. F.; Drezzon, M. A. *The Manipulation of Air-sensitive Compounds*, second ed., Wiley-Interscience, New York, **1986**, 2 edition.
47. APEX3 Version 2016.5-0 and SAINT+ Version 8.37A. Bruker AXS, Inc., Madison, Wisconsin, USA, **2016**.
48. Krause, L.; Herbst-Irmer, R.; Sheldrick G. M.; Stalke D. SADABS-2016/2. *J. Appl. Cryst.* **2015**, *48*, 3.

49. (a) Sheldrick, G. M. SHELXT. *Acta Cryst.* **2015**, *A71*, 3. (b) Sheldrick, G. M. SHELXL. *Acta Cryst.* **2015**, *C71*, 3.
50. Dolomanov, O. V., Bourhis, L. J., Gildea, R. J., Howard J. A. K.; Puschmann, H. OLEX2: *J. Appl. Cryst.* **2009**, *42*, 339.

Chapter 7

Synthesis and Characterization of a Pyridine–Functionalized Carborane

Bearing Distorted Square Planar Complex of Nickel(II)

7.1 INTRODUCTION

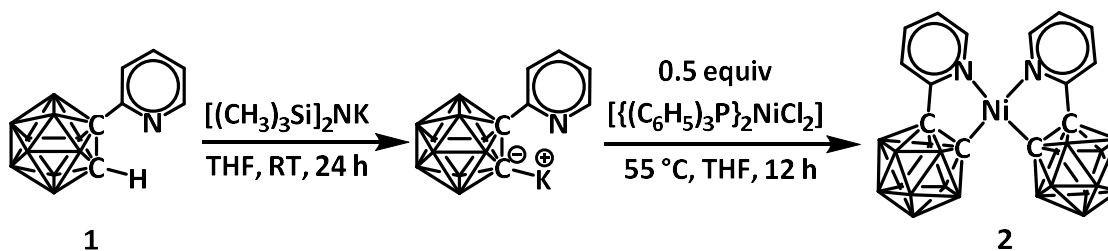
Icosahedral *closo*–(*ortho*–carborane) has attracted significant attention in recent years due to its unique structure and applications in the field of organometallic chemistry.¹ As a versatile synthon, this remarkable robust three-dimensional boron-carbon cluster can be functionalized at one or both cage carbon atoms to obtain a wide range of chelating ligands.^{2,3} The steric bulk imposed by *ortho*–carborane cluster often offers unusual geometry featuring transition metal complexes *via* deviation from idealized configuration. For instance, two bidentate *C,C'*–chelating *bis*–(*ortho*–carborane) ligands form *tetra*–coordinated Ni(II) complex with a distorted square planar geometry.⁴

Pyridine derivatized *ortho*–carborane ligands form a large number of *C,N*–chelating transition metal complexes by utilizing σ –bonding mode of carboranyl function and pendant nitrogen donor atom of pyridine moiety.⁵ The intramolecular coordination of two *C,N*–chelating picolyl–*ortho*–carboranyl ligands are known to form ideal square planar complex with Ni(II).⁶ However, to the best of our knowledge, the coordination of two (*ortho*–carboranyl)pyridine ligands to a single metal has not been reported yet.

Herein, we report the synthesis and characterization of an intramolecularly coordinated nickel(II) complex of two (*ortho*–carboranyl)pyridine ligands. Surprisingly, the two *ortho*–carboranyl clusters occupy adjacent position, and the molecular structure possesses a strongly distorted square planar geometry, in contrast to the picolyl–*ortho*–carboranyl nickel complex.

7.2 RESULTS AND DISCUSSION

The synthesis of the *tetra*-coordinated $\{(ortho\text{-carboranyl})\text{pyridine}\}_2\text{nickel(II)}$ complex (**2**) was accomplished by the addition of bis(triphenylphosphine)nickel(II) dichloride to a solution of $\{(ortho\text{-carboranyl})\text{pyridine}\}$ potassium in THF (**Scheme 7.1**). The complex **2** was isolated as a yellow powder upon washing of the dried reaction mixture by ether and methylene chloride.



Scheme 7.1: Synthesis of $\{(ortho\text{-carboranyl})\text{pyridine}\}_2\text{nickel(II)}$ (**2**).

The cyclic voltammogram (CV) of the ligand (*ortho*-carboranyl)pyridine (**1**) in 0.1 M TBAPF₆ in acetonitrile exhibited a reversible reduction event at -0.9 mV, which is attributable to the carborane cluster. The oxidation peak of **1** was observed at -0.8 mV, as shown in **Figure 7.1 (a)**. In comparison to **1**, the reduction of the carborane clusters of complex **2** in 0.1 M TBAPF₆ in acetonitrile showed a reversible peak at a higher value of -1.3 mV, presumably due to the stabilization of the carborane clusters upon coordination with the Ni(II) center *via* C-atoms. In addition, two irreversible events were observed at -2.1 mV and -2.5 mV (**Figure 7.1 (b)**). The complex **2** was also characterized by the ¹H, ¹¹B, and ¹³C NMR spectroscopic techniques and single crystal X-ray crystallography.

In the ¹H NMR spectrum of **2** in CD₂Cl₂, the disappearance of the characteristic resonance of the cluster C–H proton at 4.99 ppm of ligand **1** indicated C,N-coordination with the nickel(II) center. The resonances of the four pyridine ring protons were observed

as a set of doublets and triplets in the range from 7.93 ppm to 7.31 ppm. In the $^{11}\text{B}\{^1\text{H}\}$ and ^{11}B , a set of partially overlapping resonances were observed in the range from -3.02 ppm to -12.27 ppm.

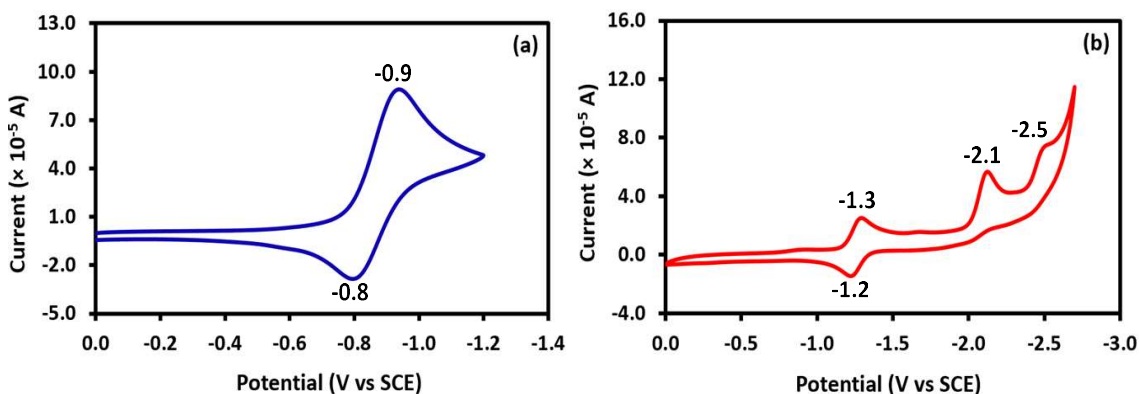


Figure 7.1: (a) Cyclic voltammogram of 1 mM of (*ortho*-carboranyl)pyridine (**1**) in 0.1 M TBAPF₆ in acetonitrile, glassy carbon (GC) as working electrode, Pt as counter electrode, scan rate 100 mVs⁻¹. (b) Cyclic voltammogram of 1 mM of complex **2** in 0.1 M TBAPF₆ in acetonitrile, GC as working electrode, Pt as counter electrode, scan rate 100 mVs⁻¹.

Single crystals of **2** were obtained by slow diffusion of hexane into a saturated solution in dichloromethane. The X-ray data unambiguously confirmed the coordination of the (*ortho*-carboranyl)pyridine ligand to the Ni(II) center through the carbon and nitrogen atoms. Presumably, the complex **2** is stabilized due to the formation of a five-membered chelate ring (**Figure 7.2** (a) and (b)). The two chelates (*C,N*) adopted a distorted square planar geometry at the Ni(II) center, and the molecular structure possesses a *C*₂ symmetry.

The *C*-functionalized *ortho*-carborane bearing *C,N*-chelating ligands, such as *ortho*-carboranylamino and picolyl-*ortho*-carboranyl are known to form square planar and distorted square planar complexes with Hg(II)^{5(c)} and Ni(II)⁶, respectively, in which two carborane clusters are located in *trans* positions. Intriguingly, in complex **2** the

carborane clusters occupy adjacent positions despite their considerable steric bulk (Figure 7.2 (a)).

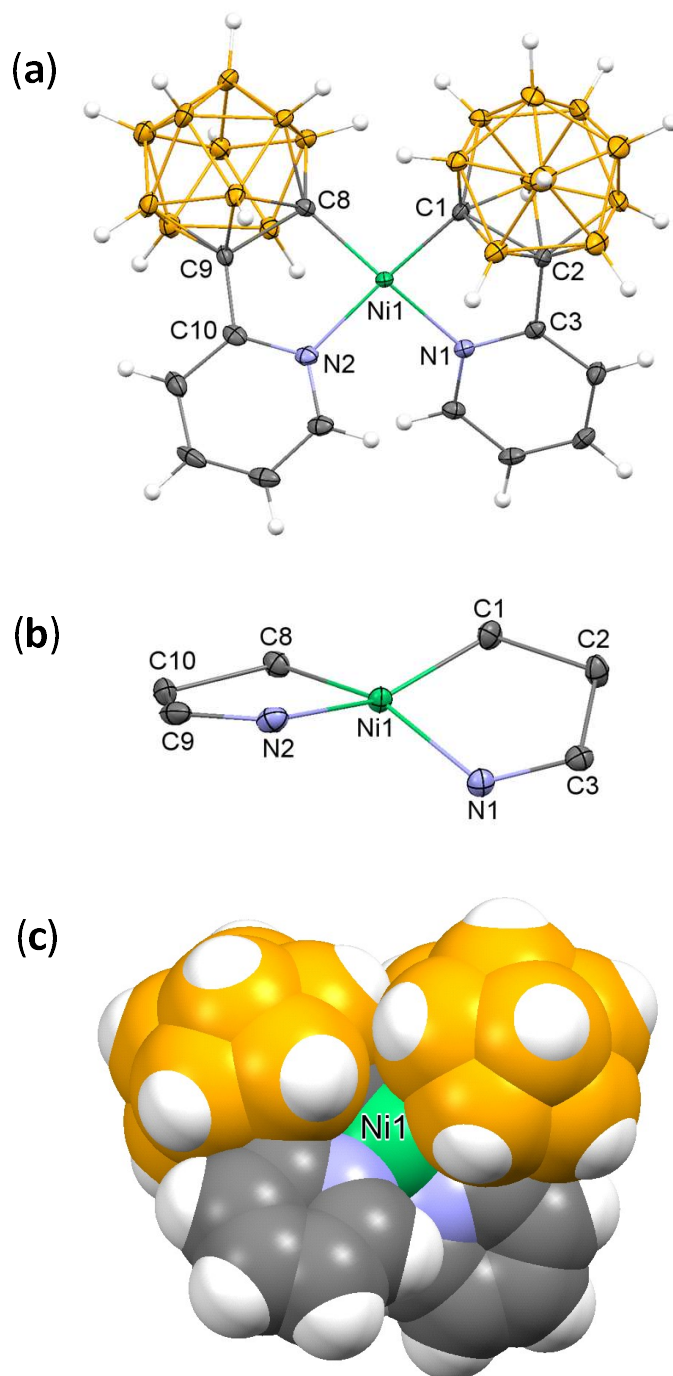


Figure 7.2: (a) 30 % probability displacement ellipsoid plot of **2**. (b) Skeletal view highlighting the C,N- coordination of the ligand **1** to the nickel(II) center to form a five-membered ring. (c) A space-filling diagram of **2**.

The space-filling diagram of **2** in **Figure 7.2 (c)** highlights the steric congestion around the metal center. Presumably, the deviation from the regular square planar geometry is due to steric constraints imposed by the two adjacent carboranyl ligands. The C1–Ni1 bond length (1.906(3) Å) is slightly shorter than the C8–Ni1 bond length (1.923(3) Å). The Ni–N bond distances in **2** (1.958(2) Å and 1.955(3) Å) are much longer than that in the corresponding picolyl-*ortho*-carboranyl ligated system bis[1-(2'-picolyl)-*ortho*-carborane]nickel (1.887(4) Å and 1.892(4) Å),⁶ but shorter than the pyridine-ligated system [*bpa*(CH₂)₂O(CH₂)₂-OH}Ni(NO₃)](NO₃) (*bpa* = bis(2-picolyl)amine; 2.0708(13) Å and 2.0765(12) Å).⁷ The angle formed by normals to the planes of the two bidentate (*ortho*-carboranyl)pyridine ligands (defined: C8, Ni1, N2 and C1, Ni1, N1) is 31.11°. Surprisingly, this value is higher than that in the corresponding *bis*-(*ortho*-carborane) analogue (26°).⁴ The *cis*-bond angles about the nickel center are 87.58(11)° (C8–Ni1–N2) to 95.66(10)° (N2–Ni1–N1), while *trans*-bond angles range from 158.36(12)° (C1–Ni1–N2) to 158.86(12)° (C8–Ni1–N1).

7.3 CONCLUSION

In conclusion, an intramolecularly coordinated nickel (II) complex containing a *C,N*-chelating ligand (*ortho*-carboranyl)pyridine was synthesized by the addition of bis(triphenylphosphine)nickel(II) dichloride into a solution of {(*ortho*-carboranyl)pyridine}potassium. The two *ortho*-carborane clusters of the two chelates are located on adjacent positions and the molecular structure possesses a distorted square planar geometry.

7.4 EXPERIMENTAL SECTION

All synthetic manipulations, unless stated otherwise, were carried out either in a nitrogen-filled VAC drybox or on a dual manifold Schlenk-style vacuum line. The solvents were sparged with nitrogen, passed through activated alumina, and stored over activated 4 Å Linde-type molecular sieves. CD₂Cl₂ was degassed and stored over activated 4 Å Linde-type molecular sieves. NMR spectra were recorded using Varian spectrometers at 400 (¹H), 100 (¹³C), 128 (¹¹B) MHz, reported in δ (parts per million) and referenced to the residual ¹H/¹³C signals of the deuterated solvent or an external BF₃(Et₂O) (¹¹B(δ): 0.0 ppm) standard.

7.4.1 Synthesis of {(C₅H₃N)(C₂B₁₀H₁₀)}₂Ni (2)

Potassium bis(trimethylsilyl)amide [{(CH₃)₃Si }₂NK] (0.7 M, 1.30 mL, 0.91 mmol) was transferred *via* a syringe to a solution of (*ortho*-carboranyl)pyridine ligand (200 mg, 0.90 mmol) in THF under nitrogen atmosphere. The resulting mixture was stirred at room temperature for 24 hours. The solvent was removed under vacuum and the solid was washed with hexane (3 × 3 mL) to remove unreacted {(CH₃)₃Si }₂NK. The solid was dissolved in THF (10 mL) in a storage flask and bis(triphenylphosphine)nickel(II) dichloride [{(C₆H₅)₃P }₂NiCl₂] (250 mg, 0.38 mmol) was added. The mixture was heated at 55 °C for 24 hours, after which time the solvent was removed under vacuum and the solid was washed with ether and methylene chloride. The complex {(*ortho*-carboranyl)pyridine)}₂Ni(II) was obtained as an orange solid (140 mg, 73 % yield).

¹H NMR (CD₂Cl₂): δ 7.91 (t, 2H, C₅H₃N), 7.62 (d, 2H, C₅H₃N), 7.49 (d, 2H, C₅H₃N), 7.32 (t, 2H, C₅H₃N), 3.25–1.40 (overlapping, 20H, B–H, C₂B₁₀H₁₀). ¹¹B{¹H} NMR (CD₂Cl₂): δ –3.48, –6.14, –7.65, –9.27, –11.57. ¹³C NMR (CD₂Cl₂): δ 159.68

(C₅H₃N), 150.66 (C₅H₃N), 140.44 (C₅H₃N), 125.54 (C₅H₃N), 122.79 (C₅H₃N), 83.43 (C₂H₁₀B₁₀), 66.83 (C₂H₁₀B₁₀) ppm.

7.4.2 CRYSTAL STRUCTURE DETERMINATION DETAILS

X-ray intensity data from a flat yellow needle were collected at 100(2) K using a Bruker D8 QUEST diffractometer equipped with a PHOTON-100 CMOS area detector and an Incoatec microfocus source (Mo K α radiation, $\lambda = 0.71073$ Å). The raw area detector data frames were reduced and corrected for absorption effects using the Bruker APEX3, SAINT+ and SADABS programs.^{1,2} The structure was solved with SHELXT.³ Subsequent difference Fourier calculations and full-matrix least-squares refinement against F^2 were performed with SHELXL-2018³ using OLEX2.⁴

7.4.2.1 X-Ray Structure Determination of {(C₅H₃N)(C₂B₁₀H₁₀)}₂Ni (2)

The compound crystallizes in the orthorhombic system. The pattern of systematic absences in the intensity data was uniquely consistent with the space group *Fdd2*. The asymmetric unit consists of one complex. All non-hydrogen atoms were refined with anisotropic displacement parameters. Hydrogen atoms bonded to carbon were located in difference Fourier maps before being placed in geometrically idealized positions and included as riding atoms with $d(\text{C-H}) = 0.95$ Å and $U_{\text{iso}}(\text{H}) = 1.2U_{\text{eq}}(\text{C})$ for aromatic hydrogen atoms. Hydrogen atoms bonded to boron were located in difference maps. Their atomic coordinates were refined freely and their displacement parameters were treated as $U_{\text{iso}}(\text{H}) = 1.2U_{\text{eq}}(\text{B})$. The largest residual electron density peak in the final difference map is 0.21 e-/Å³, located 0.81 Å from Ni1. The absolute structure (Flack) parameter after the final refinement cycle was 0.012(9), consistent with assignment of the correct absolute structure.

Crystal Data for $C_{14}H_{28}B_{20}N_2Ni$ ($M = 499.29$ g/mol): orthorhombic, space group $Fdd2$ (no. 43), $a = 33.6832(18)$ Å, $b = 42.079(2)$ Å, $c = 7.1510(4)$ Å, $V = 10135.6(9)$ Å³, $Z = 16$, $T = 100(2)$ K, $\mu(MoK\alpha) = 0.777$ mm⁻¹, $D_{calc} = 1.309$ g/cm³, 32868 reflections measured ($4.566^\circ \leq 2\Theta \leq 52.86^\circ$), 4269 unique ($R_{int} = 0.0597$, $R_{sigma} = 0.0380$) which were used in all calculations. The final R_1 was 0.0281 ($I > 2\sigma(I)$) and wR_2 was 0.0607 (all data).

REFERENCES

1. (a) Fox, M. A.; Hughes, A. K. *Coord. Chem. Rev.* **2004**, *248*, 457. (b) Teixidor, F.; Vinas, C. In *Science of Synthesis*; Thieme: Stuttgart, Germany, **2005**; Vol. 6, p 1235. (c) Grimes, R. N. *J. Chem. Educ.* **2004**, *81*, 658. (d) Plesek, J. *Chem. Rev.* **1992**, *92*, 269.
2. (a) Teixidor, F.; Vinas, C.; Abad, M. M.; Whitaker, C.; Rius, J. *Organometallics* **1996**, *15*, 3154. (b) Balema, V. P.; Somoza, F.; Hey-Hawkins, E. *Eur. J. Inorg. Chem.* **1998**, 651. (c) Calhorda, M. J.; Crespo, O.; Gimeno, M. C.; Jones, P. G.; Laguna, A.; Lopez de Luzuriaga, J. M.; Perez, J. L.; Ramon, M. A.; Veiros, L. F. *Inorg. Chem.* **2000**, *39*, 4280. (d) Lee, Y.-J.; Lee, J.-D.; Kim, S.-J.; Keum, S.; Ko, J.; Suh, I.-H.; Cheong, M.; Kang, S. O. *Organometallics* **2004**, *23*, 203. (e) Dou, J.-M.; Zhang, D.-P.; Li, D.-C.; Wang, D.-Q. *Polyhedron* **2007**, *26*, 719. (f) Laromaine, A.; Teixidor, F.; Vinas, C. *Angew. Chem., Int. Ed.* **2005**, *44*, 2220.
3. (a) Lee, J.-D.; Lee, Y.-J.; Son, K.-C.; Cheong, M.; Ko, J.; Kang, S. O. *Organometallics* **2007**, *26*, 3374. (b) Cai, S.; Jin, G.-X. *Organometallics* **2007**, *26*, 5442. (c) Kushwah, N. P.; Jain, V. K.; Wadawale, A.; Zhidkova, O. B.; Starikova, Z. A.; Bregadze, V. I. *J. Organomet. Chem.* **2009**, *694*, 4146. (d) Spokoyny, A. M.; Reuter, M. G.; Stern, C. L.; Ratner, M. A.; Seiderman, T.; Mirkin, C. A. *J. Am. Chem. Soc.* **2009**, *131*, 9482. (e) Zhang, J.-S.; Lin, Y.-J.; Jin, G.-X. *J. Organomet. Chem.* **2009**, *694*, 2069. (f) Li, Y.; Jiang, Q.; Li, Y.; Yan, H.; Bregadze, V. I. *Inorg. Chem.* **2010**, *49*, 4.
4. Harwell, D. E.; McMillan, J.; Knobler, C. B.; Hawthorne, M. F. *Inorg. Chem.* **1997**, *36*, 5951.
5. (a) Bae, H. J.; Kim, H.; Lee, K. M.; Kim, T.; Eo, M.; Lee, Y. S.; Do, Y.; Lee, M. H. *Dalton Trans.* **2013**, *42*, 8549. (b) Wang, X.; Jin, G.-X. *Chem. Eur. J.* **2005**, *11*, 5758. (c)

Lee, J-, D.; Kim, S-, J.; Yoo, D.; Ko, J.; Cho, S.; Kang, S. O. *Organometallics* **2000**, *19*, 1695.

6. Wang, X.; Jin, G-, X. *Organometallics* **2004**, *23*, 6319.

7. Kirin, S. I.; Happel, C. M.; Hrubanova, S.; Weybermueller, T.; Metzler–Nolte, N. *Dalton Trans.* **2004**, 1201.

Appendix A

Permission to Reprint



RightsLink®



Home



Help



Email Support



Sign in



Create Account

**Sterically encumbered dianionic dicarboranyl pincer ligand (C₅H₃N)(C₂B₁₀H₁₁)₂ and its CNC Nickel(II) complex****Author:** Mohammad Jahirul Islam, Mark D. Smith, Dmitry V. Peryshkov**Publication:** Journal of Organometallic Chemistry**Publisher:** Elsevier**Date:** 15 July 2018

© 2017 Elsevier B.V. All rights reserved.

Please note that, as the author of this Elsevier article, you retain the right to include it in a thesis or dissertation, provided it is not published commercially. Permission is not required, but please ensure that you reference the journal as the original source. For more information on this and on your other retained rights, please visit: <https://www.elsevier.com/about/our-business/policies/copyright#Author-rights>

BACK

CLOSE WINDOW